FINAL REPORT

Assessing Climate Change Impacts for DoD Installations in the Southwest United States During the Warm Season

SERDP Project RC-2205

MARCH 2017

Christopher L. Castro, Ph.D.
University of Arizona

SERDP
DOD ▪ EPA ▪ DOE

Page Intentionally Left Blank

REPORT DOCUMENTATION PAGE

Form Approved
OMB No. 0704-0188

1. REPORT DATE *(DD-MM-YYYY)*	**2. REPORT TYPE**	**3. DATES COVERED** *(From - To)*
10/03/2017	Final	March 2012 to March 2017

4. TITLE AND SUBTITLE

Assessing climate change impacts for DoD installations in the Southwest United States during the warm season

5a. CONTRACT NUMBER

5b. GRANT NUMBER
RC-2205

5c. PROGRAM ELEMENT NUMBER

6. AUTHOR(S)

Castro, Christopher L.

5d. PROJECT NUMBER
RC-2205

5e. TASK NUMBER

5f. WORK UNIT NUMBER

7. PERFORMING ORGANIZATION NAME(S) AND ADDRESS(ES)

University of Arizona
Dept. of Hydrology and
Atmospheric Sciences
1118 E 4th st, Rm 542
Tucson, AZ 85721

8. PERFORMING ORGANIZATION REPORT NUMBER

9. SPONSORING / MONITORING AGENCY NAME(S) AND ADDRESS(ES)

University of Arizona
Sponsored Project Services

10. SPONSOR/MONITOR'S ACRONYM(S)

UA SPS

11. SPONSOR/MONITOR'S REPORT NUMBER(S)

12. DISTRIBUTION / AVAILABILITY STATEMENT

13. SUPPLEMENTARY NOTES

14. ABSTRACT The impact of changes in extreme weather during the North American monsoon are evaluated as they may impact Department of Defense (DoD) facilities in the Southwest U.S., with respect to the concerns of exceedance of infrastructural limits and operational capability. A new methodological technique to severe weather projection is developed using convective-permitting regional climate modeling. Severe weather event days during Southwest monsoon are objectively identified within global climate models based on dynamic and thermodynamic conditions. Changes in precipitation intensity and duration from the severe weather simulations are assessed at the DoD facility scale, with respect to operational weather watch and warning criteria. Significant long-term changes in the atmospheric conditions during Southwest monsoon have occurred over the past sixty years. Though there are fewer organized monsoon convections, convection associated precipitation is tending to be more intense. Particularly in southwestern Arizona, where many DoD assets are located, it appears to be a local hot spot where historic organized convective events are becoming more intense, specific in heavier rainfall and stronger downdraft winds. These changes are verified in observed precipitation. The resulted future changes are consistent with trends from the historical record, including identifying southwestern Arizona as a region of intensifying precipitation extremes.

15. SUBJECT TERMS

16. SECURITY CLASSIFICATION OF:			**17. LIMITATION OF ABSTRACT**	**18. NUMBER OF PAGES**	**19a. NAME OF RESPONSIBLE PERSON**
a. REPORT	**b. ABSTRACT**	**c. THIS PAGE**		133	**19b. TELEPHONE NUMBER** *(include area code)*

Standard Form 298 (Rev. 8-98)
Prescribed by ANSI Std. Z39.18

Page Intentionally Left Blank

Page Intentionally Left Blank

Table of Contents

LIST OF TABLES

LIST OF FIGURES

LIST OF ACRONYMS (in alphabetical order)

Acronym	Meaning
ARK	Archival Resource Key
ATMO	Department of Atmospheric Sciences
CAPE	Convective Available Potential Energy
CCSM	Community Climate System Model
CDF	Cumulative Density Function
CMIP(3,5)	Coupled Model Intercomparison Project (Versions 3 and 5)
CORDEX	Coordinated Regional Climate Downscaling Experiment
CPM	Convective Permitting Model
CPC	Climate Prediction Center
DCAPE	Downdraft Convective Potential Energy
DCR	Data Commons Repository
DoD	Department of Defense
DOI	Digital Object Identifier
ECHAM-(5,6)	European Center Hamburg Model (Versions 5 and 6)
EMC	Environmental Modeling Center
EOF	Empirical Orthogonal Function
ESG	Earth System Grid
ESRL	Earth System Research Laboratory
GCM	Global Climate Model
GEV	Generalized Extreme Value
GFDL	Geophysical Fluid Dynamics Laboratory
GH	Geopotential Height

GHCN	Global Historical Climate Network
GP	Generalized Pareto
HadCM3	Hadley Center Coupled Model, Version3
HadGEM2	Hadley Center Global Environmental Model, Version 2
HRRR	High Resolution Rapid Refresh
IPCC	Intergovernmental Panel on Climate Change
IV	Inverted Trough
LST	Local Standard Time
MCAS	Marine Corps Air Station (Yuma, Arizona)
MCS	Mesoscale Convective System
MPI	Max-Planck Institute
MUCAPE	Most Unstable Convective Available Potential Energy
MYJ	Mellor-Yamada-Janic
NARCCAP	North American Regional Climate Change Assessment Program
NAM	North American Monsoon
NARR	North American Regional Reanalysis
NCAR	National Center for Atmospheric Research
NCEP	National Center for Environmental Prediction
NCDC	National Climate Data Center
NEXRAD	Next Generation Radar
NOAA	National Oceanic and Atmospheric Administration
NWP	Numerical Weather Prediction
NWS	U.S. National Weather Service
OWS	Operational Weather Squadron
PCMDI	Program for Climate Model Diagnosis and Intercomparison

PDF	Probability Density Function
POT	Peak Over Threshold
PV	Potential Vorticity
PW	Precipitable Water (vertically integrated)
RCM	Regional Climate Model
RCP	Radiative Concentration Pathway
RDAS	Regional Data Assimilation System
RRTM	Rapid Radiative Transfer Model
SERDP	Strategic Ennvironmental Research and Development Program
SVD	Singular Value Decomposition
WRF	Weather Research and Forecasting Model
UA	University of Arizona
UCM	Urban Canopy Model
UKMO	United Kingdom Meteorological Office
UTC	Universal Coordinated Time (local time in Greenwich, England)

KEY WORDS

Climate change projection

Convective-permitting modeling

Convective processes

Dynamical downscaling

Extreme precipitation

North American monsoon

Severe weather

Regional climate modeling

Warm season

ACKNOWLEDGEMENTS

The Principal Investigator acknowledges the contributions from the following past and present graduate students and professional staff within the Department of Hydrology and Atmospheric Sciences that have made contributions to this project:

Dr. Hsin-I Chang, Research Associate
Mr. Mike Leuthold, Research Associate
Dr. Thang Luong, Ph.D. graduate, Fall 2015
Dr. Carlos Carrillo, Ph.D. gradúate, Spring 2015
Mr. Jeremy Mazon, M.S. graduate, Spring 2013
Ms. Jennifer Stutler, M.S. graduate, Summer 2013
Ms. Megan Jares, M.S. graduate, Spring 2014
Mr. Timothy Lahmers, Ph.D. candidate
Mr. William Cassell, Ph.D. candidate

The collaborations with civilian and DoD partner organizations is gratefully acknowledged for participation and project engagement activities, provision of data and methods, and advisement of graduate students:

25th Operational Weather Squadron at Davis-Monthan Air Force Base, Tucson, Arizona
14th Weather Squadron, Ashville, North Carolina
National Weather Service, Tucson Office

The Principal Investigator is also grateful to Dr. John Hall, the prior SERDP Resource and Conservation Program manager, for his continued thoughtful guidance and feedback throughout the project.

I. ABSTRACT

Objectives: The impact of changes in extreme weather during the period of the North American monsoon in late summer are evaluated as they may impact Department of Defense (DoD) facilities in the Southwest United States, with respect to the concerns of exceedance of infrastructural limits and operational capability. The overarching research objective is to evaluate how warm season extreme weather events in the Southwest will change with respect to occurrence and intensity. The project addresses: 1) consideration of existing operational protocols for weather and climate related decision making, 2) creation of climate change projection information at an appropriate spatial scale, 3) consideration of extreme weather and climate events, and 4) use of data to inform adaptation strategies.

Technical approach: A new methodological technique to severe weather event projection is developed using convective-permitting modeling with the Weather Research and Forecasting model. The guiding principle is to use a weather forecast based approach to climate projection. Severe weather event days in the Southwest during the monsoon period are objectively identified within an atmospheric reanalysis and several global climate models from the Coupled Model Intercomparison Project (CMIP), on the basis of the thermodynamic conditions necessary for intense monsoon thunderstorms. The severe weather event days are also investigated to verify that known dynamic forcing factors also are present, including a favorable positioning of the subtropical ridge over the western United States and the presence of an upper-level disturbance, or transient inverted trough. Convective-permitting model simulations are then performed for the identified severe weather event days, similar to an operational numerical weather prediction model, with the advantage of explicitly representing convective structures and propagation. Model simulated differences between past and future periods in the various convective-permitting modeling paradigms are used to determine changes in mean and extreme precipitation and downdraft winds from thunderstorm outflows, and these results are verified against long-term changes in available observational data. Changes in precipitation intensity and duration are finally assessed at the DoD facility scale, in a manner that confirms to DoD operational weather watch and warning criteria.

Results: There have been significant long-term changes in the atmospheric thermodynamic and dynamic conditions during the period of the monsoon in the Southwest that have occurred over the past sixty years. Atmospheric moisture and instability have generally increased, but transient inverted troughs have decreased in frequency because of the expansion of the subtropical ridge. As a result, monsoon thunderstorms in the Southwest are tending to be more thermodynamically dominated, with less tendency to organize and propagate. Though there are tending to be a fewer number of strong, organized convective events during the monsoon, when they do occur their associated precipitation is tending to be more intense. In the historical climate simulations,

monsoon precipitation on average generally is decreasing in the Southwest, while the intensity of precipitation associated with organized convective events increases. In particular, the area of southwestern Arizona, where many important and spatially expansive DoD assets are located, appears to be a local hot spot where organized convective events are becoming more intense, in terms heavier rainfall and more intense downdraft winds. These changes are verified in high resolution observed precipitation data. The projected future changes using dynamically downscaled CMIP models are very consistent with trends from the historical record, including identifying southwestern Arizona as a region of intensifying precipitation extremes.

Benefits: An physically robust and computationally efficient methodological approach to the projection of extreme event weather in the Southwest is developed within this pilot project, that could be easily adapted for other regions of the United States and the world. A convective-permitting modeling approach adds substantial value to projection of extreme weather, pinpointing the spatial locations within the Southwest where precipitation is becoming more intense with a high degree of accuracy. Model data generated within this project will be made available via a cloud data storage system, so as to be widely available for DoD and civilian use.

II. OBJECTIVE

A. RELATION TO STATEMENT OF NEED

This project evaluates the impact of changes in extreme weather during the North American monsoon (NAM) at DoD facilities in the Southwest. Two principal questions therein are: 1) Will infrastructural limits be exceeded beyond some critical point? and 2) Will operational capabilities be adversely impacted? This project builds on current operational weather forecasts currently generated at the University of Arizona, Department of Atmospheric Sciences (UA ATMO) with a high resolution regional model that has been utilized by the 25th Operational Weather Squadron at Davis-Monthan Air Force Base, to develop a standardized methodology for projection of high impact monsoon weather. Dynamically downscaled "well performing" CMIP version 3 and 5 models (Taylor et al. 2012), used for Intergovernmental Panel on Climate Change (IPCC) assessment, and an atmospheric reanalysis are considered. The overall scientific research objective is to evaluate how warm season extreme weather events in the Southwest U.S. will change with respect to occurrence and intensity. The project addresses the following priorities in the Statement of Need: 1) consideration of existing operational protocols for weather and climate related decision making, 2) creation of climate change projection information at an appropriate spatial scale, 3) consideration of extreme weather and climate events, and 4) use of data to inform adaptation strategies.

B. WORKING HYPOTHESES IN RELATION TO PROJECT OBJECTIVES

The working hypotheses that underlie successful execution of project objectives, presented in the form technical questions in relation to the project tasks from the original proposal are:

- Question 1: Can a standardized methodology identify days conducive for severe monsoon weather within dynamically downscaled regional climate model data, that incorporates thermodynamic and dynamic metrics used in operational weather forecasting for the Southwest?
- Question 2: Can severe weather events can be reasonably simulated in high resolution numerical weather prediction-type simulations, in terms of storm intensity, structure, and evolution, with the recent historical period of an atmospheric reanalysis and "well performing" CMIP3 and CMIP5 models?
- Question 3: Are simulated changes in severe weather over the recent historical period (1950-present) consistent with the idea that anthropogenic global climate change is making monsoon thunderstorms more intense, because thermodynamic conditions for thunderstorms are becoming more favorable?

- Question 4: Do simulated changes in severe weather for the near future in the 21st century, using global climate change projection models, also show that monsoon thunderstorms are projected to become more intense?
- Question 5: Can high resolution atmospheric model information be utilized to assess changes in high impact weather for DoD facilities in the Southwest?

C. SCOPE OF FINAL PROJECT REPORT

This final project report reviews the extent to which all of these hypotheses have been investigated in relation to the originally proposed project tasks. The principal sections of results are organized in a manner that relates to the ordering of the work tasks. Though this report is not necessarily an all-inclusive summary of research activities performed within this project, it presents the most pertinent information and findings, as reported in conference proceedings, project-related professional publications, theses and dissertations of supported graduate students, and engagements with collaborators and SERDP through the annual in-progress review process. The work presented herein represents the contributions of all project performers at the University of Arizona, as mentioned in acknowledgements. Please note that when tables and figures are shown within this report, they immediately follow from the specific section or sub-section where they are initially mentioned in the text.

III. BACKGROUND

A. MOTIVATION FOR RESEARCH

Arid to semi-arid regions located in subtropical zones are projected to experience some of the most adverse impacts of climate change. There is likely to be an increase in heat and aridity due to the retreat of the mid-latitude jet and expansion of sub-tropical highs (e.g. Archer and Caldeira 2008; Seidel et al. 2008; Lu et al. 2009), as concluded in the recent Climate Change Assessment for the Southwest (Garfin et al. 2013) and IPCC Fifth Assessment Report (IPCC 2013). Another conclusion within these reports, more directly related to this project, is that there will be increase in extreme weather events due to the increase in mean temperature and increase in atmospheric water vapor holding capacity (e.g. Meehl et al. 2000). A number of analyses have documented significant positive trends in observed water vapor globally and within the United States, in terms of both surface specific humidity and column integrated precipitable water (e.g. Karl and Knight 1998; Karl and Trenberth 2003; Griosman et al. 2005; Santer et al. 2007; Willett et al. 2007). The recent increases in precipitation extremes have been attributed to greenhouse gas increases (e.g. Karl and Trenberth 2003; Min et al. 2009, 2011).

Our geographic area of interest in this SERDP project is the southwestern United States, henceforth referred to as the Southwest. Observed twenty-year return period thresholds of daily maximum precipitation in the Southwest have exhibited an upward trend (Kunkel et al. 2013), matching what has been documented on a more global scale. Any long-term increases in precipitation intensity should be most apparent during the NAM (Adams and Comrie 1997) in late summer (July through early September), as this is the period of warm season severe weather caused by convective thunderstorms. Two specific dangers therein most relevant to USAF-issued weather watch and warning criteria, in the area of responsibility of the 25th Operational Weather Squadron (25th OWS), are heavy rain and the wind gusts associated with convective outflow boundaries. There is some existing observational evidence to suggest that monsoon precipitation may be becoming more extreme in the Southwest (e.g. Anderson et al. 2010; Petrie et al. 2014; Chang et al. 2015).

We must necessarily depend on global and regional atmospheric models to dynamically generate future projections and retrospective simulations of the NAM for impacts assessment. Global climate models (GCMs) have been generally challenged to represent the NAM as a salient climatological feature in the Southwest, in terms of the maximum in precipitation in late July to early August and subsequent retreat of the monsoon in late August and September. This problem has been previously noted in reference to both atmospheric reanalyses and global seasonal forecast models (e.g. Castro et al. 2007; 2012) and the CMIP 3 climate change projection models (Geil et al. 2013; Bukovsky et al. 2015). There have been some notable improvements by recent IPCC models utilized within the most recent Fifth Assessment Report (Sheffield et al. 2013), and

regional climate models (RCMs) of the North American Regional Climate Change Assessment Program, or NARCCAP (Bukovsky et al. 2015). The most recent analysis of IPCC Fifth Assessment Report models suggest there will be a delay in monsoon onset in early summer due to increased atmospheric stability but an increase in monsoon precipitation in late summer (Cook and Seager 2013). Regional models that use a grid spacing on the order of 10s of kilometers tend to overestimate monsoon precipitation in mountainous regions and underestimate precipitation associated with organized, propagating convection (Castro et al. 2012; Bukovsky et al. 2013).

When considering the question of changes in extreme precipitation during the NAM, any global or atmospheric modeling paradigm that utilizes a grid spacing on the order of 10s of kilometers or coarser is not sufficient. At these relatively coarse spatial scales, atmospheric models: 1) cannot explicitly represent monsoon thunderstorms, in terms of their physical structure and evolution, and 2) the statistical representation of precipitation extremes is dependent on the spatial resolution, with improved representation at finer spatial resolution (e.g. Tripathi and Dominguez 2013). Regional atmospheric models that utilize a grid spacing approximately less than 5 kilometers are referred to as convective-permitting models, because thunderstorms may be explicitly represented without the use of convective parameterization. The overall value added of convective-permitting modeling, particularly with the representation of precipitation extremes and organized convective structures, has been well established in the recent literature, in overview articles by Prein et al. (2015) and Kendon et al. (2016). In the context of numerical weather prediction-type simulations for the NAM, convective-permitting modeling is required to reasonably represent mesoscale convective systems (MCSs), as these are one of the more common meteorological triggers for severe weather events (Cassell et al. 2016).

A convective-permitting modeling paradigm is currently being established for real-time operational numerical weather prediction (NWP) by the U.S. National Weather Service, with the recent incorporation of the High Resolution Rapid Refresh (HRRR) model that utilizes a 3 km grid spacing. Within the Southwest, the Department of Hydrology and Atmospheric Sciences at the University of Arizona has been producing convective-permitting NWP forecasts using the Weather Research and Forecast (WRF) model (with a grid spacing of 1.8 km) for nearly a decade, providing the highest spatial resolution NWP forecasts in the Southwest. The major scientific aim in this project is to use regional atmospheric modeling to address the question of possible changes in the intensity of monsoon thunderstorms under the influence of anthropogenic climate change. Convective-permitting modeling is the most viable and physically robust approach to address this question.

B. PRIOR INTERIM REPORT TO SERDP: GO/NO GO DECISION POINT

In the review of this project, SERDP required an Interim Technical Report (submitted April 2014) to evaluate a Go/No go decision point on whether or not it was appropriate to proceed on to addressing Question 4 with dynamically downscaled "well performing'' CMIP3 models. The consideration of future changes in CMIP3 and CMIP5 models would only be performed if the answers to Questions 1 and 2 were affirmative, or in other words: 1) the dynamically downscaled data used clearly represented known thermodynamic and dynamic pre-cursors for severe monsoon weather, to identify severe weather event days for high resolution NWP-type simulation; 2) the NWP-type simulations of the severe weather events with the downscaled CMIP models captured the known characteristics of monsoon storm structure and evolution associated with organized convection; and 3) these results generally comported with the counterpart results from a dynamically downscaled historical atmospheric reanalysis. Basically the Interim Report addressed the overarching question: How physically robust is the project methodological approach for representing severe weather within a regional atmospheric model. The final recommendation provided within the Interim Report and accepted by SERDP, based on the good performance of the dynamically downscaled CMIP3 models, was that the project results from the initial phases indicated it was appropriate to proceed (i.e. a ''go'' decision).

IV. MATERIALS AND METHODS

A. DATA SOURCES

1. Baseline sources of dynamically downscaled reanalysis and CMIP3 and CMIP5 data

All baseline sources of long-term dynamically downscaled data for use in the project have been produced in a consistent a manner as possible with the WRF, Versions 3.1 and higher (Skamarock et al. 2008), used as a RCM. The model physical parameterizations are approximately consistent with the existing WRF NWP system within UA-ATMO that produces quasi-operational forecasts for Arizona. They include: WRF Single-Moment 3-class microphysics (Hong et al. 2004, 1998); Kain-Fritsch convective parameterization (Kain and Fritsch 1993, Kain 2004); Goddard Shortwave radiation (Chou and Suarez 1994); Rapid Radiative Transfer Model (RRTM) Longwave (Mlawer et al. 1997); Eta surface layer (Janjic 1996, 2002); Mellor-Yamada-Janic (MYJ) planetary boundary layer (Janic 1990, 1996, 2002); and the NOAH land surface model. Spectral nudging is utilized in WRF RCM simulations, consistent with Miguez-Macho et al. (2005), to maintain the variability of synoptic-scale circulation features (i.e. upper-air ridges and troughs) and still allow the RCM to add value on the mesoscale.

Boundary forcing data for WRF-RCM simulations are from the following sources noted in bullet points below. Note that for downscaled CMIP data, either the A2 greenhouse gas emission scenario or Radiative Concentration Pathway (RCP 8.5) is utilized (Taylor et al. 2012). In practical terms this is the "business as usual" greenhouse gas emission scenario that assumes no major global economic shifts will occur to substantially reduce emissions, and this best corresponds to the currently observed trajectory of greenhouse gases in the atmosphere. Final simulations for dynamically downscaled CMIP5 data utilize the North American domain of the Coordinated Ensemble Downscaling Experiment (CORDEX)[1] and, as of the date of this report, are being transferred to a data repository at the National Center for Atmospheric Research (NCAR) for permanent archival and anticipated availability through the Earth System Grid (ESG)[2] sometime shortly after the conclusion of this project. The NCEP-NCAR global reanalysis forcing data (Kalnay et al. 2016) were obtained from the National Oceanic and Atmospheric Administration (NOAA) Earth System Research Laboratory (ESRL). CMIP3 and CMIP5 forcing data suitable for dynamical downscaling may be obtained from the Program for Climate Model Diagnosis and Intercomparison (PCMDI) website.[3]

[1] http://wcrp-cordex.ipsl.jussieu.fr/
[2] http://www.earthsystemgrid.org
[3] http://www-pcmdi.llnl.gov/

- NCEP-NCAR global atmospheric reanalysis: Completed simulation period 1948-2012 for a U.S.-Mexico domain at 35 km grid spacing.
- United Kingdom Meteorological Office-Hadley Center Coupled Model Version 3 (UKMO-HadCM3) from CMIP3: Completed simulation period 1967-2081 for a U.S.-Mexico domain at 35 km grid spacing
- Max Planck Institute-European Center Hamburg Model, Version 5 (MPI-ECHAM5) from CMIP3: Completed simulation period 1950-2100 for a U.S.-Mexico domain at 35 km grid spacing
- UKMO-Hadley Center Global Environmental Model, Version 2 (HadGEM2) from CMIP5: Completed simulation period for 1950-2100 for a North American CORDEX domain at 50 km grid spacing.
- MPI-ECHAM6 from CMIP5: Completed simulation period for 1950-2100 for a North American CORDEX at 50 km grid spacing. These forcing data were obtained directly from Dr. Susanne Grossman-Clarke at the Potsdam Institute for Climate Research during a summer research visit by Dr. Thang Luong.

Initial soil moisture within these simulations is specified according to the monthly soil moisture climatology of North American Regional Reanalysis (NARR, Mesinger et al. 2006), as it uses the same land surface model as WRF. All model simulations model simulations utilize an approximately one-year spin-up period. Global climate model data and the atmospheric reanalysis do not explicitly represent the sea surface temperatures within the Gulf of California, as this feature cannot be spatially resolved in a global climate model. Therefore, if WRF-interpolated sea surface temperatures in the Gulf of California are substantially colder than observations in the summer, sea surface temperatures within the regional model domain are bias corrected according to a 30-year optimally interpolated satellite-derived sea surface temperature product. Implementation of this bias correction substantially improved the climatological representation of monsoon precipitation, especially west of the Mogollon Rim in Arizona (not shown). The sensitivity of monsoon precipitation to sea surface temperature specification in the Gulf of California in regional atmospheric model simulations has been previously demonstrated by Ivanova and Mitchell (2003).

2. In-situ and remotely sensed observational data

To develop the methodological approach for severe weather event identification and simulation, the approximate time period of 1990-present is considered, when the following observational data are available. Web sources for these data are footnoted.

- Twice daily radiosonde data from the U.S. National Weather Service (NWS)[4]
- Historical daily precipitation from the Climate Prediction Center (CPC) united gauge-based dataset, at 0.25 degree resolution (Higgins et al. 1996)[5]. Available daily from 1948-present.
- NCEP/Environmental Modeling Center (EMC) Stage IV product[6]: Integrates NEXRAD radar with surface gauge observations at 4 km resolution (Zhang et al. 2011). Available hourly from 2002-present.
- Daily and hourly in-situ precipitation gauge data from coop stations within the Southwest[7], for those stations with sufficiently long enough records extending back to the decade of the 1950s.
- Daily gridded precipitation data from the period 1949-2010 at one-eighth degree resolution over the conterminous United States, available from Dr. Ed Maurer at the University of California, Santa Clara and originally produced at the University of Washington (Maurer et al. 2002)[8]
- Daily gridded precipitation data from the period 1915-2011 at one-sixteenth degree resolution over the conterminous United States, available from Dr. Benjamin Livneh through the NOAA ESRL (Liveneh et al. 2013)[9]. These data are essentially an updated version of the prior Maurer data mentioned in the previous bullet point.

3. Additional reanalysis or regional climate model data

In addition to the above sources of directed observed data, the following data are used as points of reference to compare with baseline sources of dynamically downscaled information:

- NARR (Mesinger 2006)[10]: generated using the NCEP Eta model combined with assimilated surface and upper air data using the Regional Data Assimilation System (RDAS) to generate a reanalysis product at 32 km grid spacing and 45 vertical levels. Available 3 hourly from 1979-present.
- Regional models from NARCCAP (Mearns et al. 2012)[11]: Employs multiple regional models to dynamically downscale select CMIP3 global climate models for the A2

[4] Can be obtained from the National Climate Data Center (http://www.ncdc.noaa.gov)
[5] Can be obtained from NOAA Earth System Laboratory (http://www.cdc.noaa.gov)
[6] Obtained from the NOAA Earth System Laboratory (http://www.cdc.noaa.gov) and NOAA Climate Prediction Center (http://www.cpc.noaa.gov), digital data set DSI-3240.
[7] Obtained from National Climate Data Center (http://www.ncdc.noaa.gov).
[8] Obtained from website of Dr. Ed Maurer, University of California, Santa Clara (http://www.engr.scu.edu/~emaurer/data.shtml)
[9] Obtained from NOAA Earth System Laboratory (http://www.esrl.noaa.gov)
[10] Available from NOAA Earth System Laboratory (http://www.esrl.noaa.gov).
[11] Available from NARCCAP website (http://www.narccap.ucar.edu)

emission scenario at 50 km grid spacing, for a historical period (1971-2000) and climate change projection period (2041-2070).

- Two dynamical downscaling model experiments from the companion SERDP project RC-2242. Dr. Rao Kotamarthi of Argonne National Laboratory is the Principal Investigator on this project. Somewhat similar in principle to the NARCCAP data, the Argonne SERDP experiments dynamically downscale a series of CMIP5 models for various greenhouse gas emission scenarios, with the Weather Research and Forecasting model at 12 km grid spacing ten year simulations of historical and future climate. In this project, we consider only two regional climate model simulations that dynamically downscale the Community Climate System Model (CCSM) for their designated historical period (1995-2004). One of these simulations uses CCSM original global climate model data directly as boundary forcing to the regional model. The other modifies the CCSM boundary forcing data to the regional model, bias correcting these data according to the climatological behavior of an atmospheric reanalysis. Additional technical details on these simulations, including the procedures for bias correction of CCSM data, can be found in Wang and Kotamarthi (2015). The downscaled CCSM experiments are used within this project only to assess the impact of the specification of lateral boundary conditions, with and without a bias correction. These data were provided to the project directly by Drs. Rao Kotamarthi and Jiali Wang, from Argonne National Laboratory.

B. TECHNICAL APPROACH

A standardized methodological protocol is necessary to identify extreme weather events in the baseline RCM simulations that dynamically downscale both the historical reanalysis and CMIP3 and CMIP5 data. This is a two-step process that first considers the thermodynamic forcing and then the dynamic forcing criteria. Then identified thermodynamically favorable severe weather event days are simulated using a convective-permitting regional model.

1. Thermodynamic criteria to select severe weather events

a) Conceptual background

Favorable thermodynamic conditions are a necessary requirement for development of any monsoon thunderstorms. Rising air occurs during the day over mountain ranges, due to the differential heating of the mountains relative to the sounding air. In a conditionally unstable atmosphere, water vapor in this rising air may condense to form cumuliform clouds. The release of latent heat due to condensation may cause the air to be warmer than its surrounding environment, in which case deep convective, or cumulonimbus (thunderhead), clouds develop.

Typically, the cumulonimbus clouds during the monsoon extend the entire depth of the troposphere. These air-mass type thunderstorms begin to develop over mountain ranges in late morning to early afternoon and produce precipitation by late afternoon. In the absence of any additional dynamic forcing, the thunderstorms remain confined over the mountain ranges and quickly dissipate after generating precipitation.

b) Convective Available Potential Energy

Convective available potential energy (CAPE) is the first-order factor in forecasting NAM thunderstorms and has a clear relationship with precipitation occurrence (Adams and Souza 2009). CAPE is the positive buoyant energy of a given parcel of air, integrated vertically through the atmosphere (Moncrieff and Miller 1976). Methodological considerations in the calculation of CAPE include: level of parcel initiation, thermodynamic path (reversible or pseudoadiabatic), virtual temperature effects, inclusion of latent heat of fusion, and water loading (Doswell and Rasmussen 1994; Emanuel 1994; Adams and Souza 2009). The study of Adams and Souza (2009) provides a detailed methodological approach for CAPE computation during the NAM and is applied to Tucson radiosonde data in this project. They demonstrated that the largest possible CAPE values for a given monsoon day is most highly correlated with widespread precipitation events across south-central Arizona. There are two general considerations for computation of CAPE that account for the uniqueness of the NAM. The first is the timing of convection. The 00 Universal Coordinated Time (UTC) (5pm Local Standard Time, LST) sounding may be unrepresentative of synoptic-scale characteristics, as prior or simultaneous convective events can contaminate these soundings, particularly the near-surface temperature characteristics. Using this reasoning, the morning soundings 12 UTC (5 am LST) are most likely to be uncontaminated by any convective precipitation. The morning sounding is then modified for appropriate afternoon maximum temperature and boundary layer moisture, for a well-mixed layer, in order to calculate a more representative CAPE.

To compute CAPE, the average of the mixing ratio in the lowest 50-mb layer of the sounding and the warmest daily surface temperature are utilized. Likewise, parcel ascent is assumed pseudoadiabatic. This calculation yields the most unstable CAPE (MUCAPE).

WRF-RCM data also provide a MUCAPE parameter derived at 3-hourly intervals, which is considered in the late morning or early afternoon hours, for all the long-term sources of WRF-generated regional atmospheric model data. This parameter is calculated as:

$$MUCAPE = \int_{z_{LFC}}^{z_{EL}} g \frac{T_{v,p} - T_{v,e}}{T_{v,e}} dz \qquad (1)$$

in which z_{EL} is the height of the equilibrium level, z_{LFC} is the height of the level of free convection, g is the gravitational constant, $T_{v,p}$ is the vitual temperature profile of an ascending

air parcel, $T_{v,e}$ is the virtual temperature profile of the environment. Per NWS guidance, a CAPE threshold for severe thunderstorms during the monsoon in Arizona is in the range of greater than 500-1000 J kg^{-1}.

c) Precipitable Water

Severe weather has been directly linked to increases in low-level moisture from the surface to 700-mb during the NAM (Maddox et al. 1995; Wall et al. 2012). The absence of this low-level moisture can stifle convection and inhibit precipitation (Adams and Souza 2009). Low-level moisture is accounted indirectly in the calculation of CAPE, but CAPE fails to depict accurately the overall influence of moisture in convective events (e.g., precipitation efficiency or downdraft strength). To account for atmospheric moisture content, we consider precipitable water vapor (PW) as an additional thermodynamic parameter to CAPE. In monsoonal regions and, in tropical continental regions in general, precipitable water (PW) provides a consistent positive correlation with precipitation (Bretherton et al. 2004; Neelin et al. 2009; Janiga and Thorncroft 2014) along with the onset and demise of the monsoon (Lu et al. 2009). PW and its temporal evolution have also been shown to have a strong positive relationship with precipitation in Arizona during the NAM, both observationally (Kursinski et al. 2008a; Serra et al. 2016) and in sensitivity experiments within a regional atmospheric model, specifically WRF (Kursinski et al. 2008b). PW has been employed in the forecasting of monsoon thunderstorms by both research scientists and operational meteorologists at the National Weather Service (Lu et al. 2009). The exact thresholds relating to severe weather development have not been specifically defined in the literature, permitting some necessary geographic subjectivity among operational forecasters. The value of PW associated with organized convection generally is above 25 mm (i.e. approximately one inch) in Tucson, Arizona, per the operational practice of the NWS Office there. This PW threshold criterion generally applies throughout the Southwest. Within the WRF model, PW is computed from the six-hourly water vapor mixing ratio (q_v) measurements at standard pressure levels (p) as:

$$PW = \int_{z_0}^{z} q_v \rho dz = -\frac{1}{g} \int_{z_0}^{z} q_v dp \qquad (2)$$

where z_o is the lowest modeling layer, z highest modeling layer and g is the gravitational constant.

d) Downdraft convective available potential energy

Another thermodynamic variable considered in the context of extreme monsoon weather is downdraft velocity, measured by the metric of downdraft convective available potential energy (DCAPE). There are two reasons why DCAPE is of interest in reference to simulation of monsoon thunderstorms. First, downdraft outflows help to maintain existing and trigger new convection via cold pool dynamics. Convective downdrafts hitting the surface can provide a lifting mechanism to trigger new convection (e.g. Lahmers et al. 2016). Second, wind gusts from downdraft outflows are associated with the severe weather hazards of microbursts and dust storms (haboobs). The operational UA-WRF model described earlier has been demonstrated to successfully simulate these types of events, for example the Phoenix haboob event of 5 July 2011 (Raman et al. 2014). DCAPE is used estimate downdraft intensity or low-level outflow strength, consistent with NWS operational practice. DCAPE is the accumulated buoyant energy from the parcel's starting point to the ground.

$$DCAPE = -g \int_{z_{sfc}}^{z_{start}} \frac{\theta(z) - \bar{\theta}(z)}{\bar{\theta}(z)} dz \qquad (3)$$

The maximum theoretical downdraft velocity w_{max} is used to represent maximum wind gust potential as calculated by

$$w_{max} = \sqrt{2\ DCAPE} \qquad (4)$$

d) Thermodynamically favorable severe weather event days

The days during the NAM with relatively high MUCAPE and PW values, as determined by a joint frequency distribution analysis, are regarded as most thermodynamically favorable for the occurrence of monsoon thunderstorms and are henceforth referred to as monsoon severe weather event days. Specifically, these are the days when both MUCAPE and PW are in the top 20% of the climatological distribution over a given period of record during the period June-September. Thermodynamically favorable severe weather event days were first considered for the period 1993-2010 using radiosonde sounding data from Tucson, Arizona, to demonstrate the robustness of the severe weather event selection methodology purely in the context of observational data. To ensure a better representation of severe weather event days of the entire monsoon region, it was necessary to develop a more regionally applicable selection criterion for the days that could be applied to gridded regional climate model data. Seven additional operational NWS radiosonde sites were used to formulate the final list of thermodynamically favorable days in all sources of baseline dynamically downscaled data. The sites included Tucson, Phoenix, El Paso, Albuquerque, Flagstaff, Las Vegas, and San Diego, as shown in *Fig. 1*. Considering each of these sites, daily maximums of MUCAPE and PW were determined for each day during the monsoon season (JJAS) for all the years in a given source of downscaled data. Individual

empirical orthogonal function (EOF) analyses (e.g. Wilks 2006) were performed on the station-time matrices of MUCAPE and PW, to determine the dominant modes of spatial coherency. The normalized principal components of the dominant modes were then regressed and correlated with gridded model data to illustrate the associated spatial patterns. If thermodynamic conditions at Tucson are generally representative of the Southwest as a whole, we would expect a priori to have relative high positive values of correlation throughout the entire Southwest in the spatial pattern maps. Moreover, when considered over a long-term record, these modes can be also used to assess the long-term changes in the thermodynamic parameters.

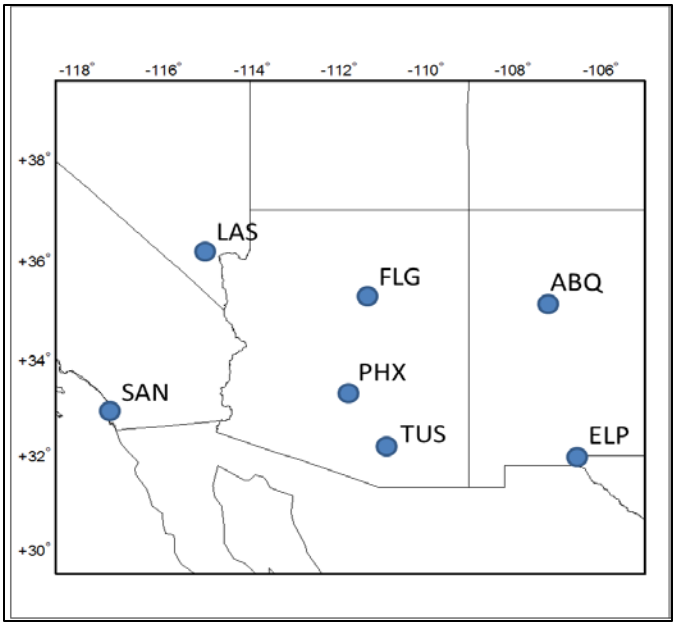

Figure 1: Locations of NWS sounding sites in the Southwest U.S. that are used in formulating final list of severe weather event days in all sources of long-term dynamically downscaled WRF model data.

2. Dynamic criteria associated with severe weather events

a) Conceptual background

- Monsoon thunderstorms that initiate over high terrain may grow and organize only if the dynamic environment is favorable. Generally speaking, strong thunderstorms in a mid-latitude environment require: 1) vertical wind shear, to sustain the updraft of warm, moist air into the thunderstorms, 2) Strong upper-level winds to provide steering and a means of outflow at the top of cumulonimbus clouds (in the anvil region), and 3) moisture

transport near the surface, for example from a low-level jet. Specifically for the NAM, severe thunderstorms are most favored when all following dynamic criteria are satisfied:

- Upper-level ridge of high pressure (or monsoon ridge) is positioned to the north of Arizona and New Mexico. Northeasterly or easterly flow around the monsoon ridge in this position facilitates the movement of thunderstorms westward off the mountain ranges. Favorable configurations of the monsoon ridge for severe weather were subjectively identified by Maddox et al. (1995) and the first two of these modes are shown in *Fig. 2*
- An upper-level disturbance, such as a transient inverted trough (e.g. Bieda et al. 2009; Douglas and Englehart 2007; Pytlak et al. 2005), is located in the vicinity of the Southwest U.S. Upper-level disturbances typically travel westward along the southern side of the monsoon ridge when the monsoon ridge is in a favorable severe weather configuration. Thunderstorm growth is promoted by the presence of large-scale upward vertical motion and/or vertical wind shear (Finch and Johnson 2010). *Fig. 3* provides a characteristic illustration of a transient inverted trough. Operationally, inverted troughs are tracked using potential vorticity at the 250-mb surface.
- There is a low-level surge of moisture from the Gulf of California, or Gulf surge, that provides low-level moisture into the Colorado River Valley and low desert areas of Southwest Arizona (e.g. Higgins and Shi 2005; Zehnder 2004; Mo and Berbery 2004; Douglas 1995). Strong gulf surges are almost always associated with the passage of a tropical disturbance (easterly wave, tropical cyclone) near the southern end of the Gulf of California.
- If all of the above conditions are satisfied, monsoon thunderstorms may grow and organize into propagating MCSs, that generally move in a westward direction off the mountain ranges toward the urban areas (Tucson and Phoenix) and low deserts of southwest Arizona and the Colorado River Valley, for example as illustrated in radar data by Nesbitt et al. (2008) and Lang et al. (2007). MCSs have characteristic leading convective lines of heavy precipitation followed by a longer period of lighter and steadier precipitation. The most long-lived MCSs in Arizona, for example, will typically reach the Colorado River Valley by late evening or the early morning hours. A schematic of this process is shown in *Fig. 4*.

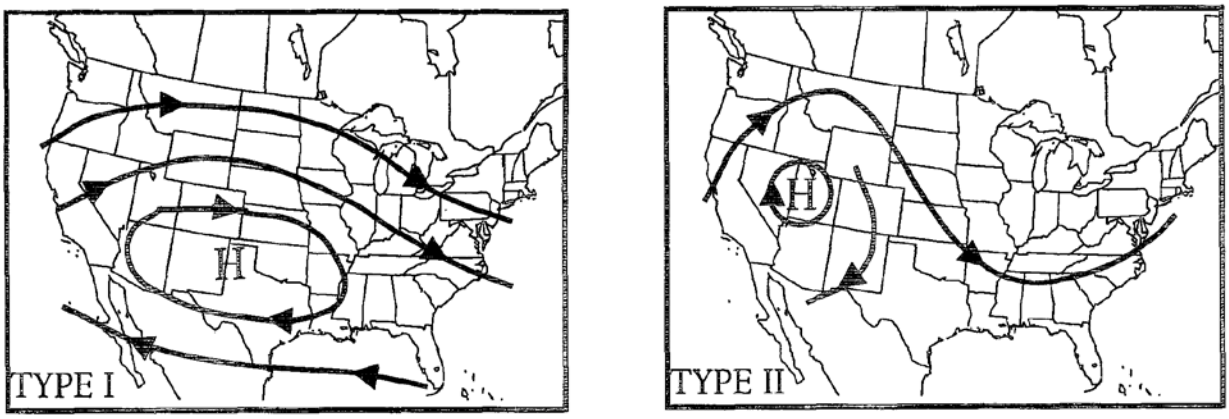

Figure 2: Streamlines and corresponding monsoon ridge positions for the first two subjectively identified severe monsoon weather patterns in Arizona, as identified by Maddox et al. (1995).

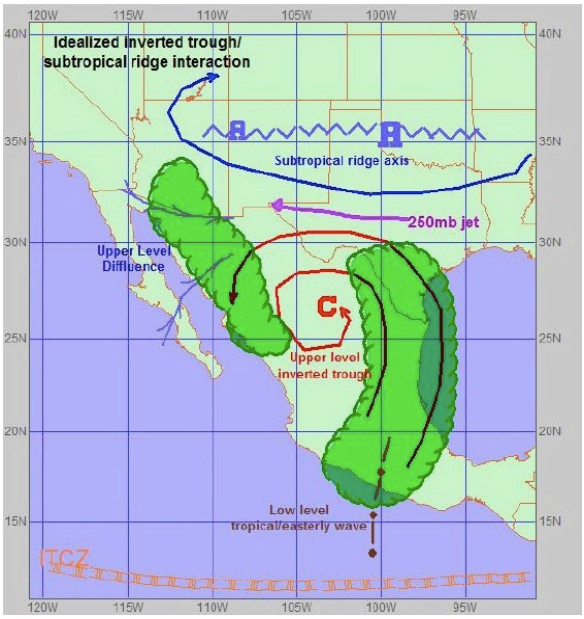

Figure 3: Idealized illustration of an inverted trough and its meteorological effects in the North American monsoon region. Adapted from Pytlak et al. (2005)

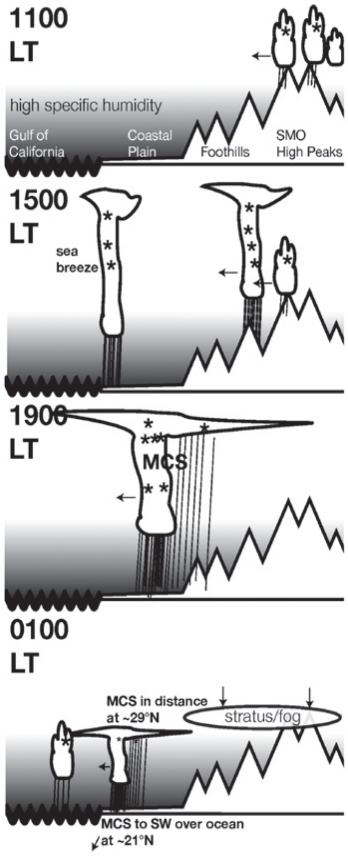

<u>Figure 4:</u> Idealized diurnal evolution of monsoon thunderstorms in northern Mexico during a convectively active day. Geographic points of reference as indicated. From Nesbitt et al. (2008).

<u>b) Monsoon ridge positioning</u>

The thermodynamically favorable monsoon severe weather event days are analyzed with respect to synoptic-scale atmospheric circulation forcing patterns in NARR and baseline sources of dynamically downscaled data. The daily 500-mb geopotential height is the proxy for monsoon ridge positioning and strength. The presence of favorable vertical wind shear for convective organization is generally implicit for monsoon ridge configurations for severe weather days in Arizona, as demonstrated by Maddox et al. (1995). The 500mb geopotential height (GH) fields of the thermodynamically favorable severe weather event days are objectively analyzed using EOF analysis (e.g. Wilks 2006). This analysis produces maps of 500-mb height patterns that specifically correspond to objectively determine dominant severe weather modes, directly comparable to the prior, subjectively determined results of Maddox et al. (1995).

c) Inverted trough tracking and track density

Inverted troughs (IVs) are tracked as normalized potential vorticity (PV) anomalies at 250-hPa from the baseline sources of dynamically downscaled data, consistent with NWS practice. For a given period of analysis years, a PV climatology is constructed for a 10-day running mean and standard deviation of PV at every grid point. Considering the PV climatology, normalized PV anomalies for specific days are computed as a Z-score. Since IVs are in tropical regions and are associated with lower PV values compared to that of a mid latitude cyclone, they would be washed out and nearly impossible to track without this normalization. An individual IV feature is tracked as a relative maximum normalized PV anomaly on the 250 hPa pressure surface. Optimization of the track locations is used to ensure accurate output, per the tracking algorithm of Hodges (1999). Each PV anomaly is assumed to contain at least 8 pixels (~ 1.15 Square Decimal Degrees) with values that exceed 2 standard deviations, to be counted by the tracking algorithm. A definable IV feature is: assumed to move at 3 m s^{-1}, last at least 21 hours (8 time steps in the 3-hour temporal resolution reanalysis product), and move from east to west along the southern side of the monsoon ridge. Eastward moving features, with a southerly component greater than the westerly component are also considered, to capture features that recurve around the NAM ridge to the west. Only definable IV features within the Southwest and northwest Mexico are considered. IV features are tracked for each season through the following time intervals: 4 June to 6 July, 19 June to 21 July, 4 July to 5 August, 19 July to 20 August, 3 August to 4 September, and 18 August to 19 September. These periods of analysis are nearly equivalent to the manual analysis of IV track density performed by Bieda et al. (2009). Track density is computed with a kernel smoothing technique described by Hodges (1996) and is based on the point density of tracks at the same time steps of the model time. Individual days in which an IV occurred in the Southwest U.S. can also be objectively identified as "trough days". Days without an IV feature are identified as "no-trough days". An example of IV tracks for a sample period is shown in *Fig. 5*.

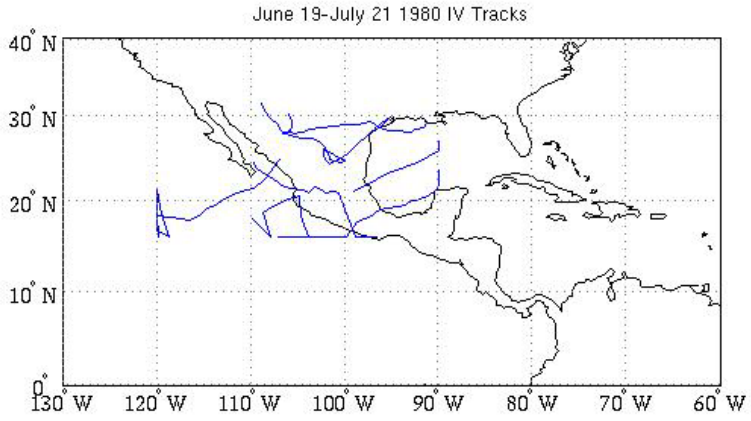

Figure 5: Example of IV tracks computed with the vortex tracking code. Period considered here is 19 June to 21 July, 1980.

d) Gulf of California moisture surges

Gulf surge events are objectively identified, per NWS practice, using Global Historical Climate Network (GHCN) hourly- observed surface data recorded at Yuma Marine Core Air Station (MCAS) (located approximately 32°N, 114°W) and the corresponding area within the sources of baseline dynamically downscaled data and NARR data. Yuma is a location in the United States that has a clear, demonstrable gulf surge signature in surface meteorological data (e.g. Douglas 1995). The NWS-based surge identification method considers a surge event as having occurred when the average daily (at least 24 consecutive hours) dew point temperature is greater than or equal to 18° C and the surface wind direction originates directly from the Gulf of California, between 160 and 180 degrees. The first time when these criteria are met marks the beginning of a surge event onset day, and it is recorded regardless of what time the event occurs during that day. NWS criteria are relaxed slightly in identifying gulf surges here: the dew point temperature exceeds 18°C for at least 24 consecutive hours (6 hours in dynamically downscaled data); and the average surface wind direction for the duration of the event lies between 140 and 200 degrees. A gulf surge event starts when the first of dew point values exceeding 18°C is noted and ends when the last of 24-consecutive dew point values exceeded 18°C is noted, provided the average wind direction criteria are also satisfied over that same period.

3. Convective-permitting simulations of severe weather events

Objectively identified severe weather event days in all baseline sources of dynamically downscaled data during select twenty-year periods are simulated using convective-permitting grid spacing with the WRF model. The WRF model experimental design for simulation of severe weather event days uses a two-domain nesting strategy as shown in *Fig. 6*, with an intermediate domain of 10 km grid spacing, and a convective-permitting domain of 2.5 km grid spacing. The course resolution domain is essentially the equivalent long-term WRF downscaled NCEP-NCAR reanalysis or CMIP3 and CMIP5 models. The intermediate domain covers the southwest United States and northwest Mexico. The convective-permitting domain encompasses all U.S. military facilities of interest in the Southwest within the scope of the project, and it covers all of Arizona and New Mexico and portions of Colorado, Utah, Nevada, and California. One-way nesting is employed, so that there is no exchange of information from the fine grid to the intermediate grid. WRF model parameterization options on the convective-permitting domain are nominally similar to what is used for generating real-time WRF quasi-operational monsoon forecasts at UA, but with two notable differences with respect to land surface modeling and convective parameterization. Common parameterization options include: a bulk microphysics scheme (Thompson et al. 2004); Mellor-Yamada-Janjic planetary boundary layer scheme (Janjic 1990, 1996, 2002) with Eta surface layer (Janjic 1996, 2002); the NOAH-MP land surface model (Niu et al. 2011); Dudhia Shortwave radiation (Dudhia 1989); and the

Rapid Radiative Transfer Model (RRTM) Longwave radiation (Mlawer et al. 1997). On the intermediate domain, the Kain-Fritsch cumulus parameterization scheme is applied (Kain and Fritsch 1993, Kain 2004), with the modified convective trigger and CAPE closure assumption of Truong et al. (2009) that better accounts for dynamic pressure effects in complex terrain. An Urban Canopy Model (UCM), with optimized anthropogenic parameters for the southwestern United States as adapted from Grossman-Clarke (2010), is applied at grid points with a defined urban land use classification, including the cities of Tucson, Phoenix, Albuquerque and Las Vegas. Note that there are some differences in model parameterization options in the convective-permitting simulations from the baseline dynamically downscaled data, which were implemented to best represent organized, propagating convection in Arizona

For a given identified severe weather event, that satisfies the thermodynamic threshold criteria as previously described, the convective-permitting model WRF simulation (henceforth referred to as CPM-simulated) is performed as follows in a numerical weather prediction-type mode. The event simulation is initialized at 6 UTC (11 pm MST) the day prior to the event and the simulation is executed for thirty hours, ending at 12 UTC (5 am MST) the day following the event. The initialization in the evening prior allows for 6 hours of model spin-up time, consistent with UA operational forecast practices. Model output from the convective-permitting grid is saved hourly, as this temporal resolution resolves well the diurnal cycle of convection. It also permits an evaluation of extreme precipitation on an hourly basis within the convective cores of thunderstorms and wind gusts in thunderstorm outflow boundaries.

One additional suite of convective-permitting regional model severe weather event simulations was performed within this project, that dynamically downscales the WRF-CCSM 12 km simulation data available from Argonne National Laboratory from SERDP project RC-2242. This particular simulation suite only utilizes the WRF-CCSM simulation using the original CCSM boundary forcing. Owing to technical challenges in dynamically downscaling the bias corrected WRF-CCSM simulation, equivalent convective-permitting simulations were unable to be performed within the timeframe of this project.

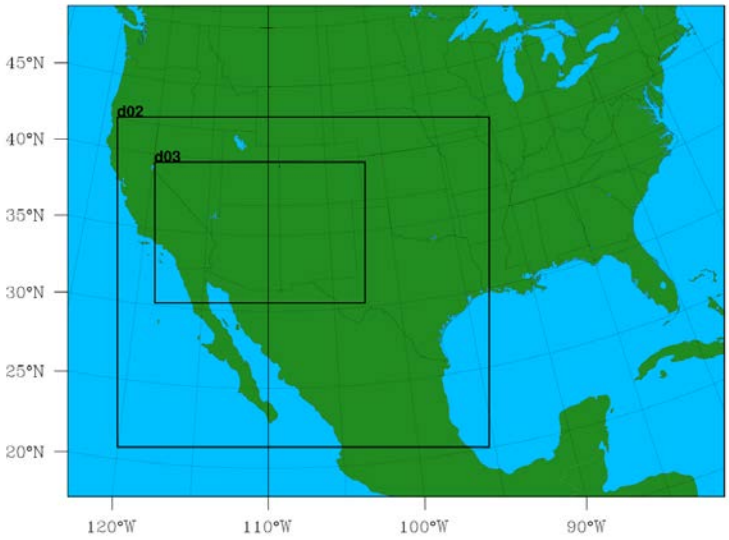

Figure 6: WRF model simulation domain for NWP-type simulations of identified severe weather event days. Grid spacings on the three domains shown (in km) are 35, 10, and 2.5.

4. Statistical analysis methods to characterize distributions and trends

The representation of the likelihood of receiving a specific quantity, for example precipitation amount, is best accomplished by fitting a theoretical probability density function (PDF). The advantage to a theoretical PDF is that it is a continuous function with no discontinuity that can be determined for every local grid point on the map. These distributions make it possible to estimate the likelihood of rainfall being within a specified range. The gamma distribution typically yields a good PDF fit of a total precipitation distribution. However, extreme precipitation values in the right tail of the distribution typically do not fit well to the theoretical PDF of the entire data set.

To account for precipitation extremes, a generalized Pareto distribution, a peak-over-threshold (POT) method, is utilized to better describe the behavior in the tail (e.g. Katz 2010; Dominguez et al. 2012; Rivera et al. 2014). This methodology is useful when dealing with a limited number of time slices (on the order of 200). It allows for a larger sample size than the generalized extreme value (GEV) approach. A Poisson distribution is used to characterize the extreme precipitation rate at which the threshold is exceeded and a Generalized Pareto (GP) distribution is used to characterize the amount at which the threshold is exceeded (termed "Poisson–GP model"). For the distribution of excesses above a high threshold, the cumulative distribution and quantile functions for the GP are given by:

$$F(x;\sigma^*,\gamma) = 1 - \left[1+\gamma\left(\frac{x}{\sigma^*}\right)\right]^{-\frac{1}{\gamma}}, \qquad \sigma^* > 0;\ 1+\gamma\left(\frac{x}{\sigma^*}\right) > 0 \qquad (5)$$

$$F^{-1}(1-p;\sigma^*,\gamma) = \frac{\sigma^*}{\gamma}(p^{-\gamma}-1), \qquad 0 < p < 1 \qquad (6)$$

Here σ^* and γ are the scale and shape parameters, respectively. We set the threshold for the POT distribution to the 90th percentile. The tails of the distribution with an intensification of events above this threshold is what is of interest.

Once the parameters are estimated, their accuracy in approximating the true rainfall distribution is evaluated. This study tests the goodness-of-fit using a χ^2 test that compares the histogram and the discrete density function. In this statistical test, the null hypothesis is that the data are consistent with the specified distribution. The test statistic random variable χ^2 is defined by the following equation.

$$\chi^2 = \sum_{classes} (O_i - E_i)^2 / E_i \qquad (7)$$

where O_i is the observed frequency count for the i^{th} level of the categorical variable, and E_i is the expected frequency count for the i^{th} level of the categorical variable. The local statistical significance (for each grid box) of the estimated daily precipitation above the 90th percentile is determined by a bootstrap resampling procedure using a total of 1000 samples. The future changes in the return values are considered statistically significant at the 0.1 (90th percentile) level if their 90% confidence intervals do not overlap (Kharin and Zwiers 2005).

5. Intensity, duration analyses for variables of interest at the DoD facility scale

An effective way to translate high-resolution model information for decision making is through intensity, duration analyses of model-simulated variables such as precipitation, as originally described by Kendon et al. (2014). The methodological approach for these analyses is summarized in the top portion of *Fig. 7*. For a given geographic area, a joint probability density function (PDF) is generated as a two-dimensional plot that expresses intensity (y-axis) versus spell duration (x-axis) using model-simulated information over a designated period. The "designated period'' in the context of this project is the WRF-simulated severe weather event days with convective-permitting modeling, given a particular applied boundary forcing (e.g. reanalysis, CMIP3, CMIP5 models). The spell duration metric is defined as the time length of the event, and the intensity is defined as the peak intensity within the spell duration. This type of analysis can be applied to any variable of interest. Of greatest interest for DoD, per operational watch and warning criteria of the 25th OWS, are the variables of precipitation and wind speed (computed from DCAPE).

The difference in the joint PDF between a particular past and a future period can be computed. As shown in the first application of the intensity, duration analysis by Kendon et al. (2014), the significant changes in the joint PDF can be highlighted (*Fig. 7*). Statistical significance may be assessed using a Monte Carlo method, such as bootstrapping or permutation. In the example

shown in the bottom portion of *Fig. 7*, future projected changes of precipitation intensity and duration are considered for the southern United Kingdom (UK) during the warm season (June-August). The plot on the left is from the coarser resolution 12 km model and the plot on the right is from the convective-permitting 1.5 km model. Note that the convective permitting model simulations in this case project the most significant precipitation changes for the relatively high intensity, short-duration events (greater than 2 mm hr^{-1}, less than five hours long). These types of diagrams may be constructed for any DoD facility of interest within the convective-permitting modeling domain, in a manner that is directly relatable to weather watch and warning criteria.

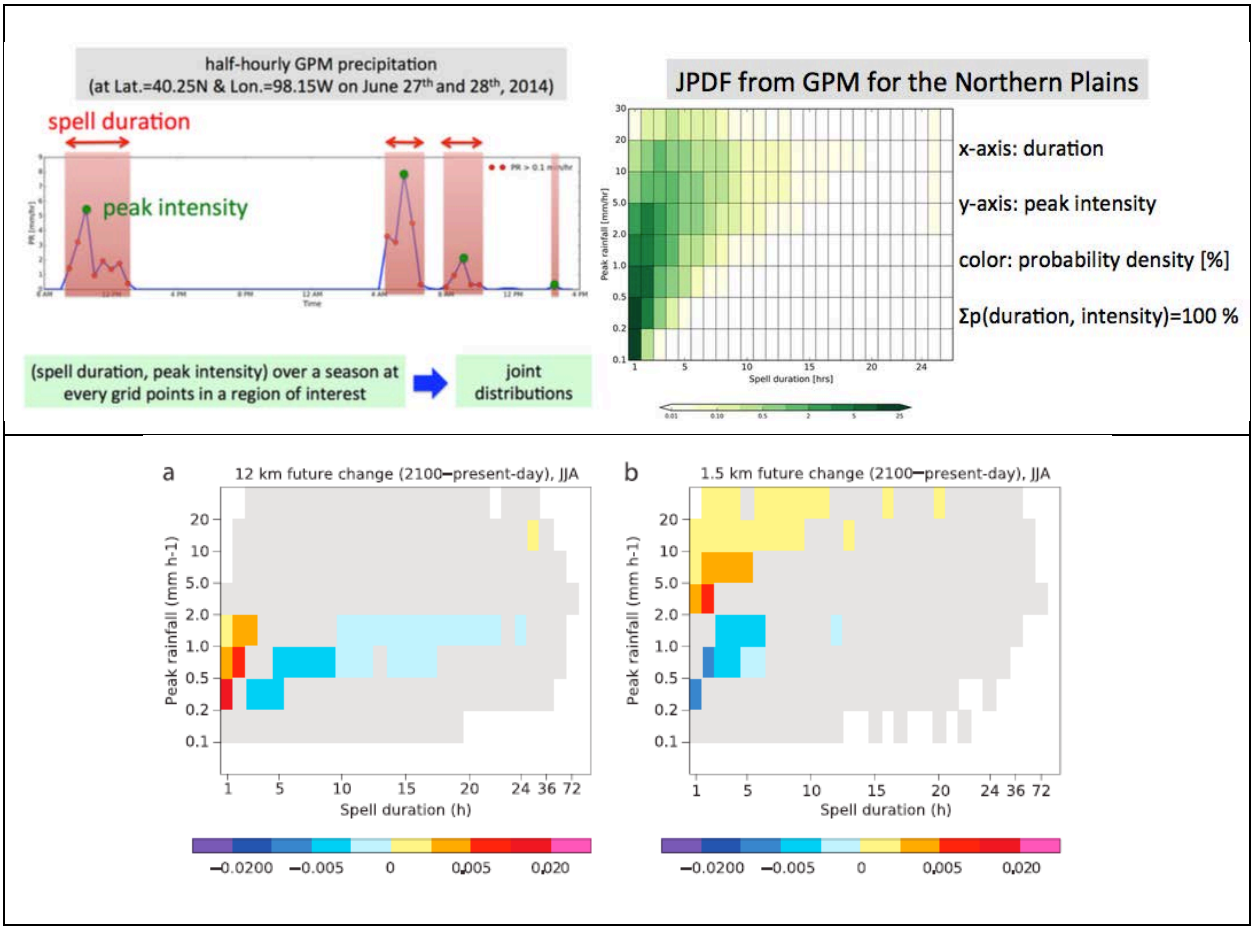

Figure 7: Top: Summary of methodological approach of producing joint PDFs of rainfall duration and intensity (Courtesy of Huikyo Lee, NASA Jet Propulsion Laboratory). Bottom: Simulated climatological difference in the joint distribution of wet spell duration and peak precipitation intensity for the southern UK and for June, July, and August (JJA) from (a) 12 km model and (b) a 1.5 km model. The differences are computed between periods 1996-2009 and 2087-2099. Gray shaded areas show no significant differences at the 1% level. (Kendon et al. 2014)

V. RESULTS AND DISCUSSION

A. COMPARISON OF DOWNSCALED CMIP DATA TO NARCCAP

Before any consideration of determining severe weather events for high resolution, convective-permitting simulations, it is necessary to verify that the baseline sources of dynamically downscaled CMIP data compare reasonably to counterpart NARCCAP data. This step ensures that downscaled CMIP data produced at UA-ATMO is falling within the range of a standard community product that has already undergone thorough vetting in the literature. *Fig. 8* shows the monthly precipitation climatology within the region of the Southwest U.S approximately corresponding to the finest (2.5 km) of the convective-resolving WRF simulations. *Fig. 9* shows the change in precipitation from the historical climate versus climate change period, for just the downscaled CMIP3 models. *Fig. 8* includes CPC-derived precipitation (during the period 1971-2000), several of the NARCCAP models, and all of the UA-ATMO downscaled CMIP models for their period of record as described in the Methods section. Note that the NARCCAP models that dynamically downscale the CMIP3 Geophysical Fluid Dynamics Laboratory (GFDL) model are excluded from *Fig. 8*, as these models tended to substantially overestimate monsoon precipitation, as recently reported in Bukovsky (2015). This overestimation in precipitation by NARCCAP models that downscale the GFDL model is quite clear in *Fig. 9*, where they are included. In comparison to NARCCAP models, the UA-ATMO downscaled CMIP models exhibit the following characteristics:

- UA-ATMO downscaled CMIP3 HadCM3 and MPI-ECHAM5 tend to simulate wetter than observed precipitation (on the order of 1 mm per day) and delay the peak in monsoon precipitation by about a month, with a maximum occurring in September instead of August.
- UA-ATMO downscaled CMIP3 HadCM3 and MPI tend to simulate the rapid increase in early monsoon precipitation either in a manner that is at least as good as or better than the counterpart NARCCAP models. About half of NARCCAP models do not simulate a seasonal maximum in monsoon precipitation in the Southwest.
- UA-ATMO downscaled CMIP5 HadGEM2 and MPI-ECHAM6 improve the timing of monsoon onset and correctly represent the seasonal maximum in monsoon precipitation in August. Downscaled CMIP5 MPI-ECHAM6 still has a wet bias similar to CMIP3 MPI-ECHAM5. Downscaled CMIP5 HadGEM2 has the closest climatological representation of monsoon precipitation, as compared to gauge-derived observations.
- Simulated monsoon precipitation in the UA-ATMO downscaled CMIP3 GCMs do not exceed the bounds of precipitation in the counterpart NARCCAP models.

For these reasons, UA-ATMO downscaled CMIP models were deemed to compare reasonably to the community-produced NARCCAP models, as part of the go/no go decision criteria for the interim report.

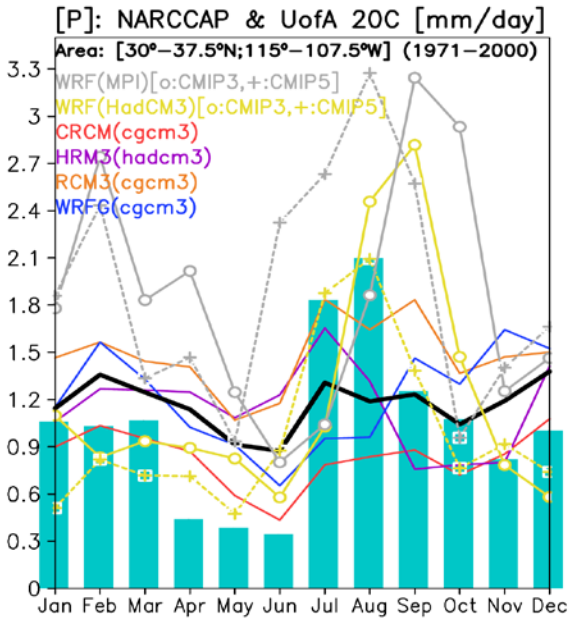

<u>Figure 8</u>: Climatological evolution of precipitation in the Southwest U.S. (mm day^{-1}), for CPC observed precipitation (bars), selected NARCCAP models and UA-ATMO downscaled CMIP models (colored lines as indicated). The average of the NARCCAP simulations is shown by the black line.

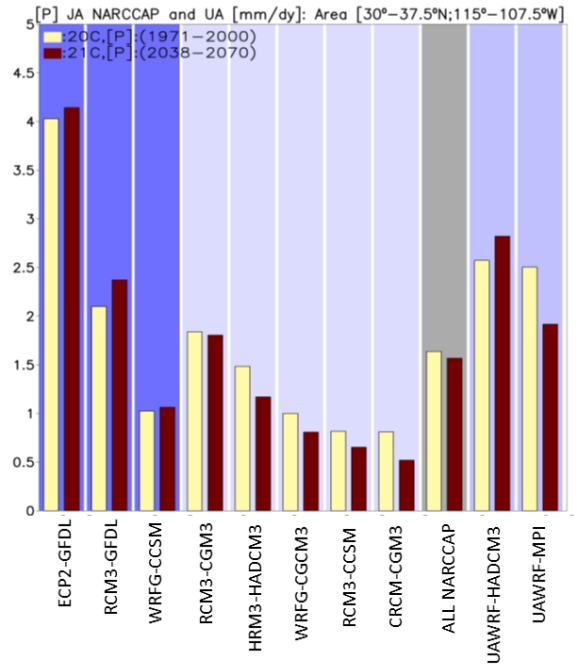

<u>Figure 9</u>: July-August precipitation (mm day^{-1}) during the period of historical climate versus climate change period of NARCCAP, considering all NARCCAP models and UA-ATMO downscaled CMIP3 models.

B. THERMODYNAMIC IDENTIFICATION OF SEVERE WEATHER EVENT DAYS

1. Identifying thermodynamically favorable severe weather event days for Tucson, Arizona

a) MUCAPE and PW distributions, scatterplots

Thermodynamically favorable monsoon severe weather event days were identified using MUCAPE and PW for the Tucson sounding during the period June through September (JJAS) for the years 1993-2010. The histograms of these distributions are shown respectively in *Fig. 10* and *Fig. 11*. We do not employ theoretical distribution fits to these data, as this is not really essential to our objective of determining the severe weather event threshold points. Nonetheless, there are some important distributional characteristics of these raw histograms that should be at least qualitatively described. The MUCAPE histogram is clearly positively exponentially distributed, due to a high frequency of MUCAPE values at or near zero. Such days with virtually no appreciable atmospheric instability occur either prior to the onset of the monsoon (mostly during the month of June) or during monsoon breaks. These are very hot, dry periods when the monsoon ridge is typically located directly over southern Arizona. According to the National Weather Service, a 500-mb geopotential height above 5950 m over Arizona in is indicative of a strong monsoon ridge. For days with some appreciable MUCAPE, exceeding 500 J kg^{-1}, there is a fairly uniform frequency of occurrence within the MUCAPE bins up to about the 70^{th} percentile, to about 3000 J kg^{-1}. Maximum MUCAPE in Tucson is in the range of 6000 J kg^{-1}. This type of extreme MUCAPE event occurs on the order of about 10 times during the 1993-2010 period, or roughly just one event in a given monsoon year. It should be emphasized that MUCAPE values from the modified morning soundings tend to be on the high end. Typically, boundary layer ventilation, which is not accounted for in Adams and Souza (2009) would tend to decrease near surface moisture during the course of the day, thereby reducing CAPE, all else being equal.

PW, as shown in *Fig. 11*, tends to be more normally distributed, albeit slightly negatively skewed. The 25 mm nominal operational forecast threshold for a convectively active monsoon day is roughly in the middle of the distribution. Even though Tucson is a semi-arid climate, on rare occasions PW values can exceed 50 mm, values that are reminiscent of a deep tropical environment such as the Amazon rainforest (Adams et al. 2013). Documented severe flooding events during the monsoon in Arizona, for example the Sabino Canyon flood in Tucson have values of PW on this order (Magirl et al. 2007; Griffiths et al. 2009)

A scatterplot of MUCAPE vs. PW for Tucson is shown in *Fig. 12*. The solid black line indicates the upper 70^{th} percentile threshold for both MUCAPE and PW. Days falling in to the category of the upper right quadrant (i.e. above the 70^{th} percentile in both MUCAPE and PW) are hence defined, in an objective way, as thermodynamically favorable severe weather event days. For the 1993-2010 period, 404 days met these criteria, where MUCAPE exceeds approximately 3000

J kg^{-1} and PW exceeds 45 mm. As expected, a strong relationship between CAPE and PW exists, their correlation coefficient being 0.86.

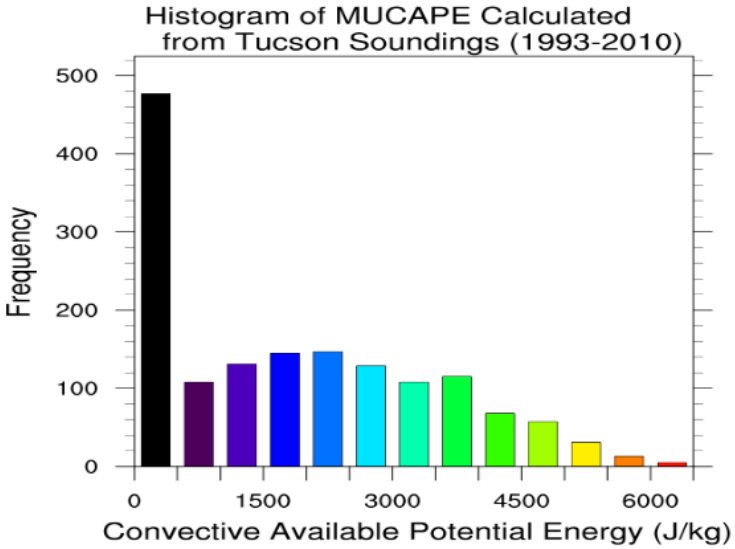

.

Figure 10: Histogram of derived MUCAPE (J kg^{-1}) values based on raw observational rawindsonde data during June, July, August, and September for Tucson, AZ (1993-2010).

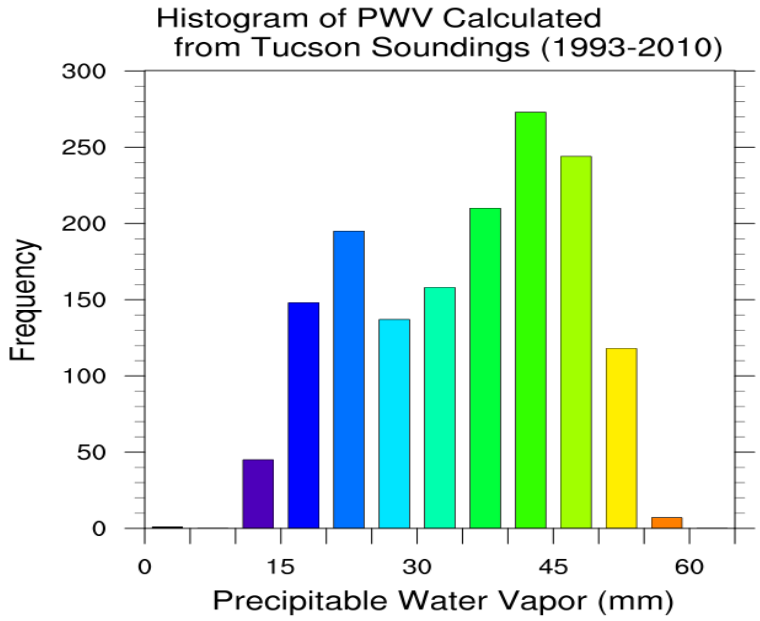

Figure 11: Histogram of integrated PW (mm) values based on raw observational rawindsonde data during June, July, August, and September for Tucson, AZ (1993-2010).

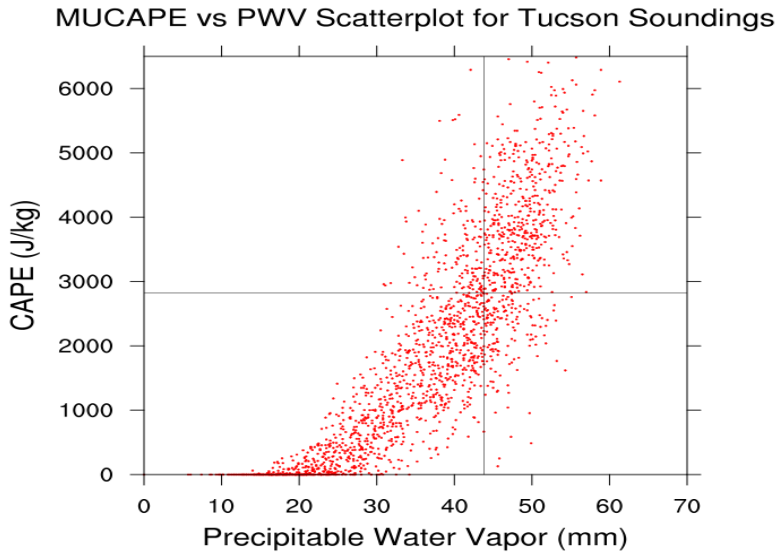

Figure 12: Scatter plot of CAPE (J kg^{-1}) versus PW (mm) in Tucson, Arizona, considering all days during the monsoon (JJAS), derived from original raw radiosonde upper-air sounding data (1993-2010). The 70% (horizontal and vertical lines) threshold levels for PW and CAPE, respectively, to select severe weather event days indicated.

b) Identified severe weather event days in comparison to storm reports

The identified severe weather event days were compared to NWS Storm Based warning verification data from the Iowa Mesonet (http://mesonet.agron.iatate.edu/cow/) for the period 2005-2010 for the region of southern Arizona, basically from the latitude of the city of Phoenix and points further south. These reports are based on NWS warnings and public reports of occurrences of severe weather phenomena, such as damaging winds, large hail, or flash flooding. Roughly 58% of the convective event days objectively identified using our methodology corresponded with reported severe weather phenomena between 2005 and 2010. While these reports provide an independent source of data to verify the effectiveness of the objective approach to classify severe monsoon weather, the reporting of severe weather is highly dependent on population density and participation of the general public. Areas with limited or no population in southern Arizona, mostly outside of the Tucson and Phoenix metropolitan areas, are generally under-accounted for in severe weather reporting. We suspect that at least some of the unaccounted for severe weather events may be associated with recurving East Pacific tropical cyclones. Though not explicitly investigated in the scope of this project, objective analysis techniques have been used in other studies to characterize tropical cyclone-related precipitation in the southwestern U.S. (e.g. Wood and Ritchie 2013). Though these types of events are associated with extreme, more widespread precipitation, the atmosphere is actually relatively stable, as compared to the more typical convectively active monsoon day with well-organized MCSs.

2. Analysis of MUCAPE and PW in baseline sources of WRF dynamically downscaled data

An identical analysis was performed on MUCAPE and PW derived from all baseline sources of WRF dynamically downscaled data. Sample scatter plots of MUCAPE and PW for the downscaled reanalysis are shown in *Fig. 13* for the period 2002-2010, within the record of the Stage IV product, with cumulative density function (CDF) thresholds as indicated on the figure. MUCAPE is generally higher as computed in the Tucson morning sounding-derived CAPE than WRF model-computed MUCAPE, for the reasons mentioned earlier. Maximum PW values are also lower in the WRF model, with the peak of the distribution occurring in the range of 30-35 mm. Similar scatter plots of MUCAPE versus PW for all sources of dynamically downscaled data are shown in *Fig. 13*. Characteristics common to all the scatter plots include: 1) a positive relationship of MUCAPE and PW and 2) a CDF threshold of 80% that exceeds 1000 J kg^{-1} for MUCAPE and 30 mm for PW that are above the operational thresholds for forecasting severe monsoon thunderstorms. As expected, there is variability in CAPE and PW among the downscaled CMIP models, with CMIP 5 MPI-ECHAM6 having the greatest amounts of atmospheric moisture and instability. When considering thermodynamically favorable severe weather days with an 80% CDF threshold in the WRF downscaled reanalysis during the period, the correspondence of those days with severe weather reports in the Tucson Weather Service forecast area nearly 70%, similar to what is obtained using observational 12 UTC Tucson sounding data.

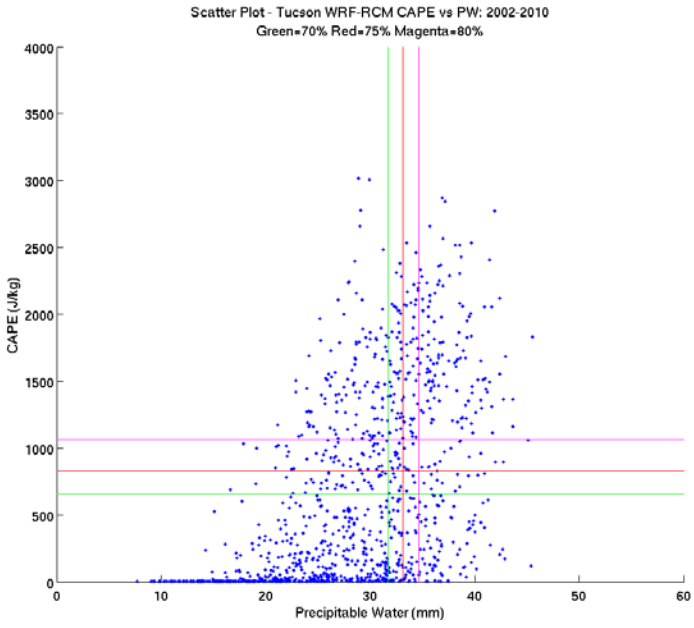

<u>Figure 13:</u> Scatter plot of CAPE (J kg^{-1}) versus PW (mm) area-averaged around Tucson, Arizona, considering all days during the monsoon period (JJAS) from 2002-2010, derived from the dynamically downscaled reanalysis.

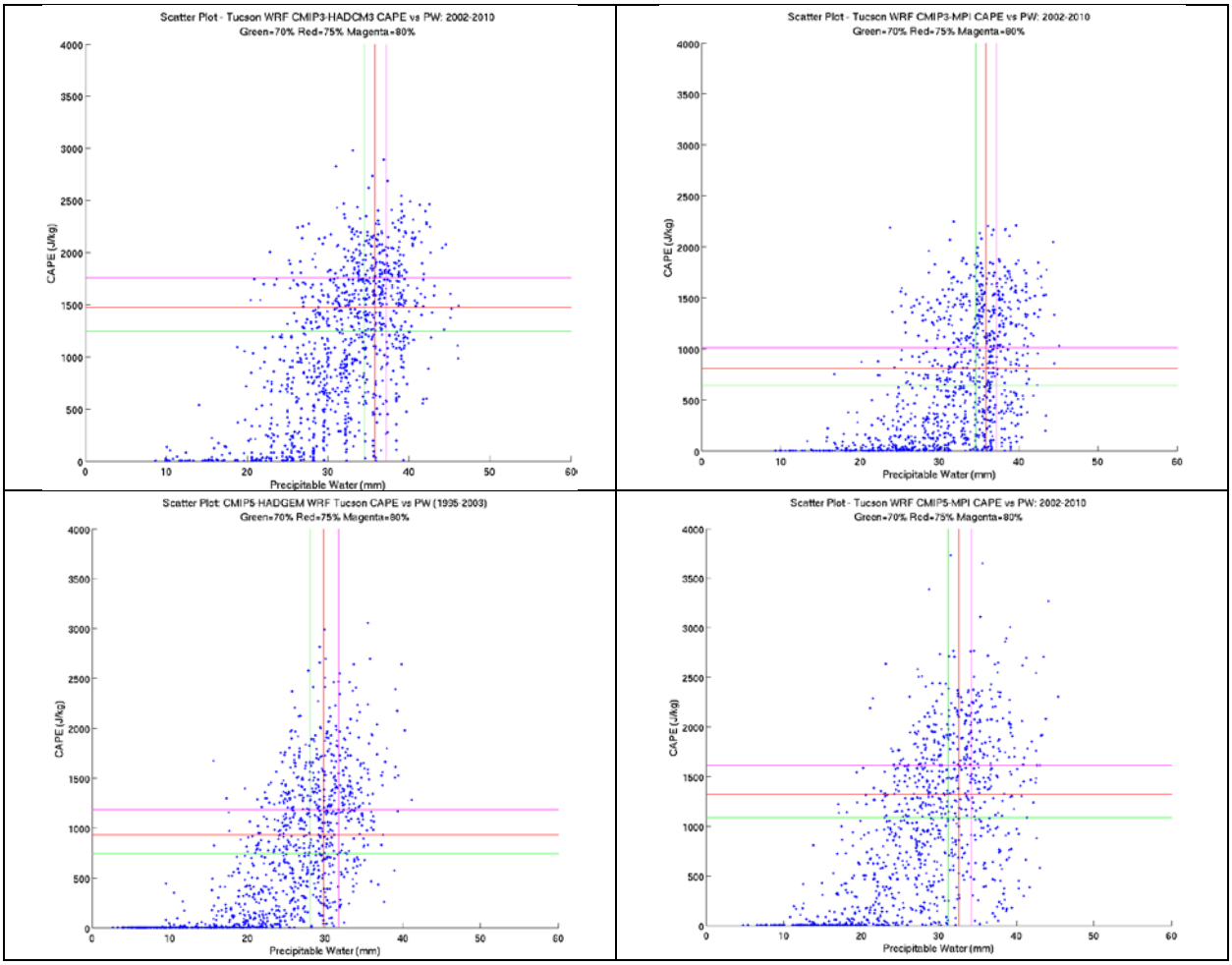

<u>Figure 14:</u> Same as Fig. 13 for dynamically downscaled CMIP models as indicated.

3. Coherency of MUCAPE and PW across the Southwest U.S. in downscaled reanalysis

The EOF analysis of MUCAPE and PW using the downscaled reanalysis at operational radiosonde sites, as described in the Methods section, is used to develop one final list of thermodynamically favorable days that is applicable for the Southwest U.S. region as a whole. *Fig. 15* shows the linear regression and correlation of gridded MUCAPE with the two statistically significant dominants mode of MUCAPE of the radiosonde sites. The regression coefficients for the dominant mode of MUCAPE are largest in southern Arizona and southern New Mexico (near 700 J kg^{-1}), because this is where the highest amounts of monsoon precipitation in the Southwest occur. The correlation coefficients for MUCAPE are positive and statistically significant (greater than 0.5) throughout all of Arizona and western New Mexico. San Diego is the one station that does not behave as the others, and that would be expected since this station does not typically experience any monsoon-related precipitation. *Fig. 16* shows the same for gridded PW with the one statistically significant dominant mode of PW of the radiosonde sites. The largest values of regressed PW (9-10 mm) occur in the low western desert regions of Arizona and extend southwestward towards the Gulf of California, clearly indicating the influence of a gulf surge. The dominant mode of PW is statistically significantly correlated throughout the entire Southwest, with the highest values (greater than 0.8) in southern and central Arizona. Because the correlation coefficients of the dominant mode(s) of MUCAPE and PW are positive and statistically significant throughout most of the Southwest, it is viable to use the one time series of these dominant mode(s) to define thermodynamically favorable severe weather event days. Expressed more plainly and succinctly, when severe monsoon weather occurs, the thermodynamic conditions are generally the same throughout the Southwest. Though the spatial coherency of MUCAPE and PW has only been assessed for the downscaled reanalysis here, it is reasonable to assume that downscaled CMIP3 and CMIP5 data behave similarly.

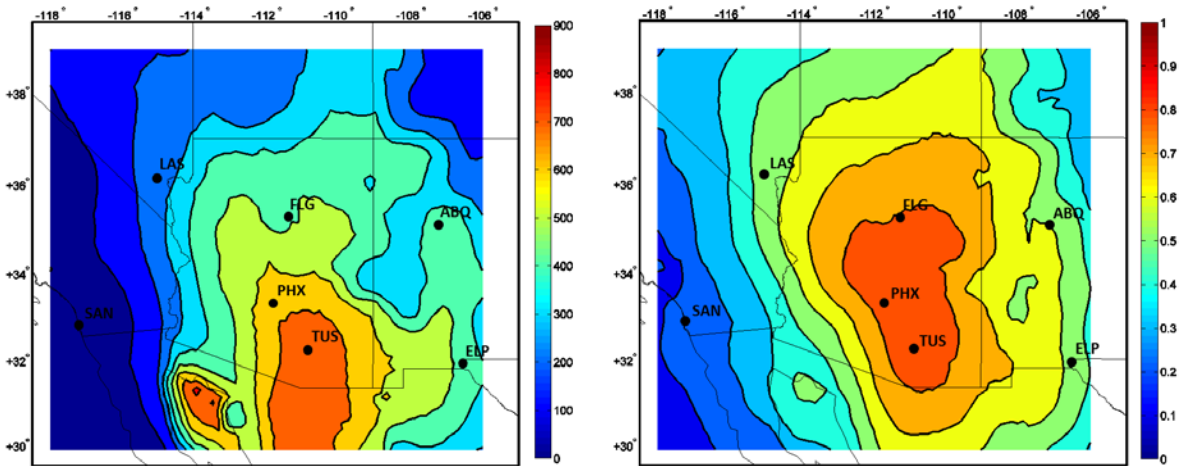

Figure 15: Linear regression (left) and correlation (right) of MUCAPE with the two dominant modes of MUCAPE at the Southwest U.S. radiosonde sites, using downscaled reanalysis. MUCAPE in linear regression in J kg^{-1}.

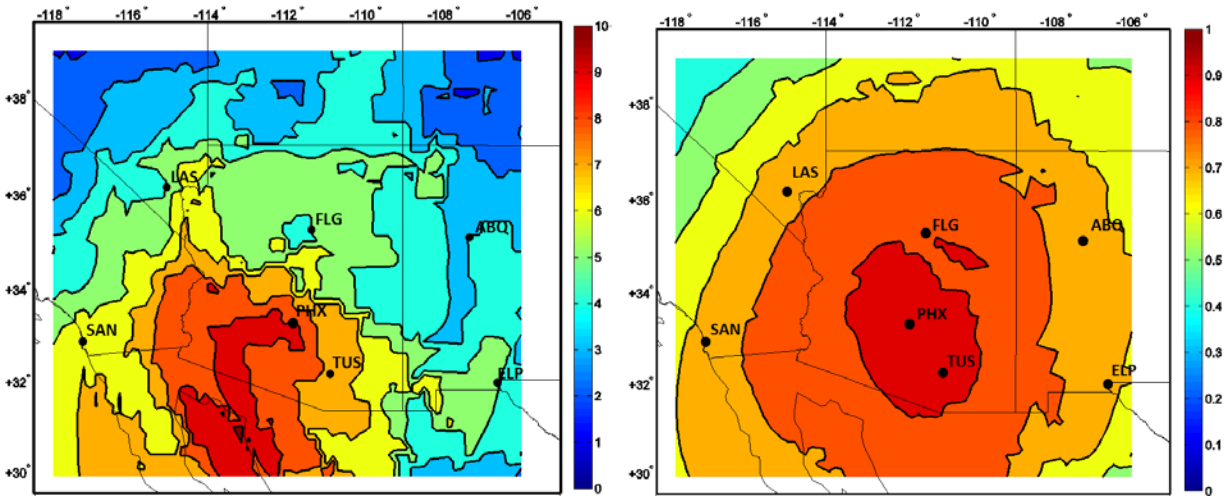

Figure 16: Linear regression (left) and correlation (right) of PW with the dominant mode of PW at the Southwest U.S. radiosonde sites, using downscaled reanalysis. PW in linear regression in mm.

C. DYNAMIC FORCING MECHANISMS FOR SEVERE WEATHER

1. Monsoon ridge positioning and precipitation during observed severe weather event days

The mean of the 500-mb heights and anomalies for the severe weather event days is shown in *Fig. 17*, along with the average precipitation anomaly from the Stage IV product. The average synoptic pattern of all thermodynamically favorable monsoon severe weather event days shows a strong monsoon ridge, centered slightly north of its favored climatological position in the Four Corners region in late summer. The highest local 500-mb geopotential height anomalies are located just to the north of the center of the monsoon ridge. The average precipitation (bottom of *Fig. 17*) reflects an active monsoon pattern over the Southwest, with precipitation generally maximized on the peaks of the terrain, for example the Mogollon Rim in Arizona, with maximum values on the order of 7 mm day^{-1}. This constitutes the baseline climatological map for observed severe weather events in the period 1993-2010.

a) Dominant monsoon ridge patterns

Considering the thermodynamically favorable severe weather event days identified in the Tucson morning sounding analysis during the period of the Stage IV precipitation record, the dominant modes of 500-mb geopotential height in NARR are objectively determined using empirical orthogonal function (EOF) analysis (e.g. Kutzbach 1967; Probhaska 1976; Bretherton et al. 1992; Wallace et al. 1992). The EOF analysis here is performed using singular value decomposition (SVD). To prepare the data prior to SVD, considering only the identified monsoon severe weather event days, the mean values of 500-mb geopotential height at each grid point are removed and the grid points are weighted based on the square root of the cosine of latitude. This analysis produces maps of 500-mb height anomaly patterns. The synoptic patterns associated with the mean 500-mb height of the monsoon severe weather event days and dominant modes of the severe weather event days may then be compared with the prior subjectively determined results of Maddox et al. (1995).

The 500-mb height patterns associated with the first two dominant EOF modes of the severe weather event days are shown in *Fig 18*. Taken together, the first five modes explain about 25% of the 500-mb height variance, albeit not necessarily statistically distinct by standard tests of eigenvalue separation (e.g. North et al. 1982). The first two modes are physically important because they correspond approximately to Maddox et al. Type I and II severe monsoon weather patterns. The Maddox et al. Type I severe weather pattern in EOF 1 is related to a north and east displacement of the ridge into the central U.S. The Maddox et al. Type II severe weather pattern in EOF 2 is related more to a north and west displacement of the ridge into Nevada and Utah.

These Type I and II patterns tend to be associated with monsoon severe weather in the Southwest, particularly Arizona, for several reasons. First, these orientations of the monsoon

ridge would favor enhanced easterly flow at upper-levels with a more southeasterly component for Type I and a more northeasterly component for Type II. In both cases, westward propagating upper-level disturbances (inverted troughs) are favored as well as weakened subsidence over Arizona (e.g. Bieda et al. 2009). Likewise, in both cases, a concomitant increase is observed in low to mid-level moisture from the eastern Pacific and Gulf of California, as well as convectively mixed moisture over western Mexico (Maddox et al 1995). This increased low-level moisture, decreased subsidence and more favorable wind shear profiles may act in concert to increase the likelihood for organized convective events which may propagate westward/southwestward off the higher terrain in central and southeastern Arizona.

c) Precipitation associated with dominant severe weather event synoptic patterns

In order to capture the precipitation associated with these synoptic patterns, the total daily precipitation was averaged over a three day time frame for each burst event for the dates with the highest positive z-scores (above 85%, or top 15%) relating to the associated combined PC time series. The precipitation anomaly patterns are shown in *Fig. 19*. The anomaly is constructed as the average precipitation for the top 15% of the events in a given monsoon severe weather mode minus the average precipitation of all the identified severe weather event days. The top events for both Type I and II modes exhibit even more enhanced precipitation across all of Arizona and New Mexico, exceeding greater than 1 mm day^{-1} above the average of all identified severe weather events. The pattern of precipitation associated with the average of all severe weather event days in *Fig. 17* would indicate maximum precipitation values centered on the peaks of the terrain, where monsoon precipitation is most climatologically favored to occur. However, the top precipitation events within this set for the strongest expressions of the Type I and II modes show maximum positive precipitation anomalies (above the severe weather event average) tending also to occur the south and west of the Mogollon Rim in Arizona, where organized convection plays a relatively more important role in monsoon precipitation (e.g. Hales 1977; Castro et al. 2007).

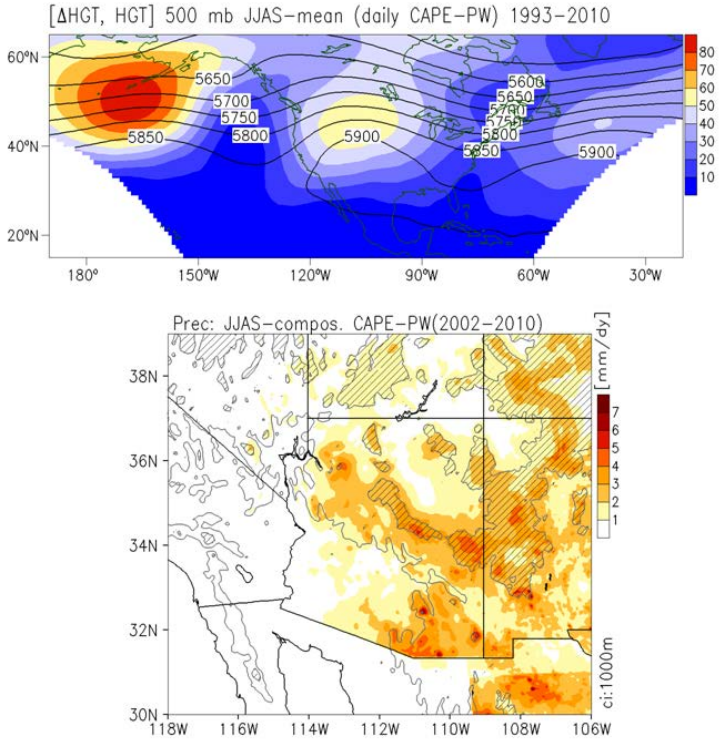

<u>Figure 17:</u> Top: 500-mb geopotential height (m) and anomaly (shaded) related to the total climatology (contour) for thermodynamically favorable severe weather events during the period 1993-2010, as identified by Tucson sounding data. Bottom: Average precipitation (mm day^{-1}) from Stage IV product for the same thermodynamically favorable severe weather event but during the period 2002-2010. Elevation terrain indicated as contours at intervals of 1000 m. Regions over 2000 m shown in hatching.

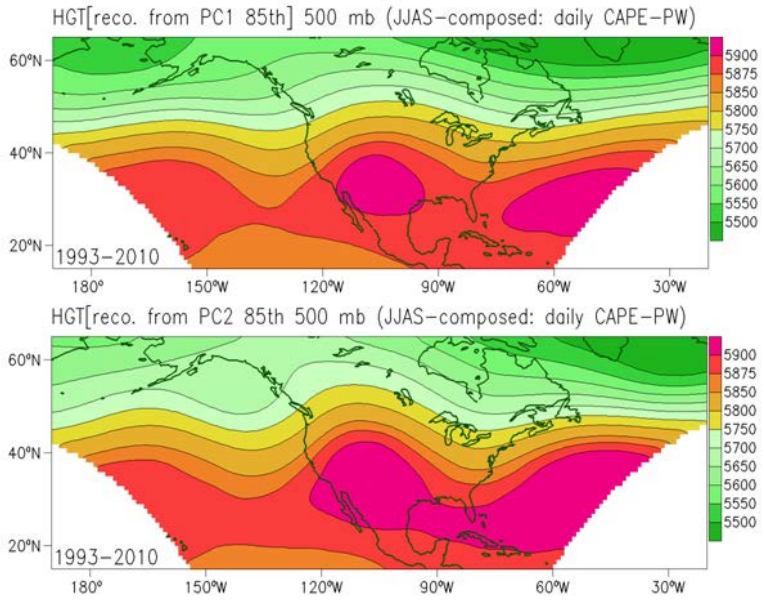

Figure 18: Objectively determined severe weather event 500-mb geopotential height patterns (m) that correspond to Type I (top) and Type II (bottom) modes of Maddox et al. (1995). Modes constructed by considering mean of 500-mb geopotential height of all severe weather event days plus the average of 500-mb height anomalies for events that project most strongly (top 15%) on the positive phase of severe-weather event of EOF1 (top) and EOF2 (bottom) modes.

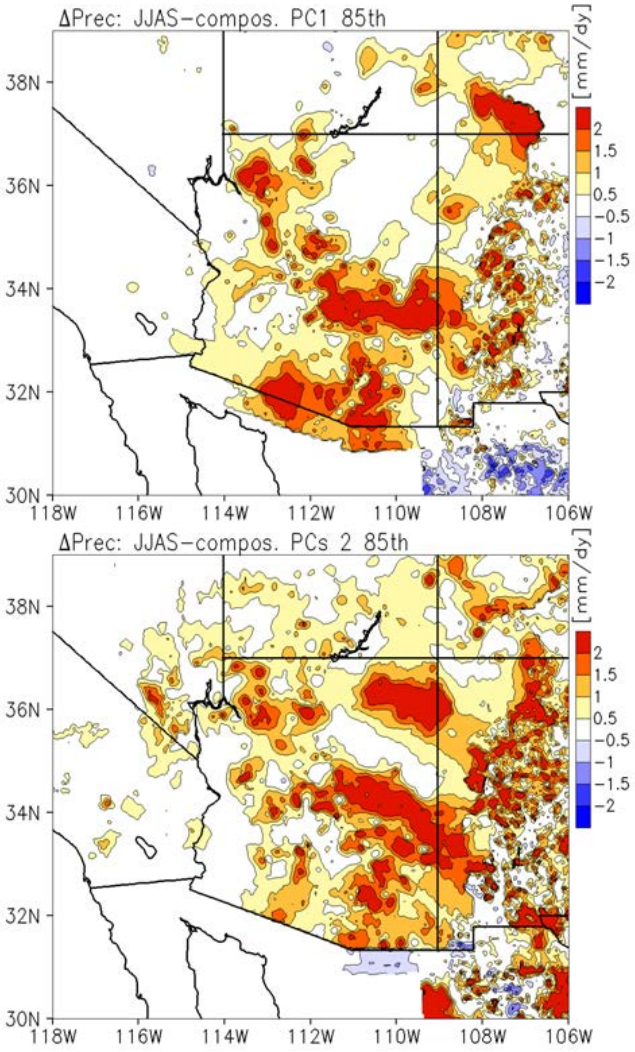

Figure 19: Precipitation anomalies (mm day-1) associated with the EOF objectively defined Type I (top) and Type II (bottom) severe weather event days from mode reconstruction. Anomalies constructed by averaging precipitation for events that project most strongly on combined EOF modes (top 15%) minus the average precipitation for all thermodynamically-favorable severe weather events.

2. Monsoon ridge positioning in CMIP3 and CMIP5 data

The same analysis was repeated with downscaled CMIP3 and CMIP5 data. The mean positioning of the monsoon ridge (during the period JA) and corresponding dominant monsoon ridge modes of thermodynamically favorable severe weather event days are shown for all downscaled CMIP models in *Figs. 20-23*. Note that for the CMIP3 and CMIP5 analyses only the months July and August are considered, as this is when the monsoon ridge is most pronounced

anyway and when most monsoon precipitation occurs in the Southwest within these models, per *Figs. 8-9* presented earlier. For the most part, the CMIP models all have a reasonable climatological positioning of the monsoon ridge (from west Texas to the Four Corners region of the Southwest) and the severe weather modes of the monsoon ridge of Maddox et al. (1995) appear as either the first or second dominant mode. The one important exception appears to be MPI-ECHAM6 in CMIP5, as the climatological positioning of the monsoon ridge is too far to the south and east. Though the dominant monsoon ridge modes do show variation in ridge positioning to the north and east or north and west, the monsoon ridge is still not located to the north of Arizona and New Mexico, as in the other three models.

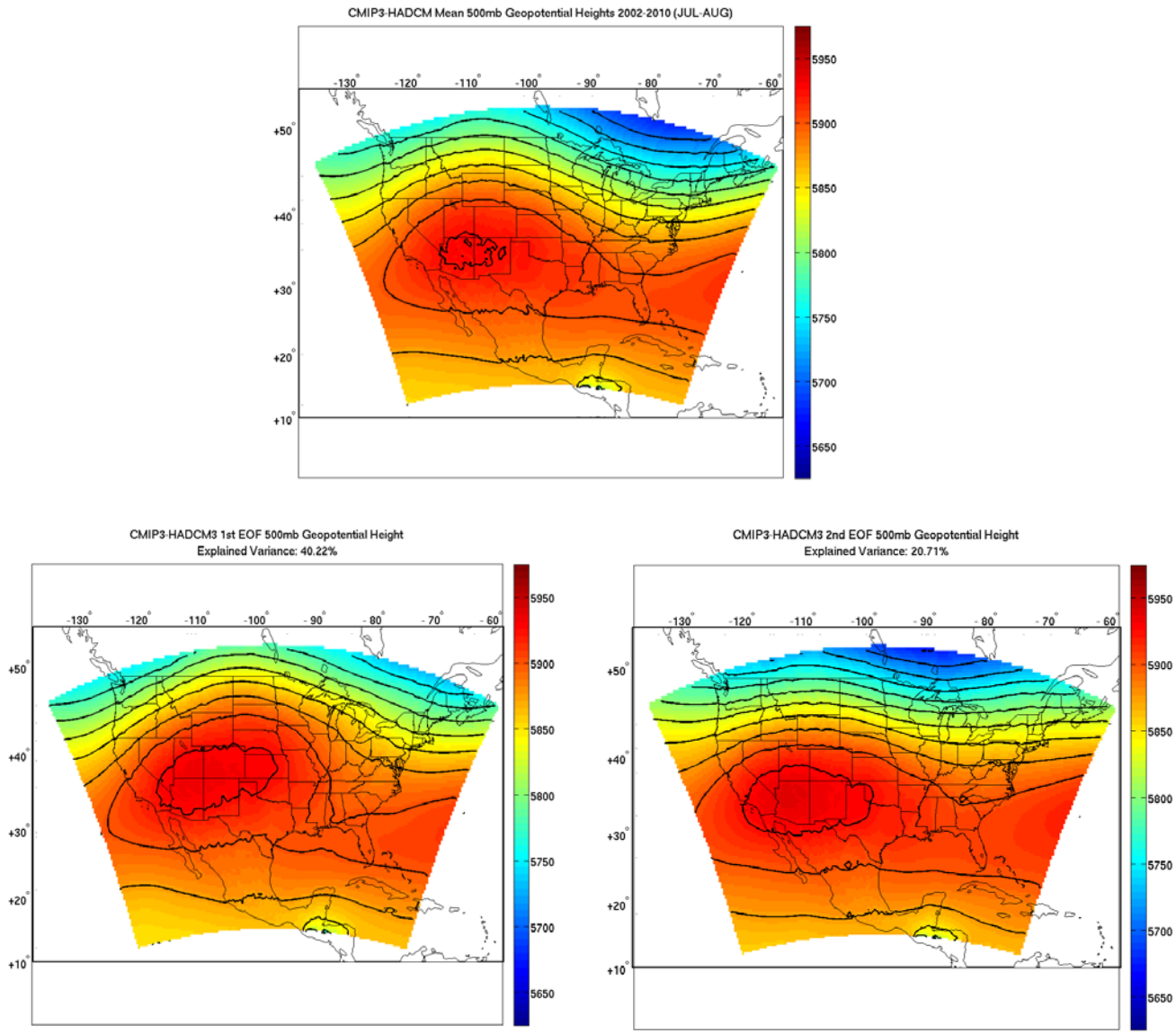

<u>Figure 20</u>: Top: mean 500-mb geopotential height (m) in July-August for downscaled CMIP3 HadCM3 for period 2002-2010. Bottom left: 500-mb geopotential height related to first dominant mode of thermodynamically favorable severe weather event days. Bottom right: 500-mb geopotential height related to second dominant mode. Percent variance explained as indicated.

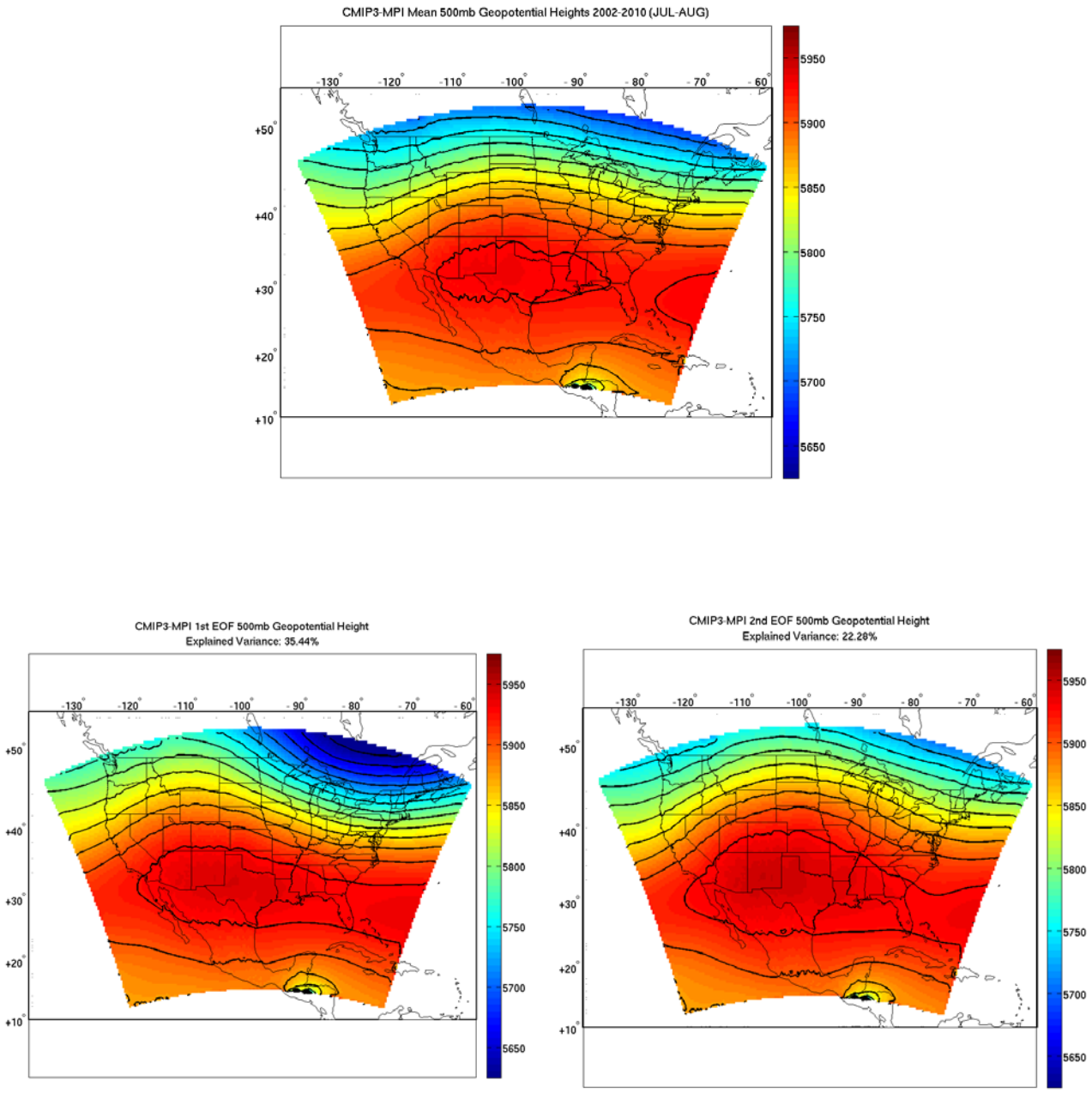

<u>Figure 21</u>: Same as Fig. 20 for dynamically downscaled CMIP3 MPI-ECHAM5.

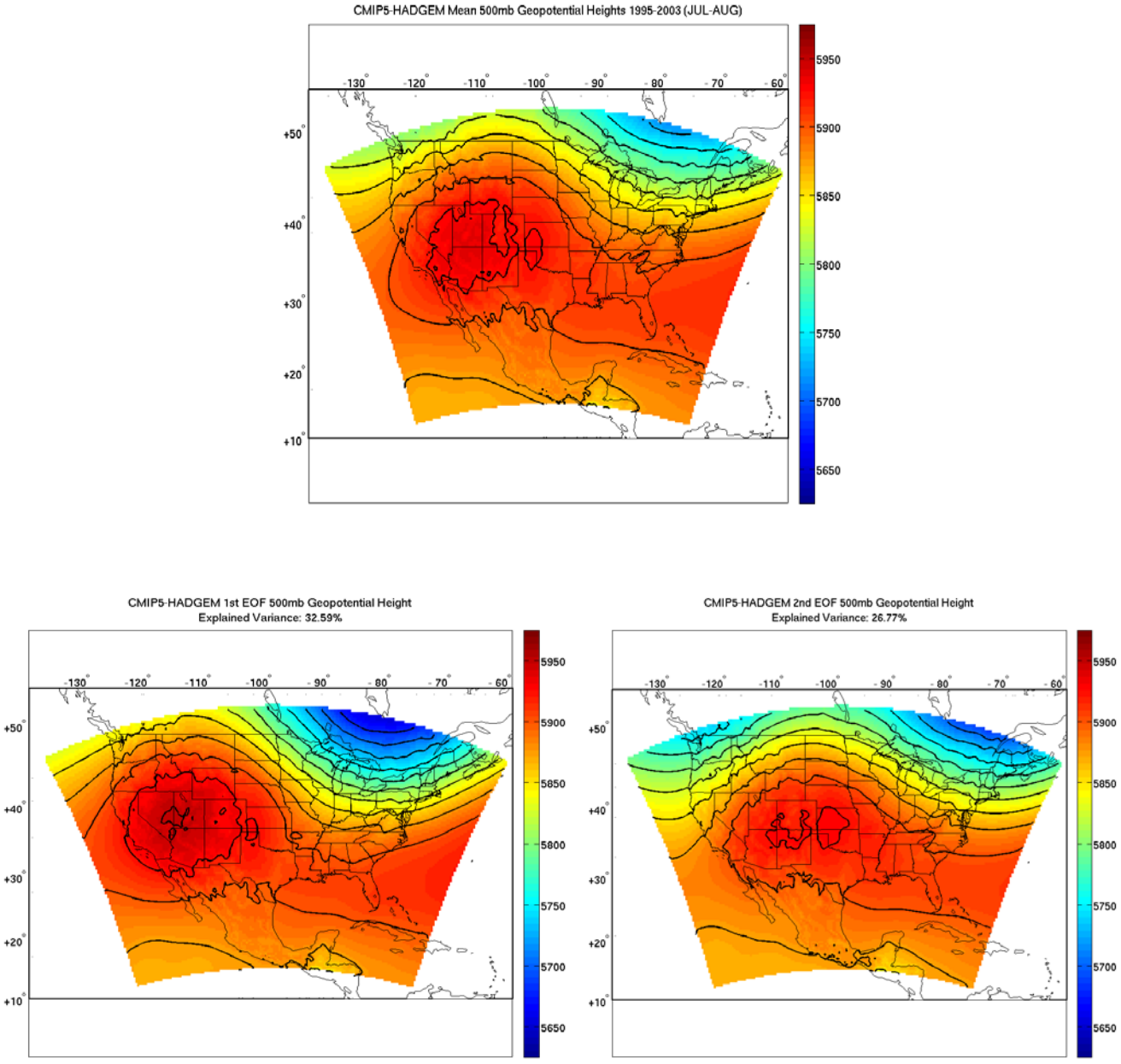

<u>Figure 22</u>: Same as Fig. 20 for dynamically downscaled CMIP5 HadGEM2.

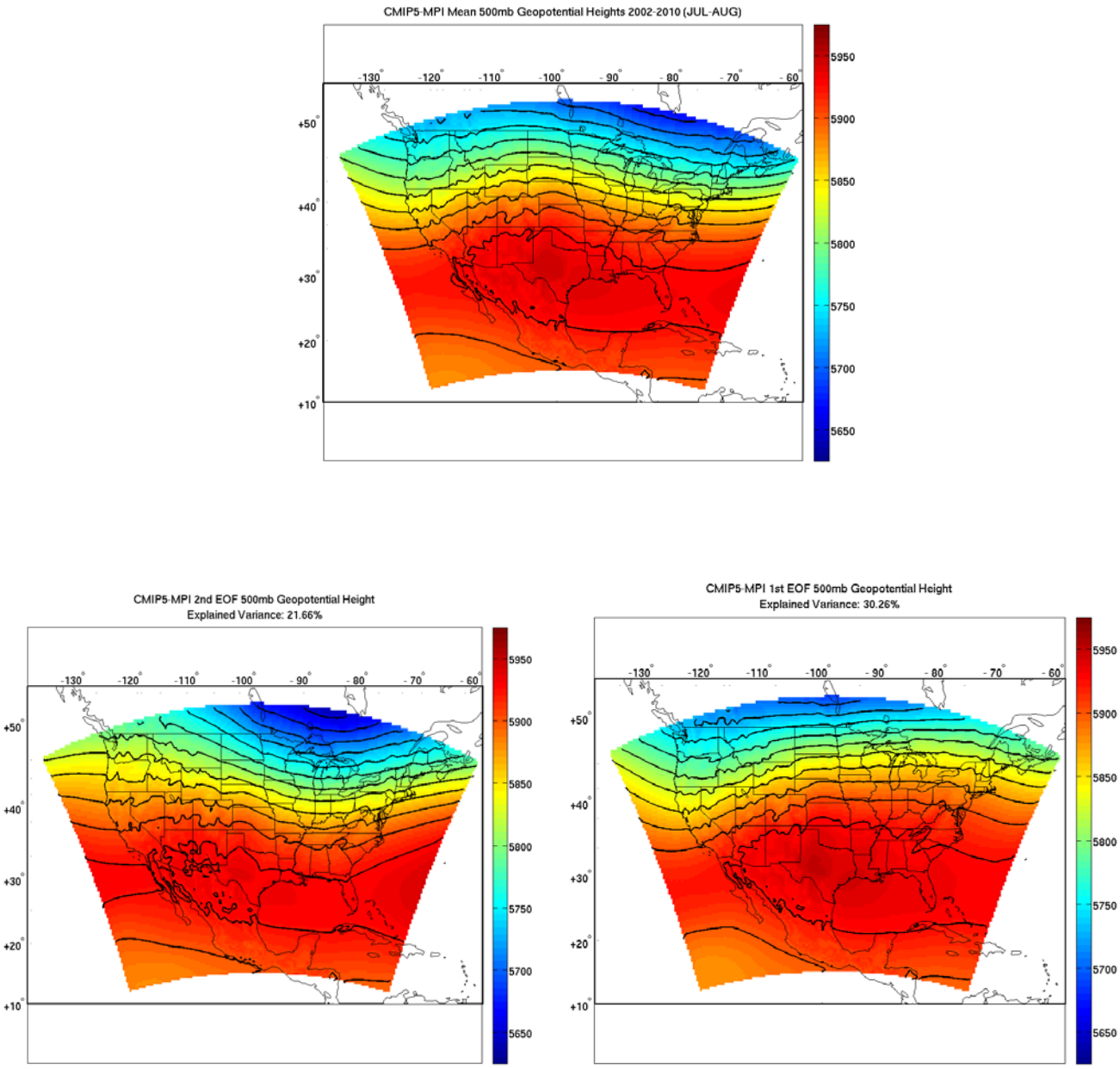

<u>Figure 23</u>: Same as Fig. 20 for dynamically downscaled CMIP5 MPI-ECHAM6.

3. Gulf of California moisture surges

Considering the period of the Stage IV precipitation record during JJAS, wind rose histograms for Yuma MCAS were constructed for gulf surge days and all days (*Fig. 24*) There are two distinct orientations of wind directions during the warm season, either out of the west, between 270 and 290 degrees, or from the southeast, between 145 and 160 degrees. The distinct orientations reflect the fact that much of the monsoon in Yuma is dominated by dry westerlies, while the remainder is characteristic of a relatively moister regime with winds out of the south and southeast. The difference in precipitation associated with gulf surge days in the Stage IV precipitation data is shown in *Fig. 25*. Not surprisingly, gulf surges tend to enhance precipitation mostly in the low desert area of southwest Arizona. A relatively greater amount of the gulf surge-related precipitation tends to fall over areas of relatively higher elevation such as the small mountain ranges near Yuma and over the Tohono O'odham nation (located approximately 50-70 miles to the west of Tucson) than surrounding low elevation areas. These relatively minor orographic features therefore act as lifting mechanisms for terrain-forced precipitation occurrence in the form of local air mass thunderstorms, provided there is an influx of moisture and instability in the low deserts during the surge events.

Using the Yuma MCAS record, major gulf surges were identified, basically with the largest dew points and longest event duration. *Fig. 26* shows the composite of simulated low-level (925-mb) winds of major gulf surge events in the downscaled reanalysis during the period of the Stage IV record. Even at 35 km grid spacing, WRF is able to simulate the gulf surge well, with relatively stronger low-level winds (4-5 m s^{-1}) at the northern end of the Gulf of California from a southeasterly direction. Applying the Yuma gulf surge criteria to thermodynamically favorable severe weather event days in downscaled CMIP data resulted in a very high correspondence with gulf surges (not shown).

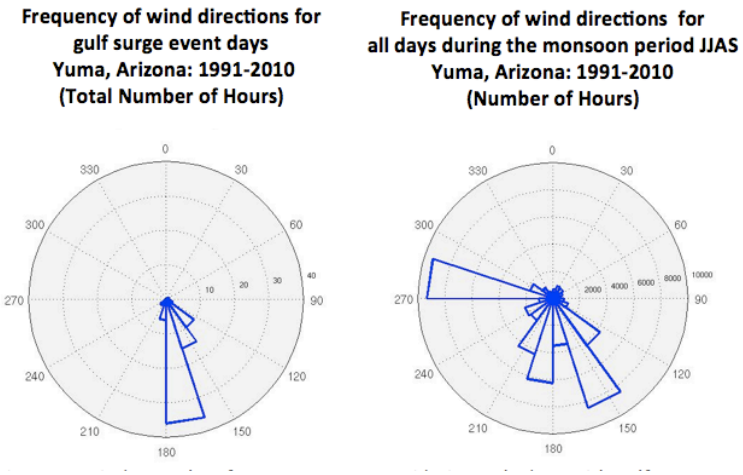

Figure 24: Left: Frequency of wind directions for gulf surge event days at Yuma MCAS for the period 1991-2010. Right: corresponding frequency for all days during the monsoon period (JJAS).

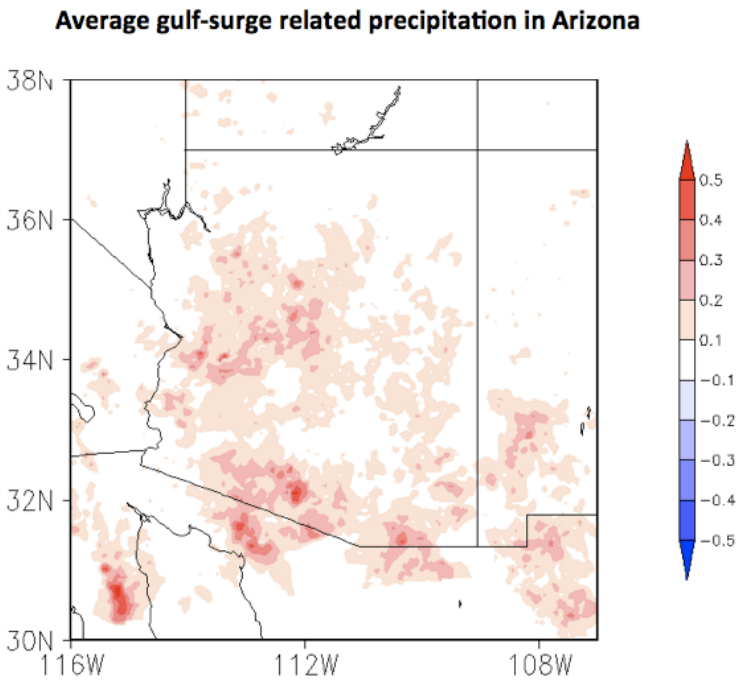

<u>Figure 25:</u> Average gulf surge associated precipitation (mm hr^{-1}) in Stage IV precipitation product over Arizona, shown as the difference with climatological monsoon precipitation.

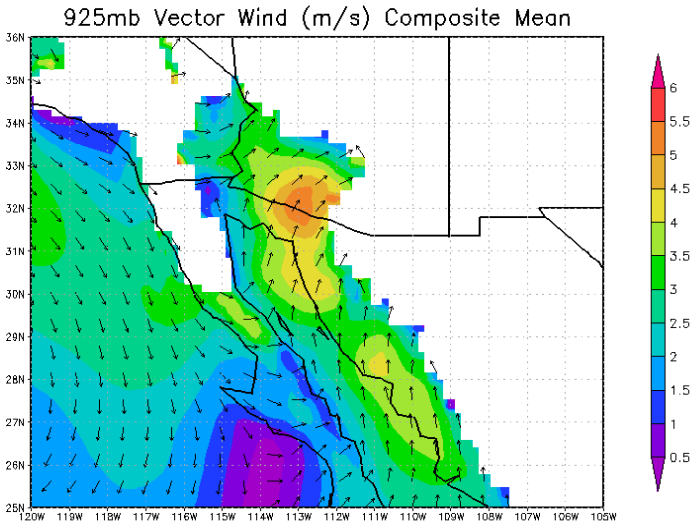

<u>Figure 26:</u> Composite winds (m s^{-1}) and wind vectors at 925-mb in downscaled reanalysis for most pronounced "major" surges at Yuma MCAS, with the longest duration and highest dew point temperatures (1991-2010).

4. Transient Inverted troughs (IVs)

a) Downscaled reanalysis

Track densities for each subsection of the monsoon season (1981-2010 analysis period) within the downscaled reanalysis are plotted in *Fig. 27*. By mid June through mid July, tracks increase in coverage, as would be expected when the monsoon season begins. Qualitatively, the IV track density computed in the downscaled reanalysis WRF RCM is similar to the manual analysis of IV track density compiled by Bieda et al. (2009) (their Figure 8). One noticeable difference with Bieda et al. (2009) is the lack of IV tracks over the Northern Baja Peninsula, extending into extreme southern California. These features that are missed by the objective feature tracking methods may be IVs that curve northward to the west of the monsoon ridge and are eventually advected eastward by the westerly wind flow in the mid latitudes. Some of these features may be omitted due to the elimination of most east moving disturbances during the processing of the track data.

b) Downscaled CMIP models

The same objective methodology for analyzing IV track data from the downscaled reanalysis is repeated on three of the CMIP3 and CMIP5 dynamically downscaled GCMs. Analysis of IV tracks from the MPI-ECHAM5 and HadCM3 products encompass the years 1981-2010. Both of these datasets have 6-hour, rather than 3-hour, temporal resolution, so the experimental methodology to track IVs differs slightly from that used on the dynamically downscaled reanalysis data. IV features that last for 4 or more time steps (~18 hours) are kept when analysis is performed on both downscaled GCM simulations, which is consistent with the analysis performed on the WRF RCM. Otherwise, settings to the Hodges (1999) tracking code are kept constant. The seasonal track density climatology for the CMIP3 MPI-ECHAM5 simulation is shown in *Fig. 28*, and the climatology for the CMIP3 HadCM3 simulation is shown in *Fig. 29*. Both of these RCM solutions appear to slightly underestimate the magnitude of the IV track density throughout the region. Despite the slight low bias of IV track density compared to the WRF RCM climatology, the CMIP models considered reasonably match the temporal and spatial patterns associated with IV tracks throughout the NAM season. The downscaled MPI-ECHAM5 product tends to systematically place the NAM ridge (and consequently IV features) too far south, while the HadCM3 product places the same ridge slightly north of its climatological position, per the reanalysis product. The CMIP3 runs of the MPI-ECHAM5 and HadCM3 show the climatological increase in IV track density during the early season and the decrease by early September.

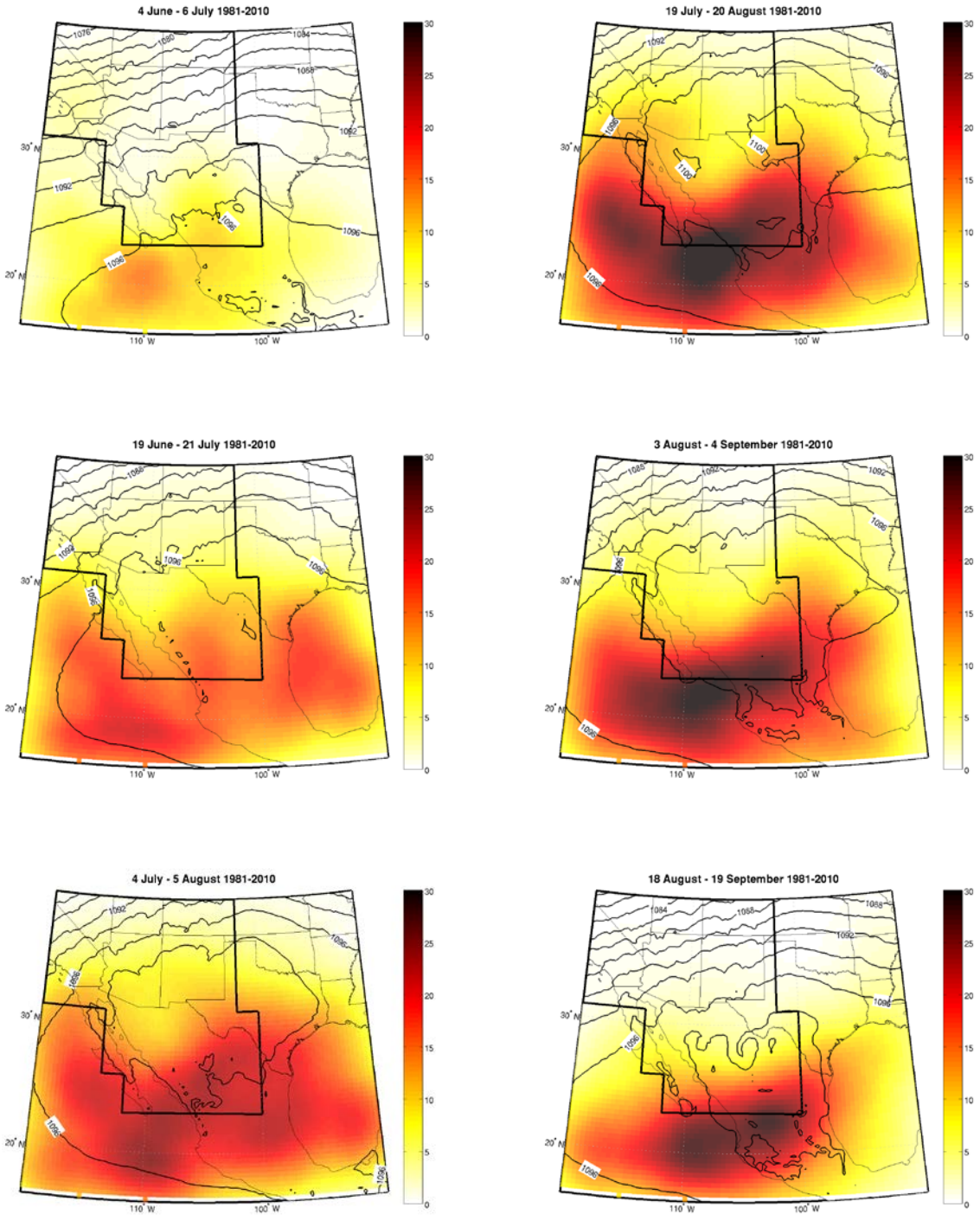

<u>Figure 27:</u> IV track density for six intervals in dynamically downscaled reanalysis for the period 1981-2010 (going from top to bottom, then left to right): 4 June – 6 July, 19 June – 21 July, 4 July – 5 August, 19 July – 20 August, 3 August – 4 September, and 18 August – 18 September. Mean 250-hPa geopotential heights are shown with black contours

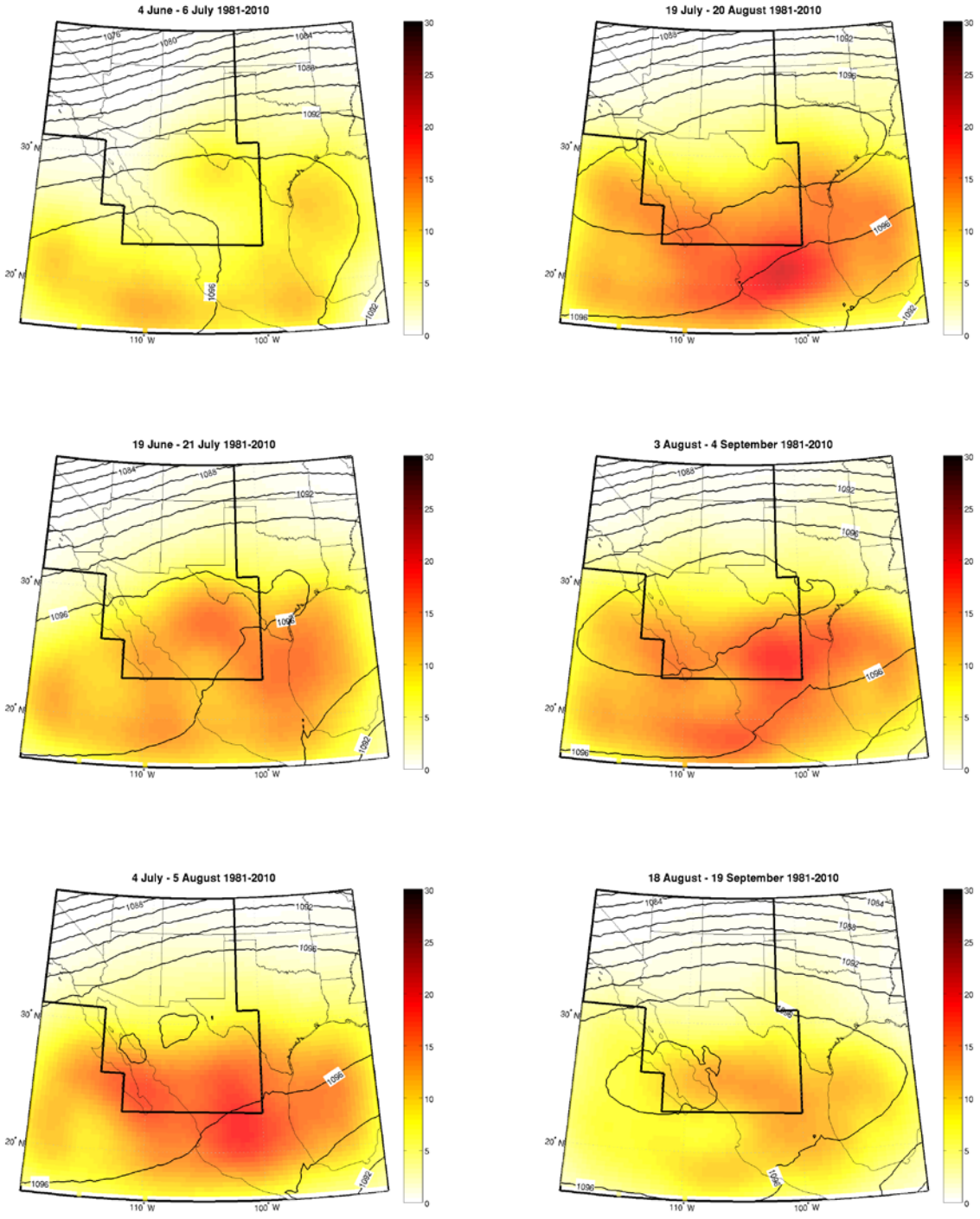

<u>Figure 28</u>: Same as Fig. 27 for IV track density and mean 250-hPa geopotential height climatology in downscaled CMIP3 MPI-ECHAM5 (1981-2010).

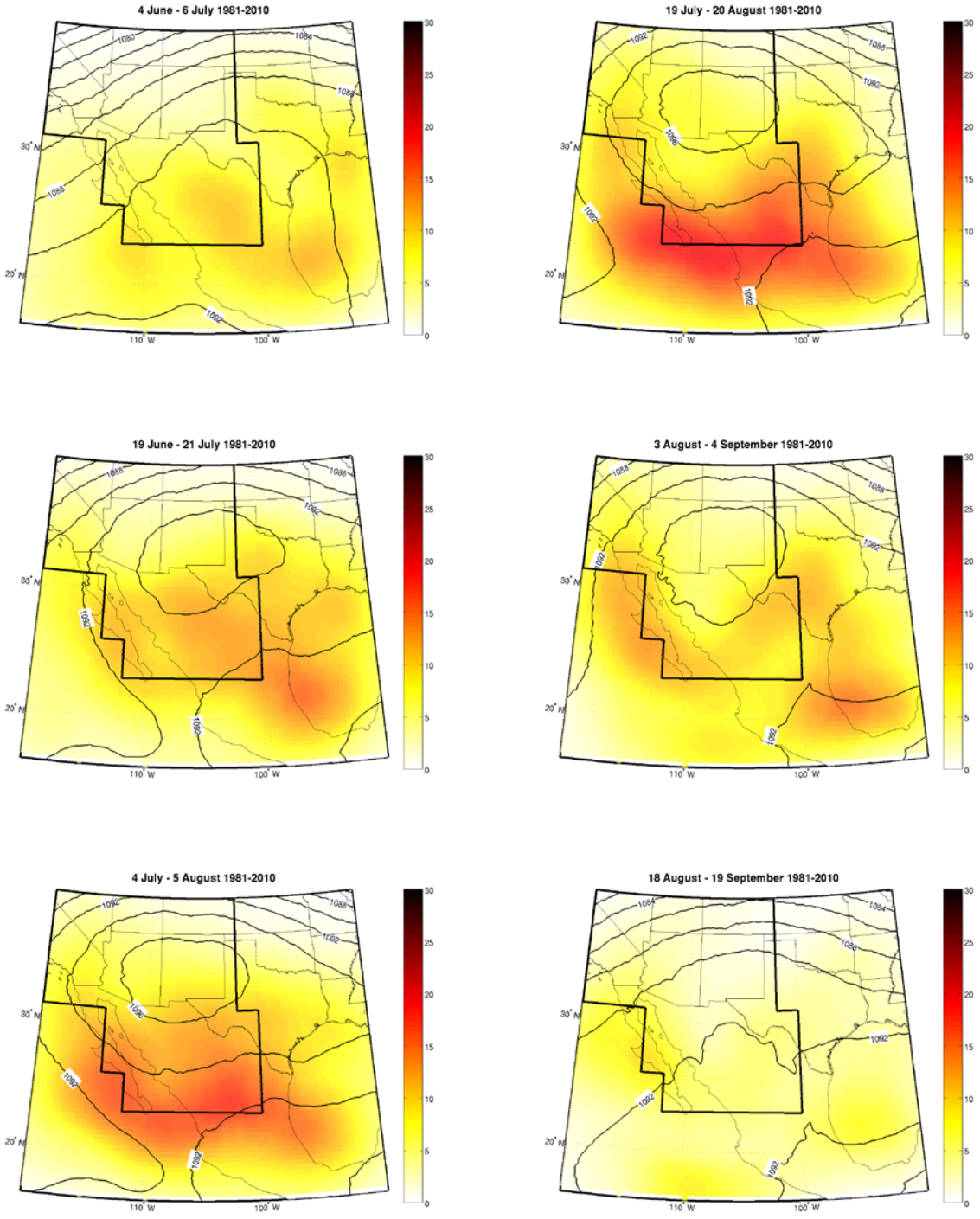

<u>Figure 29</u>: Same as Fig. 27 for IV track density and mean 250-hPa geopotential height climatology in downscaled CMIP3 HadCM3 (1981-2010).

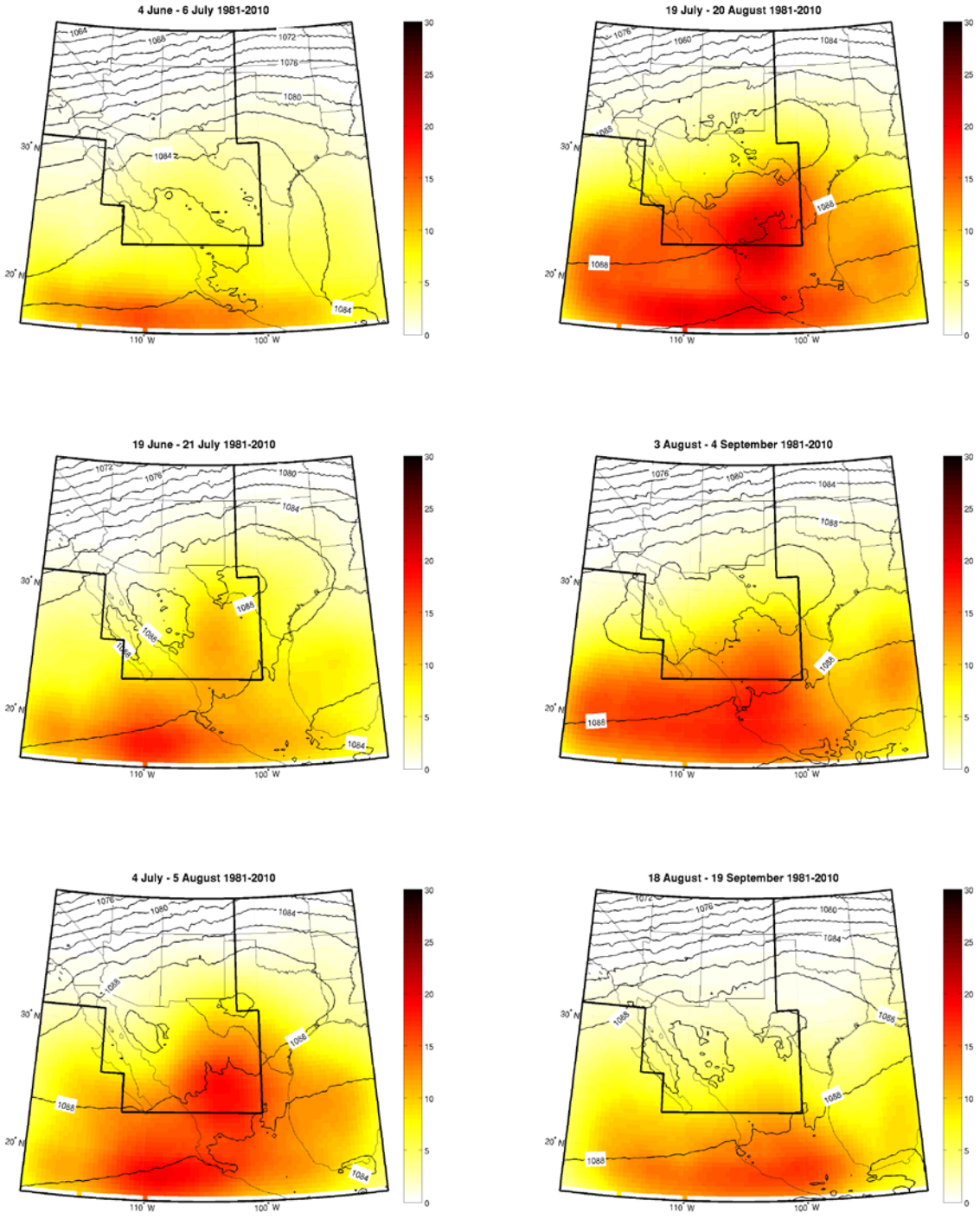

<u>Figure 30</u>: Same as Fig. 27 for IV track density and mean 250-hPa geopotential height climatology in downscaled CMIP5 MPI-ECHAM6 (1981-2010).

The WRF-downscaled MPI-ECHAM6 that was run as part of CMIP5 is also analyzed for the 1981-2010 monsoon seasons. The downscaled data are available at 6-hour temporal resolution, so IVs are tracked using the same settings as what were used for the other dynamically downscaled GCM simulations. The track density climatology for this model is shown in *Fig. 30*. Like the previously discussed track density climatologies, this downscaled GCM matches the spatial and temporal patterns associated with IVs throughout the NAM season. This climatology also tends to depict the NAM ridge, and IV features, too far south compared to the downscaled reanalysis product. Like the other downscaled GCM products, the MPI-ECHAM6 product also underestimates the track density of IVs, particularly near the peak of the NAM season. It should be noted that the comparative statements between the dynamically downscaled reanalysis and the dynamically downscaled CMIP models with respect to track density climatology presented here are more descriptive in nature. Doing a formal statistical comparison with the downscaled reanalysis results to find somehow the 'best' performing CMIP model is arguably problematic, as each of these CMIP models have errors in the climatological evolution of atmospheric circulation features that are a function of both space and time. The main objective in the analysis of IVs and their variability within the downscaled CMIP models is to ensure they are reasonably represented at least in a qualitative sense. But even given this level of analysis, it is clear that some of the CMIP models perform better than others in the aspect of representing IVs.

D. LONG-TERM HISTORICAL CHANGES IN THERMODYNAMIC AND DYNAMIC CHARACTERISTICS OF THE NORTH AMERICAN MONSOON IN THE SOUTHWEST

What is ultimately desired is that all sources of dynamically downscaled CMIP3 and CMIP5 data exhibit similar long-term changes in atmospheric thermodynamic and dynamic conditions. Within the project, long-term climate change changes in the baseline dynamically downscaled reanalysis and downscaled CMIP models have been considered. Long-term climate changes during approximately the last 30 years (since 1980) are deemed to be anthropogenically influenced, and these long-term climate trends are specifically assessed considering the differences in the downscaled reanalysis between the periods 1980-2010 and 1950-1979.

1. Changes in atmospheric thermodynamic conditions

The atmospheric thermodynamic characteristics during the monsoon have substantially changed over the past thirty years in the WRF downscaled NCEP-NCAR reanalysis, specifically considering the (late) period 1980-2010 to the (early) period 1948-1979. The mean difference in MUCAPE (*Fig. 31*, left) shows an increase in atmospheric instability over the entire monsoon region, excluding the Gulf of California. This increase of MUCAPE is maximized over northern Arizona and southern parts of Nevada and Utah, where the monsoon is at its northernmost extent. The corresponding results for PW (*Fig. 31*, right) show that PW has increased throughout the entire monsoon region. The increase is maximized at the northern end of the Gulf of California and extends northward to the region where increases in MUCAPE were observed. The

largest increase in PW occurs over the highly populated area of central Arizona where Phoenix lies. The increase in atmospheric moisture and instability over the monsoon region during the past 63 years in the downscaled reanalysis is entirely consistent with the hypothesis that long-term anthropogenic warming increases the atmospheric water vapor holding capacity of the atmosphere and makes the thermodynamic environment more favorable for heavier convective precipitation. The same types of positive trends are also found in radiosonde data throughout the Southwest during the warm season, confirming the modeled results (*Table 1*).

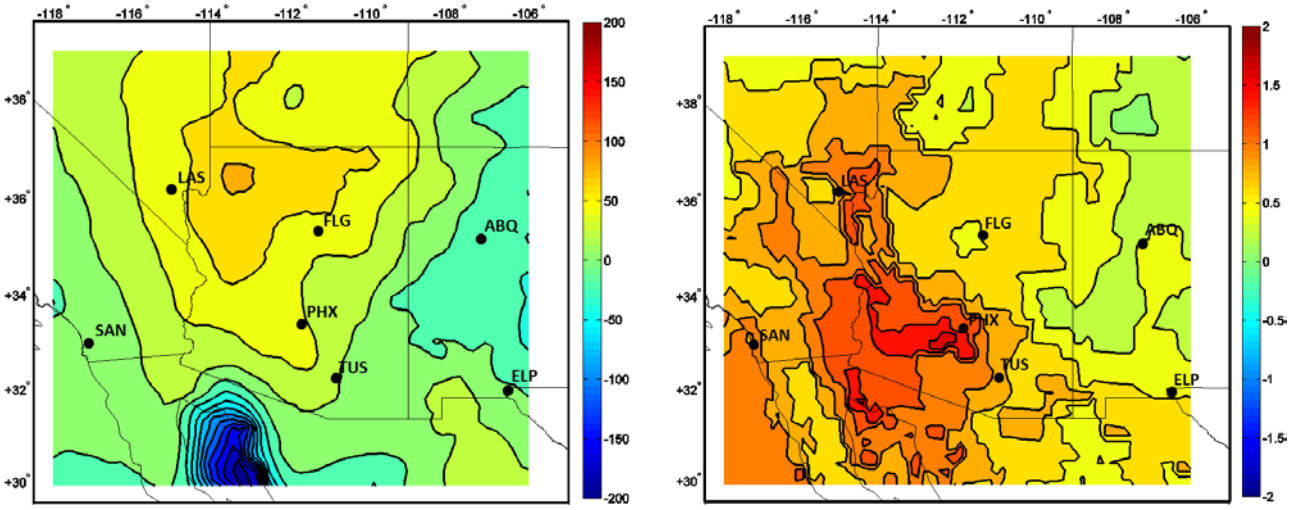

<u>Figure 31</u>: Long term differences in downscaled reanalysis between the period 1950-1979 and 1980-2010 for MUCAPE (left) in J kg^{-1} and PW (right) in mm. Months considered are JA.

Correlation Coefficient	CAPE	PW	Years Analyzed
Albuquerque, NM	**0.854**	**0.598**	1950-2014
Desert Rock, NV	**0.588**	**0.275**	1953-2014
El Paso, TX	**0.895**	**0.513**	1950-2014
Flagstaff, AZ	**0.441**	**0.490**	1996-2014
San Diego, CA	-	**0.375**	1956-2014
Tucson, AZ	**0.788**	**0.263**	1952-2014
Winslow, AZ	0.097	0.077	1961-1995

Table 1: Correlation coefficients for the observed annual average CAPE and PW (15 June – 15 September) trends at selected radiosonde sites throughout the southwest CONUS. Years used for analysis of trends shown in right column. Bold font indicates statistical significance at the 90% level.

To explore the long-term changes in distribution of MUCAPE and PW over time in the Southwest, changes in these thermodynamic variables are also analyzed individually for the location of Tucson, Arizona. This particular site is generally representative of the region as a whole during the monsoon because the local variation of MUCAPE and PW is statistically very similar to other radiosonde sites in the Southwest, as demonstrated by the dominant spatial modes of these quantities presented earlier in *Fig. 15* and *Fig. 16*. These analyses are meant to show in a qualitative, descriptive way the changes in the distributions of MUCAPE and PW at the Tucson radiosonde site as an illustrative example, to complement *Fig. 31* which shows the mean changes in these variables across the Southwest. Formal assessment of the statistical significance of the changes in the distributions of CAPE and PW at Tucson have not been performed here, but this has been performed for changes in historically observed and model simulated precipitation, as will be shown in the following Section E. The distributions histograms of PW are appear very similar in both periods but with distinguishing characteristics (*Figure 32a*). The bin of maximum frequency occurs between ~32 mm during both periods. Evaluating the percent change between the two periods, the early period has a higher frequency in the bins between 0-32 mm. The late period dominates the frequencies of the PW measurements greater than 32 mm as evidenced by the positive percent change values. This shows that PW measurements have increased with time from the early to the late period with the greatest increase, of 73%, occurring in the higher PW values (near 40 mm). Comparing the individual distributions of the two periods, these dominant frequencies in each distribution are also observed, although the fitted gamma distribution functions appear very similar. The PW

distribution of the early period (*Figure 32b*) has a greater frequency of measurements between 25-30mm than that of the late period (*Figure 32c*). The late period has a higher frequency of PW measurements between 30-45mm.

The histograms of MUCAPE appear very similar for both of the time periods. Both histograms show a very large frequency of low MUCAPE value days with MUCAPE measurements falling between 0-200 J kg^{-1} and much lower frequencies as the value of MUCAPE increases to 3500 J kg^{-1} (*Figure 33a*). Based on the percent of change in the MUCAPE measurements over time, the early period has the highest frequency between 0-1250 J kg^{-1}, as seen in the negative percentage values. The late period has higher frequencies for MUCAPE values between 1250-3500 J kg^{-1}, given the positive percentage values, except for the bins between 2250-2750 J kg^{-1} . Overall, the early period shows higher frequencies in the lower half of MUCAPE values and the late period shows higher frequencies in the higher MUCAPE values. The greatest percent of change occurs for the highest MUCAPE values, where there is a 33% increase. The distributions of the individual time periods look very similar with almost identical gamma distribution functions for each (*Figure 33b, c*). In Tucson, WRF-modeled MUCAPE has increased by 64-84 J kg^{-1} and modeled PW has increased by ~1.8mm over the past 63 years. This equates to roughly a ~10% increase in MUCAPE and a ~6% increase in PW. Broadly speaking, the modeled distributions of MUCAPE and PW become broader and flatter with time. These same types of shifts toward a broader and flatter distribution are also evident in the change in the distribution of daily precipitation at selected observing sites in the Southwest (Phoenix and Flagstaff), and these changes are statistically significant as will be shown in Section E.

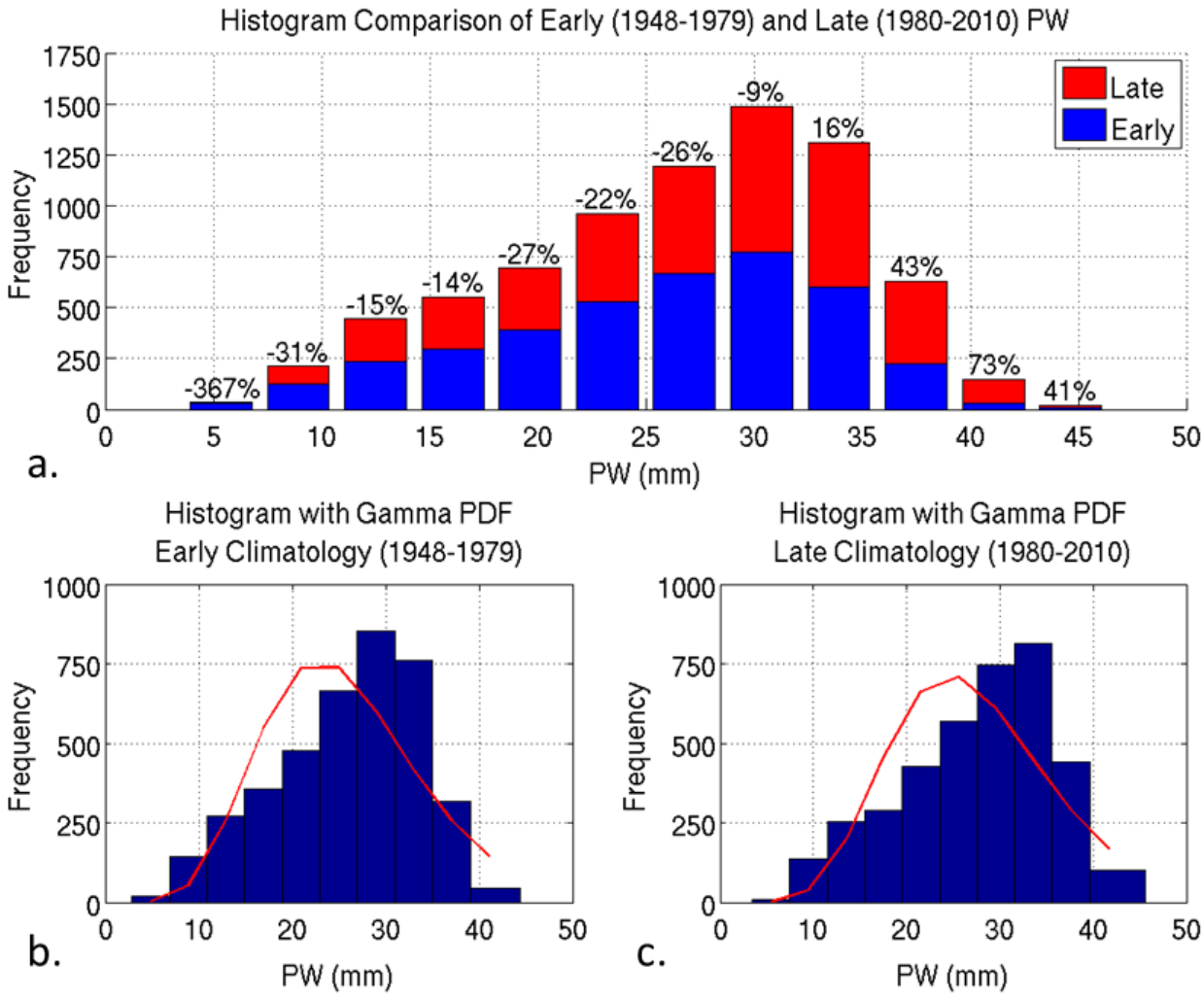

<u>Figure 32:</u> Histogram comparison of PW (in mm) values based on dynamically downscaled WRF-RCM regional atmospheric reanalysis data for all days during the monsoon period (JJAS) for an area averaged over Tucson, Arizona. The figure includes: a. stacked histogram comparison of the early (1948-1979) and late (1980-2010) period where the percentage of change over the two periods is indicated for each bin and histograms, along with the consequent gamma probability distribution functions (red), for the b. early period and c. the late period.

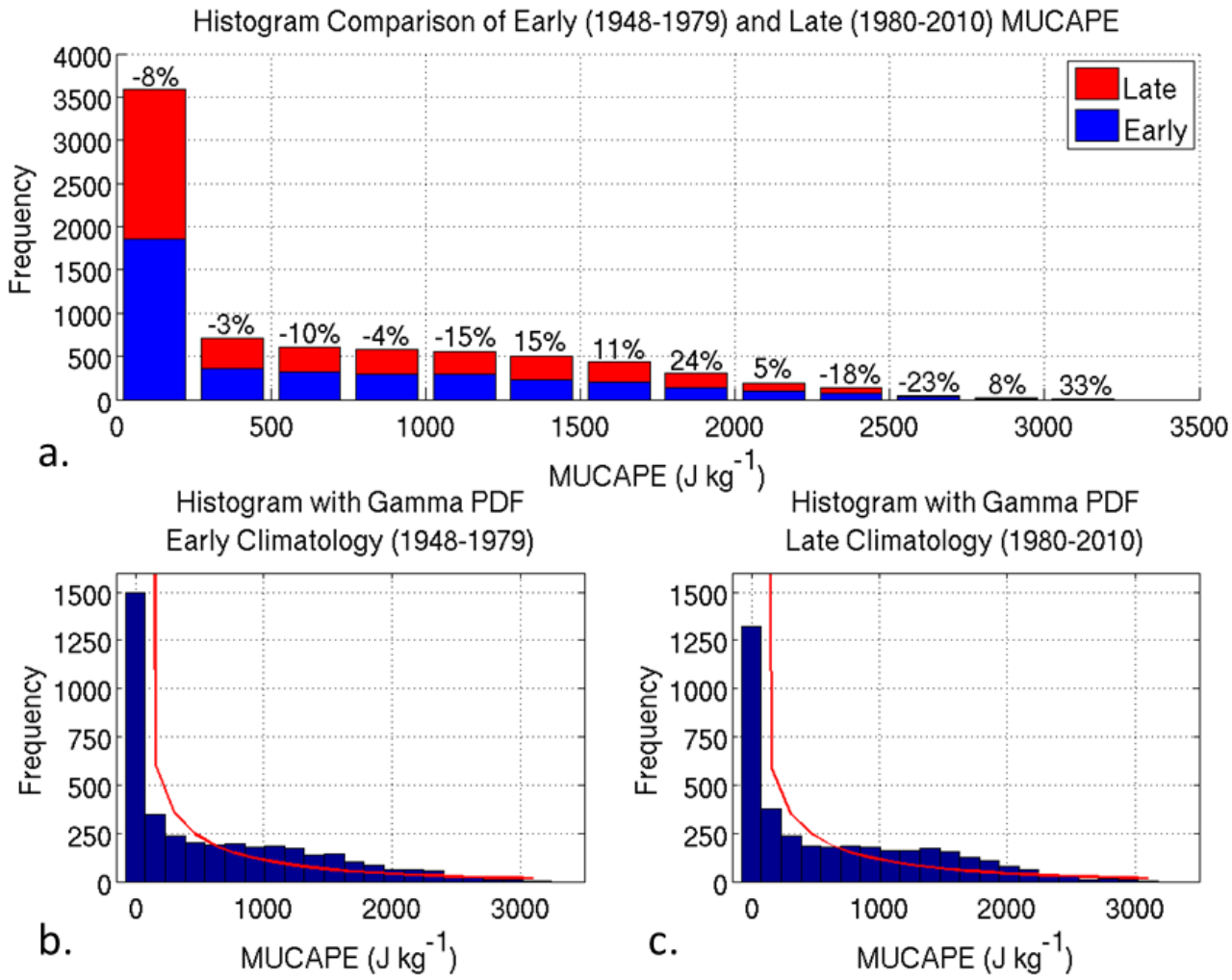

<u>Figure 33</u>: Histogram comparison of MUCAPE (in J kg^{-1}) values based on dynamically downscaled WRF-RCM regional atmospheric reanalysis data for all days during the monsoon period (JJAS) for an area averaged over Tucson, Arizona. The figure includes: a. stacked histogram comparison of the early (1948-1979) and late (1980-2010) period where the percentage of change over the two periods is indicated for each bin and histograms, along with the consequent gamma probability distribution functions (red), for the b. early period and c. the late period.

c) Observed changes in monsoon precipitation from CPC data

The corresponding long-term precipitation differences during early and late summer in the CPC gauge-derived precipitation (*Fig. 34*) appear to be consistent with the overall projected changes in monsoon precipitation in CMIP5 models as recently reported by Cook and Seager (2013). Their analysis suggests that early season monsoon precipitation will decrease and late season monsoon precipitation will increase. Indeed, observed long-term trends in the CPC precipitation data show a decrease in monsoon precipitation in Arizona during June-July and an increase during August-September. However, the largest increases in precipitation occur over the highest elevations. For example, in Arizona during August-September, precipitation has been increasing over the Mogollon Rim in central Arizona and the other mountain ranges in southeast Arizona, but decreasing in the far western part of the state near the Colorado River valley. These types of spatial differences in monsoon precipitation are important, in the sense that they bear on monsoon climate change impacts assessment on DoD facilities located in the eastern versus western part of the state. But they simply cannot be resolved within the CMIP models.

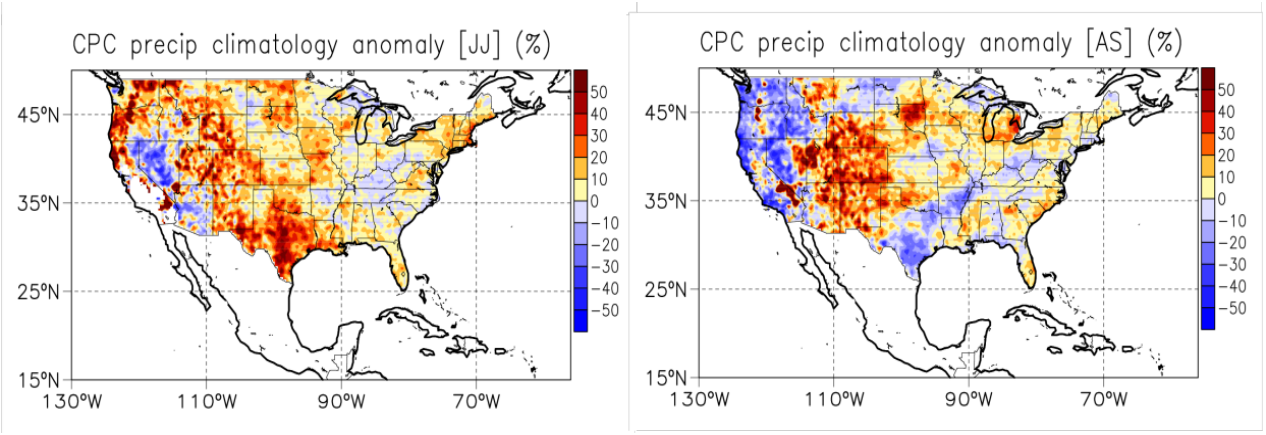

Figure 34: Long term percentage changes in early (JJ) and late (AS) warm season precipitation in CPC gage precipitation, considering the periods 1980-2010 vs. 1950-1979.

2. Changes in transient inverted troughs and response of monsoon precipitation

The analysis of long-term changes in atmospheric thermodynamic conditions during the monsoon just shown suggests that the thermodynamic environment in the Southwest is generally becoming more favorable for monsoon thunderstorms. However, long-term changes in observed monsoon precipitation show that monsoon precipitation in some areas, like the low desert areas of western Arizona and the Colorado River Valley, has been decreasing. In these areas away from the mountain ranges, the dynamic forcing mechanisms are much more important for

monsoon precipitation. In particular, organized, westward propagating mesoscale convective systems in Arizona are usually associated with a transient inverted trough and a gulf surge.

Long-term changes in IV tracks from the downscaled reanalysis are examined to determine whether or not this aspect of dynamic forcing for monsoon thunderstorms has significantly changed over the last thirty years as compared to the previous thirty years, and these results are shown for time slices during the monsoon in *Fig. 35*. Statistical and field significance of mapped changes in track density are computed using Monte Carlo randomization methods, consistent with Livezey and Chen (1983). During the early part of the monsoon, no statistically significant changes in IVs track density are found. However, during the latter part of the monsoon, in particular the month of August, the frequency of inverted troughs in the Southwest has significantly decreased while they have significantly increased further to the south in central and western Mexico. These long-term changes in IV tracks are due to the fact that the monsoon ridge over western North America is becoming spatially larger and more intense in late summer, shifting the tracks of IVs further south on its southern side (*Fig. 36*).

Changes in monsoon precipitation based on observed CPC precipitation data are considered for trough versus no-trough days in *Fig. 37* and *Fig. 38*. Trough days are defined when there was an objectively identified IV that occurred anywhere in the Southwest U.S. and northern Mexico (approximately corresponding to the intermediate domain of WRF severe monsoon weather event simulations) by the tracking algorithm. Where there is no statistically significant change in inverted troughs in the early part of the monsoon (June-July), the model simulated monsoon precipitation on both the trough and no-trough days has increased. However, when the frequency of inverted troughs significantly decreases in August, there are decreases in precipitation localized to central and western part of Arizona, away from the mountain ranges. The 35 km downscaled reanalysis is not able to simulate these changes well (not shown), because of its poor representation of organized convection.

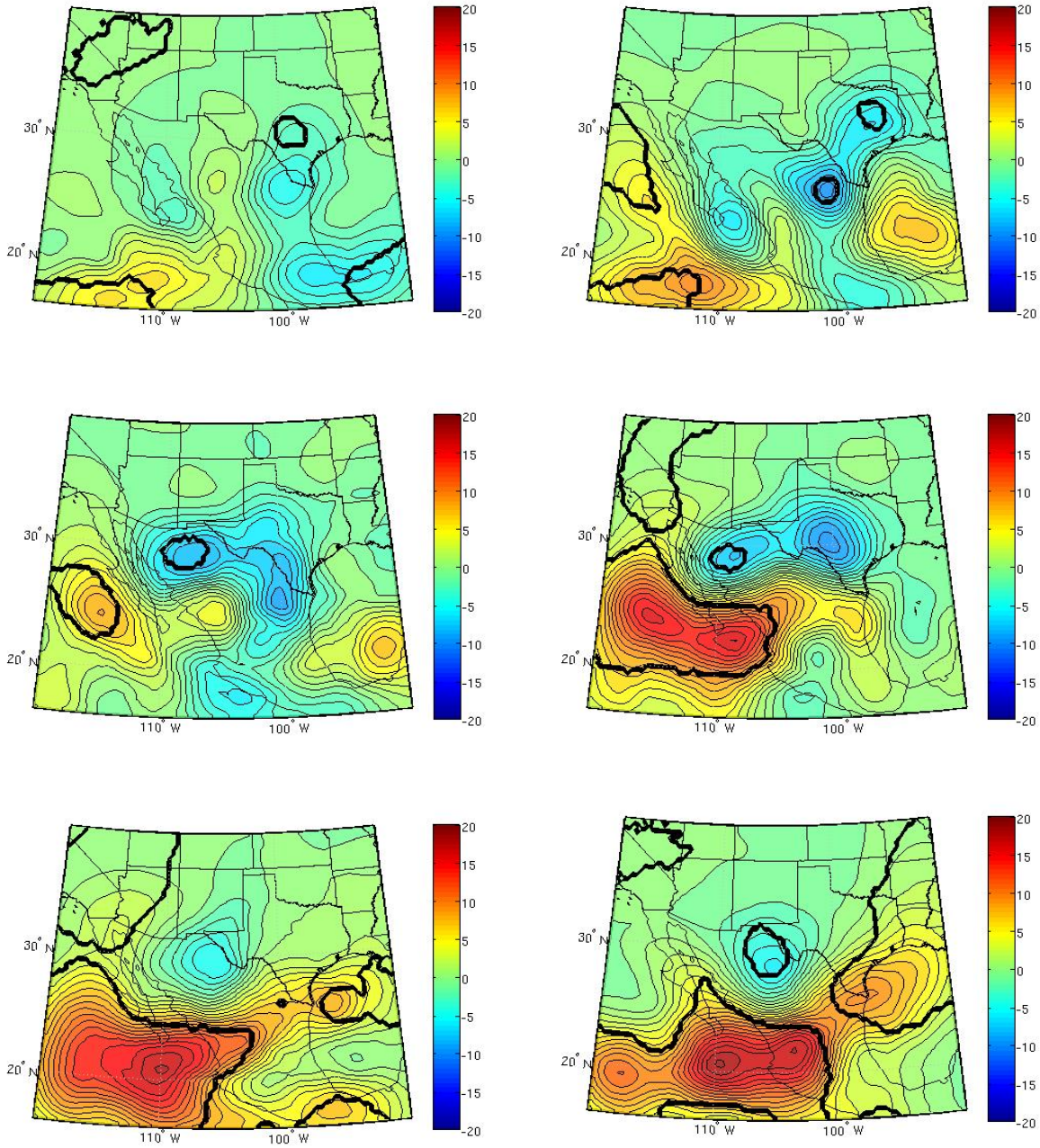

<u>Figure 35:</u> Long-term changes in IV track density in downscaled reanalysis, period 1980-2010 minus 1950-1979 (going from left to right, top to bottom): 4 June – 6 July, 19 June – 21 July, 4 July – 5 August, 19 July – 20 August, 3 August – 4 September*, and 18 August – 18 September*. Locally statistically significant areas indicated by dark black line. An asterisk indicates periods in which differences are field significant.*

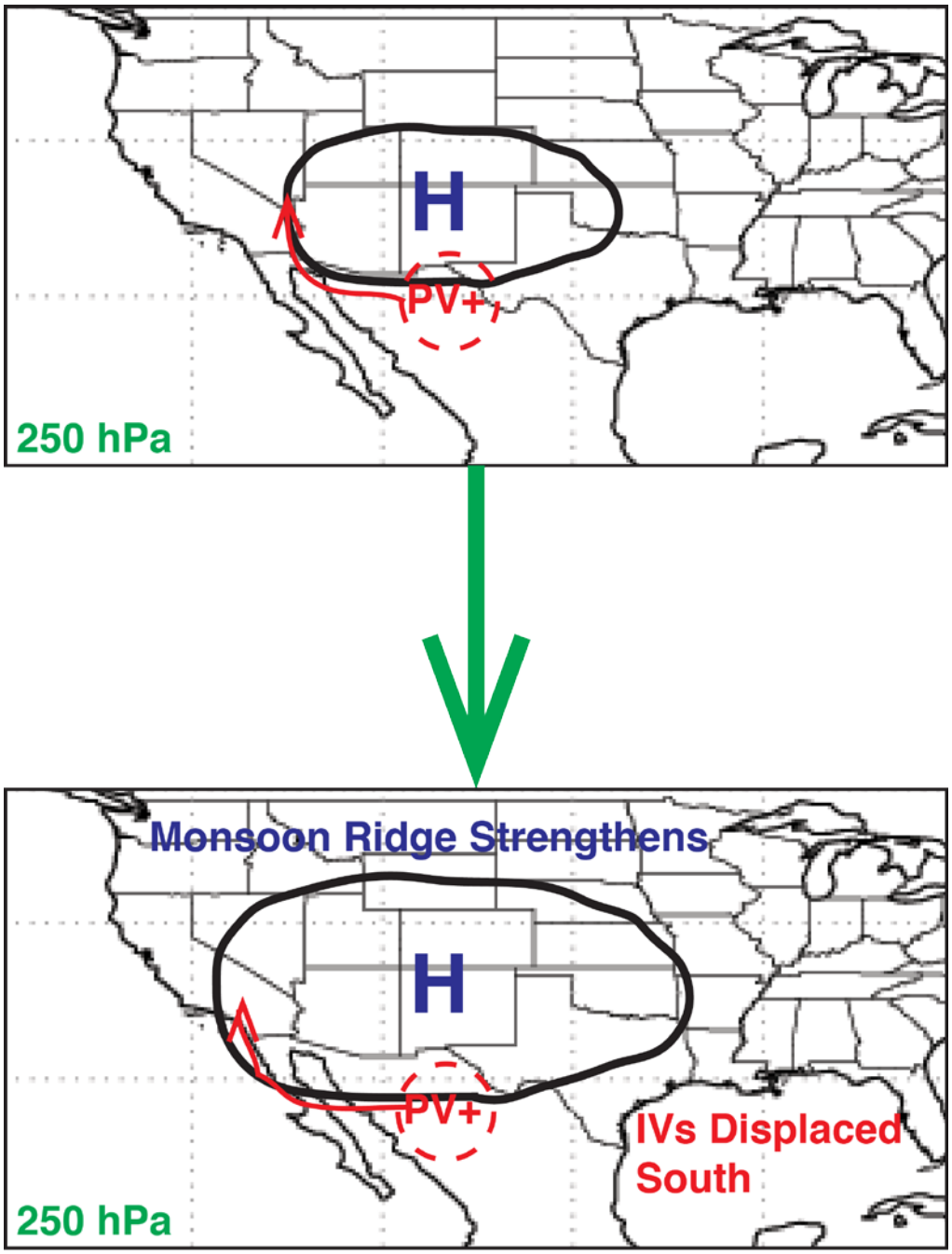

Figure 36: Conceptual illustration of changing upper troposphere (250 hPa) dynamics during the NAM season. The strengthening monsoon high is displacing PV anomalies (IVs) away from its center.

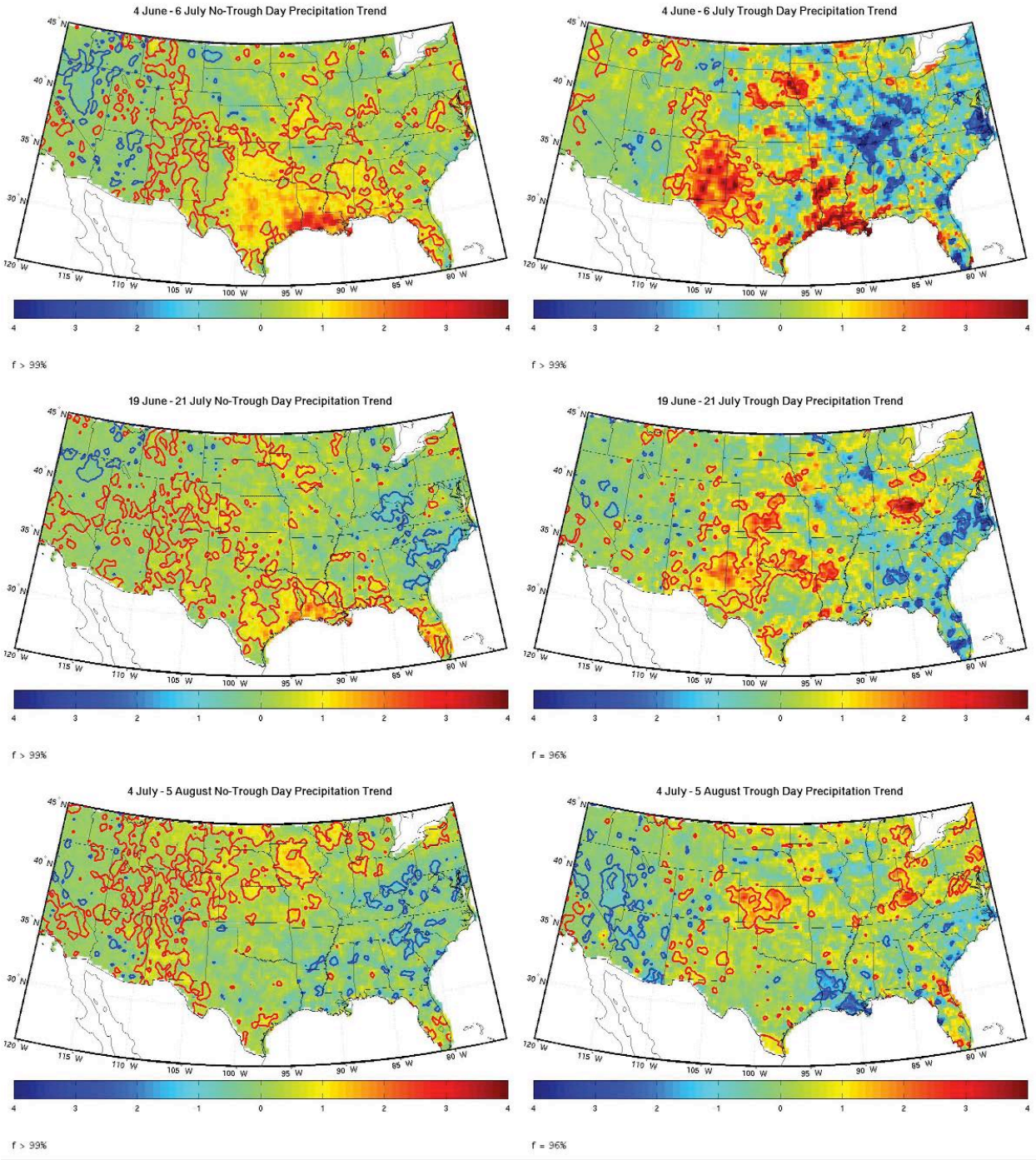

<u>Figure 37</u>: Daily 24-hour average precipitation (mm) change between the early and late periods for no-trough days (left) and trough days (right). Dates include 4 June – 6 July (top), 19 June – 21 July (middle), and 4 July – 5 August (bottom). Statistically significant positive (negative) areas are contoured in red (blue). Precipitation data are from the CPC gridded precipitation dataset. Field significance is shown in the bottom left corner of each plot.

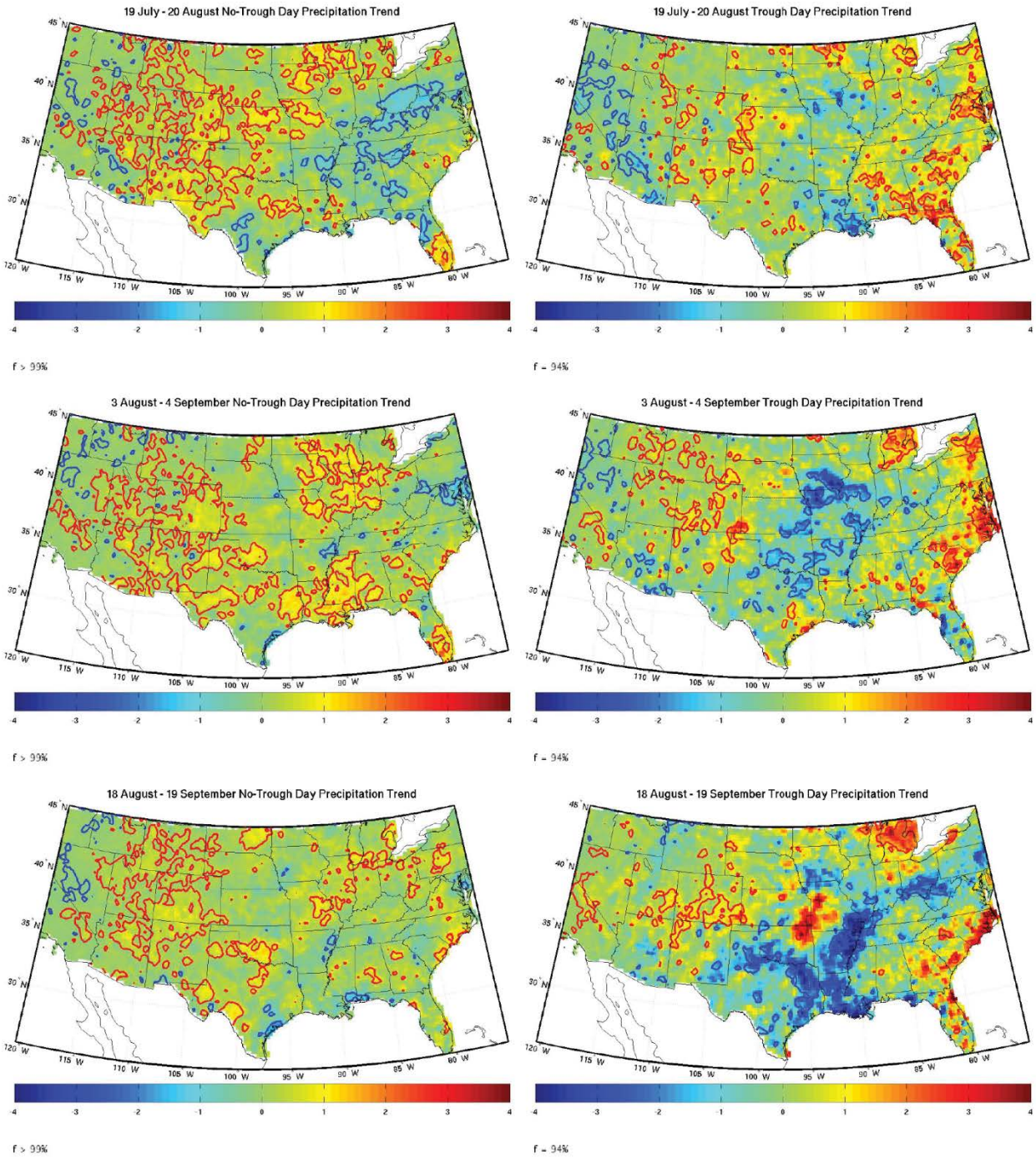

Figure 38: Daily 24-hour average precipitation (mm) change between the early and late periods for no-trough days (left) and trough days (right). Dates include 19 July – 20 August (top), 3 August – 4 September (middle), and 18 August – 19 September (bottom). Statistically significant positive (negative) areas are contoured in red (blue). Precipitation data are from the CPC gridded precipitation dataset. Field significance is shown in the bottom left corner of each plot.

E. CONVECTIVE-PERMITTING MODEL SIMULATIONS OF SEVERE WEATHER EVENT DAYS, PART ONE: DOWNSCALED NCEP-NCAR REANALYSIS

Thermodynamically favorable severe weather event days identified in the WRF dynamically downscaled reanalysis during a retrospective "present day" period (1991-2010) are first simulated with a convective-permitting grid spacing of 2.5 kilometers. Results from these simulations are compared with hourly observed precipitation (derived from gauge and radar data), to verify that the atmospheric model can reasonably represent the diurnal cycle of precipitation and its relationship to convective organization and propagation. Severe weather event days within a retrospective "historical past" period (1951-1970) are then simulated. Differences in the behavior of precipitation between the "present day" and "historical past" periods help reveal the impact of long-term observed changes in atmospheric moisture and instability on severe monsoon weather. The total number of simulated days in the "present day" and "historical past" periods is 255 and 268, respectively.

1. Performance of severe weather event day simulations during period of Stage IV product

To verify the performance of the WRF severe weather event simulations on the CPM grid prior to any evaluation of long-term trends in precipitation intensity, we compare model-simulated precipitation to the Stage IV combined radar-gauge observed precipitation product during the nine-year period 2002-2010. We first consider precipitation climatology of the severe weather event days, and then the modeled treatment of the diurnal cycle of precipitation from the hourly data.

a) Daily precipitation evaluation

The model simulated daily average precipitation (over 24 hours of the convective day) and corresponding Stage IV precipitation for all thermodynamically favorable severe weather event days, based on the 35 km downscaled NCEP Reanalysis, is shown in *Fig. 39*. The Stage IV data shows that the thermodynamically identified severe weather event days have widespread precipitation over all of the Southwest, particularly Arizona and New Mexico. The average observed daily precipitation is a maximum (greater than 5 mm) over the highest elevations because the mountains are the focal point for convective initiation. For example, the highest average observed precipitation in Arizona occurs over the Mogollon Rim, which roughly bisects the state from the southeast to the northwest corners (*Fig. 39*, top-right). Generally, the CPM severe weather event simulations exhibit similar behavior in terms of capturing the terrain-dependence of monsoon precipitation and show precipitation occurring throughout the Southwest. There is an underestimation of precipitation in the CPM simulations on the order of

1-2 mm day^{-1} (*Fig. 39*, top-left). In contrast, similar to the WRF simulations of Tripathi and Dominguez (2013), there is a widespread area of overestimation of precipitation from the coarser resolution simulation, generally on the order of 3-5 mm day^{-1} and even high within in mountainous areas (*Fig. 39*, bottom-right). Overall, the CPM yields precipitation amounts and a spatial pattern that better corresponds to the Stage IV product than the equivalent coarse resolution model grid.

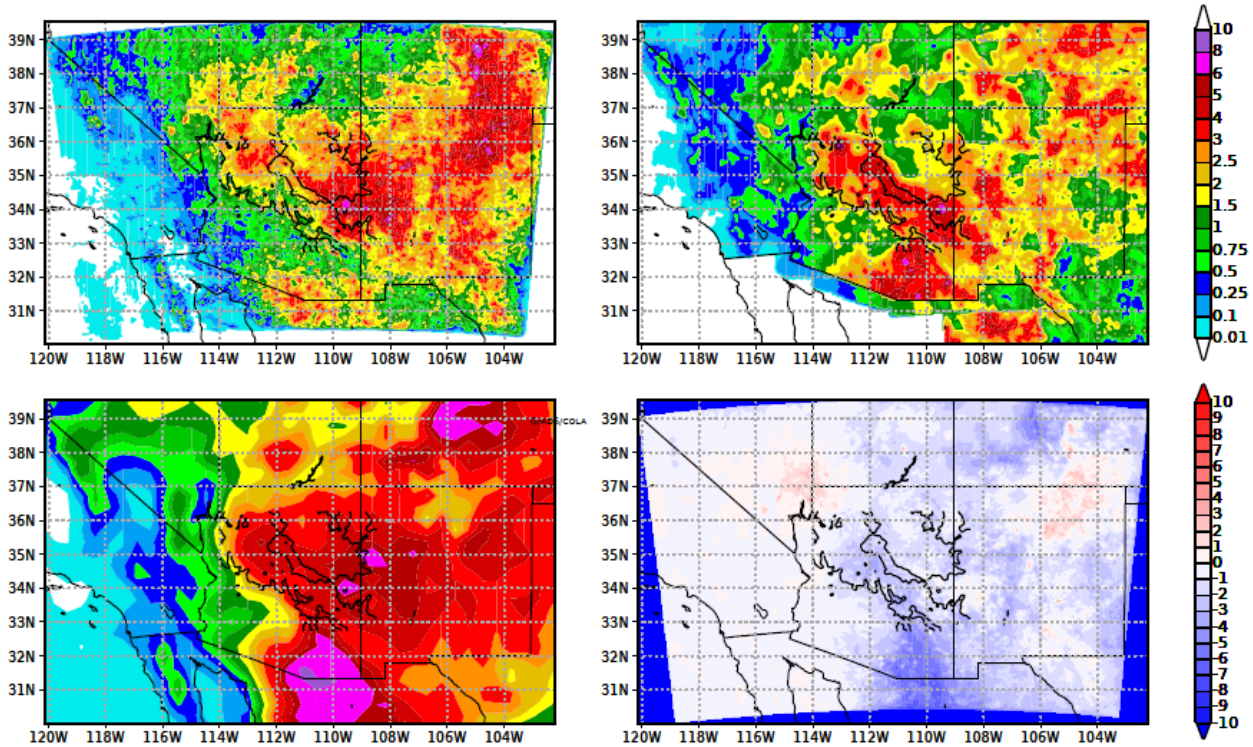

*<u>Figure 39</u>**:** Composite daily means of precipitation (mm day^{-1}) for all selected severe weather event days during 2002-2010 of convective-permitting simulation (top-left), Stage IV observation (top-right), course resolution simulation (bottom-left), and difference in convective-permitting minus course resolution (bottom-right). Location of the Mogollon Rim indicated by terrain relief contours (in black) at 1000 m intervals within the state of Arizona.*

<u>b) Diurnal cycle of model simulated precipitation</u>

The CPM simulations are also able to reasonably simulate the diurnal cycle of convection, with a maximum in precipitation centered over areas of high terrain during the afternoon (11am to 5pm local time), westward propagation of the precipitation off the terrain of the Mogollon Rim during early evening (5pm to 11pm local time), and weakening and dissipation of precipitation during

the late evening to early morning (11pm to 5am local time). The propagation of monsoon precipitation during the late afternoon to early evening is demonstrated in *Fig. 40* in terms of the precipitation rate averaged over the six-hour time period. The precipitation at later times in the day reflects the presence of westward-propagating MCSs as previously mentioned. Evolution of rainfall in the state of New Mexico is also well captured in terms of pattern and intensity at selected peak hours from 11 am to 11 pm. The CPM simulations are, therefore, capable of reproducing the heavy rainfall event precipitation climatology at the very high resolution spatiotemporal resolution (2.5 km, hourly).

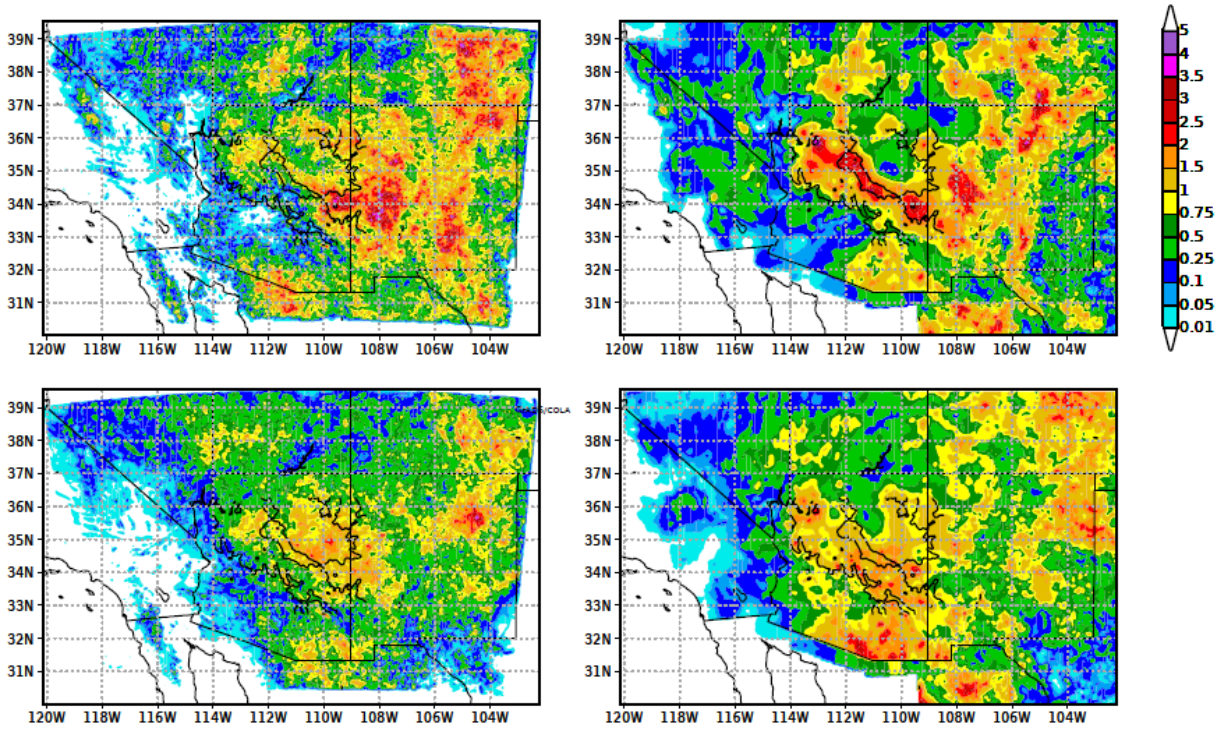

Figure 40: Peak-hour composite 6-hourly means of precipitation [mm hour^{-1}] for all selected severe weather event days during 2002-2010 of convective-permitting simulation (left), and Stage IV observation (right) plotting from 11am to 5pm (top), and from 5pm to 11pm (bottom). Location of the Mogollon Rim indicated by terrain relief contours (in black) at 1000 m intervals within the state of Arizona.

2. Observed and simulated long-term changes in monsoon thunderstorms in the Southwest

Long-term changes in monsoon precipitation are evaluated from the perspective of both observations and results of the CPM severe weather event simulations. Observations in this case are station National Climate Data Center (NCDC) coop precipitation data and the daily gridded CPC precipitation product. In the presentation of these results, we attempt to distinguish between the mean changes in precipitation versus the changes in precipitation extremes in the tails of the distribution. For evaluation of the latter, we apply the extreme value statistical analysis peak over threshold technique described earlier.

a) Observed and model-simulated changes in daily precipitation distribution

The histogram of NCDC coop station precipitation data shows that Phoenix and Flagstaff have experienced an increase in precipitation extremes during the "present" period 1991-2010 as compared to the "historical" period 1951-1970 (*Fig. 41*, left). The red and blue lines on the figure are the peak-over-threshold generalized Pareto distributions fitted to the right tail of the PDF for precipitation events above the 90^{th} percentile. The fitted distributions satisfy the Chi square goodness-of-fit test at significance level $\alpha = 0.1$. The increase in extremes in monsoon precipitation in Phoenix can be interpreted as a broadening and flattening of the daily precipitation distribution. The differences are statistically significant tested with bootstrapping at significance level $\alpha = 0.1$. The right side of *Fig. 41* shows the same analysis performed for the CPM-simulated severe weather events. Though CPM-simulated precipitation exhibits a dry bias, as discussed earlier with reference to comparison with the Stage IV product, it shows basically the same type of broadening and flattening of the distribution as the observed station data.

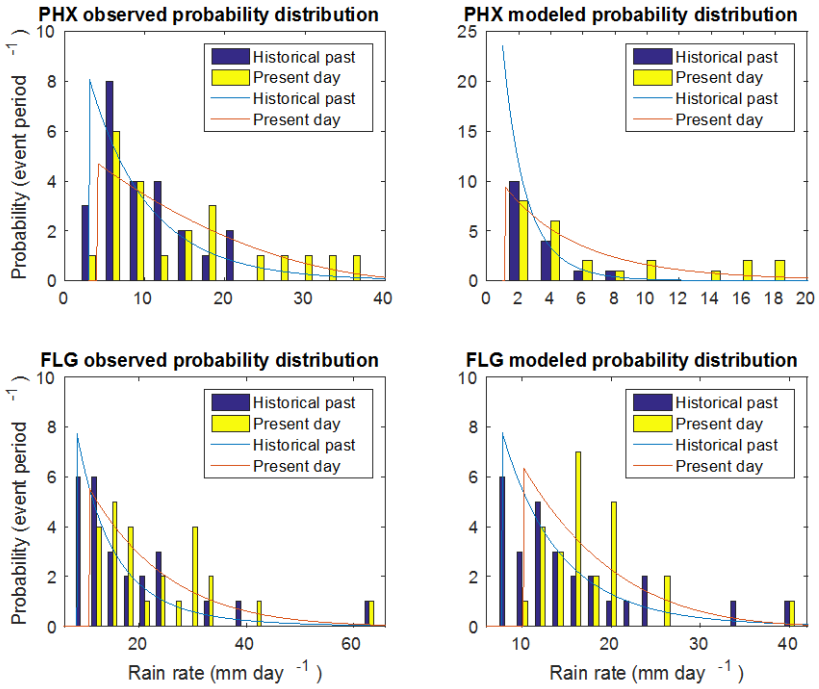

<u>Figure 41:</u> Probability distributions of daily precipitation extremes in Phoenix (top), and Flagstaff (bottom) of NCDC coop (left) and convective-permitting simulation (right). Blue and yellow bars are station histograms. Light blue and red lines are peak-over-threshold General Pareto distributions fitted into the right tail of the PDF with events on the right of 90 percentile.

<u>b) Spatial patterns of changes in precipitation mean and extremes</u>

The idea of a broadening and flattening of the daily precipitation distribution also holds over the entire Southwest, in the context of comparing the observed CPC gridded precipitation product with the simulated severe weather events within the CPM domain. The "present day" minus "historical past" period change in mean daily CPC and coop observed precipitation for all days during the monsoon months of July and August is shown in *Fig. 42* (left), in terms of the absolute change. From the observational standpoint, mean daily monsoon precipitation has decreased as a whole in Arizona in recent decades. The largest absolute precipitation decreases in the CPC product occur over the Mogollon Rim (1 mm day^{-1} or greater than 30%). The largest precipitation percentage decreases occur in the Colorado River Valley and over southwest Arizona (40-50%), an area of the state where the more infrequent, organized convection accounts for the majority of monsoon precipitation (e.g. Castro et al. 2007).

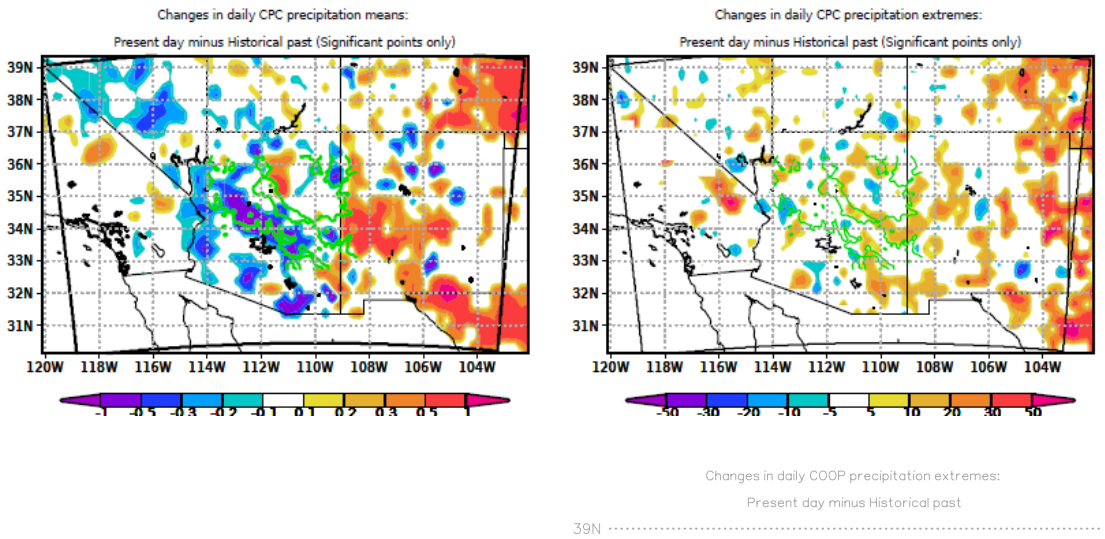

<u>Figure 42:</u> Changes (present day minus historical past) in CPC (top), and NCDC coop (bottom) of mean (left), and extreme (right) precipitation (mm day^{-1}). Only grid points that satisfied a statistically significant test are plotted in top panels. Stations that satisfy a statistically significant test in bottom panels are circled. Location of the Mogollon Rim on CPC data indicated by terrain relief contours (in green) at 1000 m intervals within the state of Arizona.

However, the corresponding pattern of changes in extreme monsoon precipitation is quite different than that of the mean just shown. Characterizing the changes in extreme event precipitation within the CPC daily precipitation data is done with the top 20% of heavy precipitation days for each grid pixel. Using this limited subset of days, we characterize the changes in extreme precipitation above the 90th percentile using peaks over threshold analysis technique. With these filters applied (*Fig. 42* top right) the CPC data would seem to indicate that observed extreme event monsoon precipitation is, at least, not decreasing. The patchy nature of areas with significant changes in precipitation increases likely reflects the fact that the gridded CPC product is relatively more challenged to represent the long-term changes in extreme monsoon precipitation as compared to changes in mean, we suspect due to the limitations in availability of long-term station data in the Southwest and/or its data interpolation techniques. The corresponding coop station precipitation data analysis presents a clearer picture of the

changes in extremes (*Fig. 42*, bottom right). The largest and most statistically significant increases in extreme precipitation in the Southwest occur at the stations located in the southwestern portion of Arizona, namely Yuma (30 mm) and Alamos (45 mm). The change in sign of the precipitation change from the mean trends, at least in the actual coop station data in Phoenix and other stations in southwest Arizona, is consistent with the conceptual idea of a broadening and flattening of the precipitation distribution as discussed earlier.

In addition to the CPC daily precipitation product and the coop station precipitation, the equivalent changes in means and extremes were calculated in the Maurer and Liveneh gridded daily precipitation datasets (*Fig. 43*). As noted earlier in the description of data, the Liveneh daily precipitation product is essentially an upgraded version of the Maurer product at higher resolution. There are some very important comparisons and contrasts to be made with these data to the CPC product over the same time period. The pattern of change in mean precipitation is nearly identical, with the maximum decrease in precipitation centered on the Mogollon Rim. However, the pattern in the changes of extreme precipitation is quite different. Both Maurer and Liveneh datasets indicate a statistically significant increase in extreme event precipitation throughout the western half of Arizona, especially south and west of the Mogollon Rim, better corresponding to the actual coop station data.

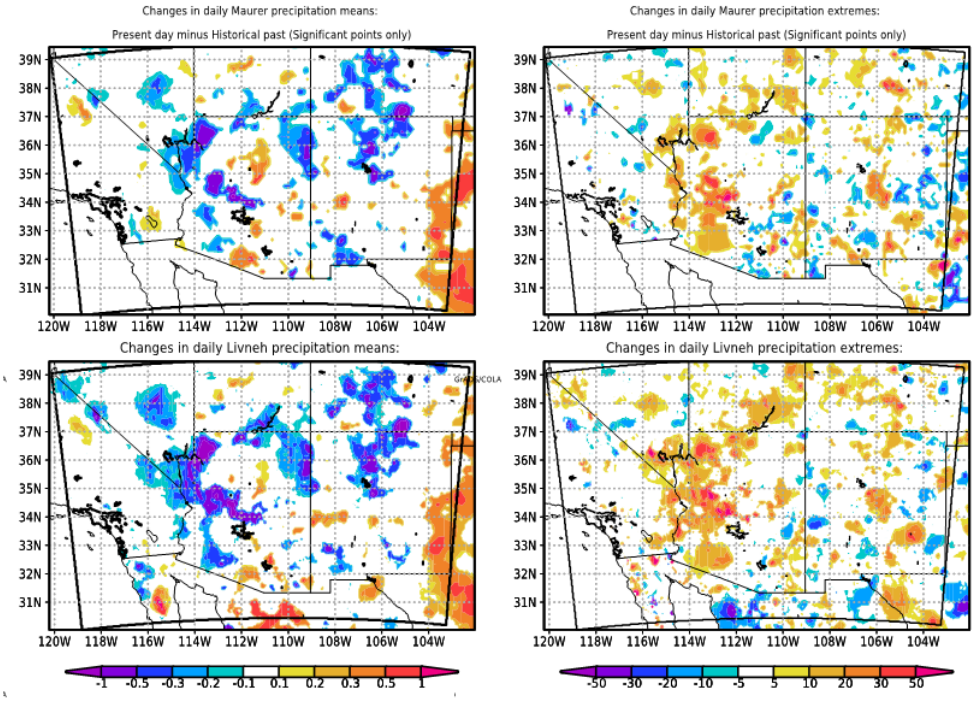

Figure 43: Equivalent to CPC analysis presented in Fig. 42, but for Maurer and Liveneh daily precipitation datasets as labeled. Precipitation changes in mm day^{-1}.

The simulated precipitation changes from the "present day" to "historical past" are shown in *Fig. 44* for the severe weather event simulations at the course resolution 35 km (top) and the CPM 2.5 km grid spacing (bottom), for the significant changes in mean precipitation (left) and extreme precipitation beyond the 90th percentile (right). As in the CPC and NCDC coop observations for the entire warm season in *Fig. 42*, both the course resolution and convective-permitting simulations show a decrease in mean precipitation for the simulated severe weather events between the two simulation periods, with decreases maximized in Mogollon Rim of Arizona. As has been suggested by observational coop station precipitation data, the course resolution and convective-permitting simulations show statistically significant increases in extreme precipitation in the Southwest for the region as a whole.

The exact geographic locations where the modeled extreme precipitation is becoming more intense and the spatial extent of the increases are markedly different between the two simulations. The CPM simulations show: 1) a relatively coherent and larger geographic area where extreme precipitation is becoming more intense; 2) the most dramatic increases in Arizona occur in areas immediately to the west (downwind) of the Mogollon Rim, where organized MCS-type convection accounts for a greater proportion of the monsoon precipitation and the greatest increases in precipitable water occur in the downscaled reanalysis; and 3) corresponds to the same geographic location where the coop station data and Maurer and Liveneh observational precipitation products show the largest increase in precipitation extremes, including the Phoenix metropolitan area and southwestern low desert areas of the state. In these areas the increase in extreme daily monsoon precipitation is on the order of 10 mm day^{-1} (approximately one-half inch) or greater. By contrast, the coarser resolution model does not capture the correct geographic location of where extreme precipitation in increasing, as its increases are more centered over mountainous areas like the Mogollon Rim (*Fig. 44*, right). The CPM substantiates the conceptual idea of a broadening and flattening of the distribution of daily monsoon precipitation in the areas where the changes in precipitation extremes are statistically significant in *Fig. 42* and *Fig. 43*, with decreasing mean daily precipitation but increasing extreme event precipitation intensity.

To further substantiate that the convective-permitting simulations are providing the best representation of the observed changes in precipitation, a quantitative comparison of the spatial patterns of precipitation trends is made between the modeled versus the Liveneh observed precipitation product. The comparison is made in the following way. Model trends from the coarse resolution (35 km) and convective-permitting resolution (2.5) severe weather event simulations as shown in *Fig. 44* are regridded to match the Liveneh data. Then a trend comparison metric is computed at those points that exhibit statistically significant trends in the precipitation observations. The trend in model is divided by the trend in the model and multiplied by 100%, and these results are shown in *Fig. 45*. Using this metric, a positive value means that the trends from observations and model simulations are both statistically significant

and of the same sign. A value of 100 means that the model trend perfectly matches the observed trend. A negative value means that trends from observations and model simulations are both statistically significant but of opposite sign. The most important message this quantitative comparative analysis between models and observations yields is that the convective-permitting model simulations produce trends in extreme event precipitation that better match the spatial location of the observed extreme event increases in the Liveneh data. The spatial pattern of changes in means may be represented better in the coarse resolution 35 km simulation, but the modeled precipitation decreases are substantially overestimated. Repeating the same procedure with the Maurer data yields a nearly identical result (not shown).

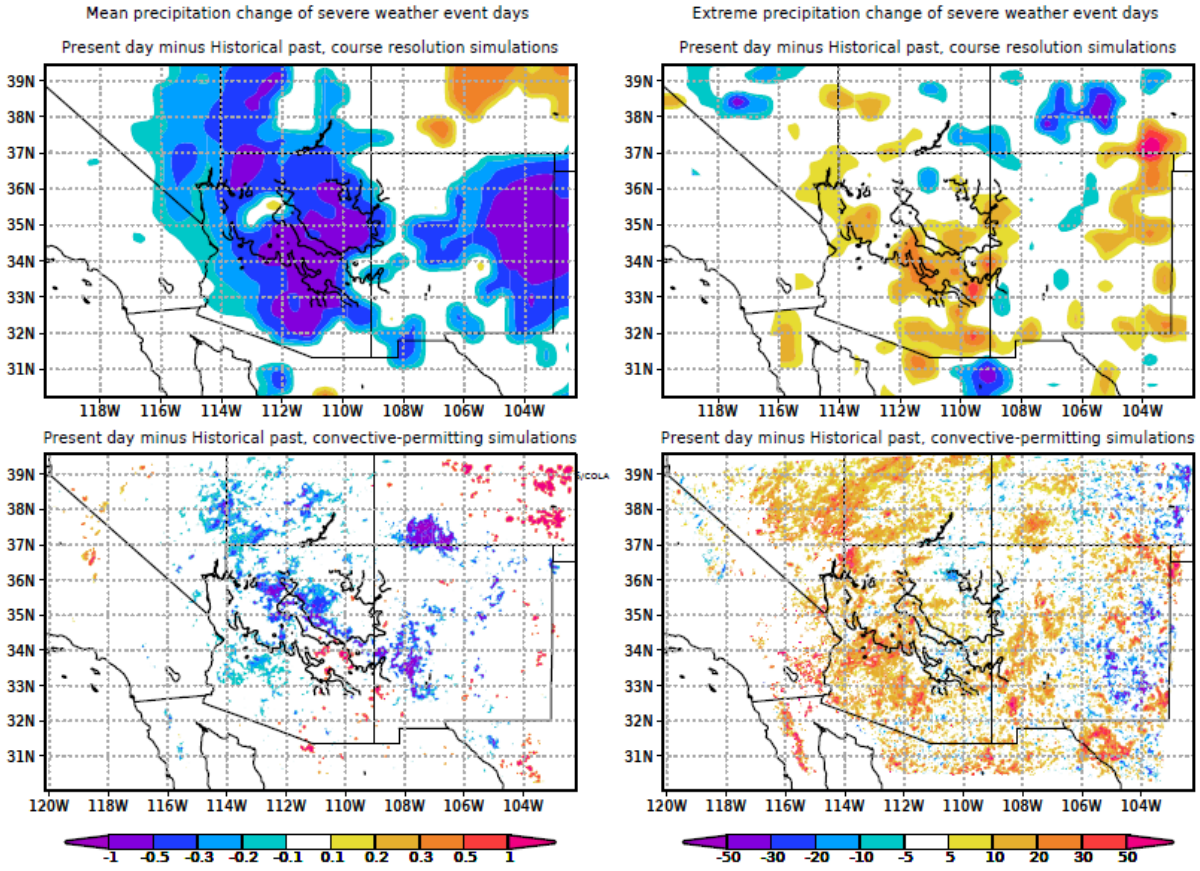

Figure 44: Changes (present day minus historical past) in course resolution (top), and convective-permitting simulations (bottom) of mean (left), and extreme (right) precipitation (mm day^{-1}). Only grid points that satisfied a statistically significant test are plotted. Location of the Mogollon Rim indicated by terrain relief contours (in black) at 1000 m intervals within the state of Arizona.

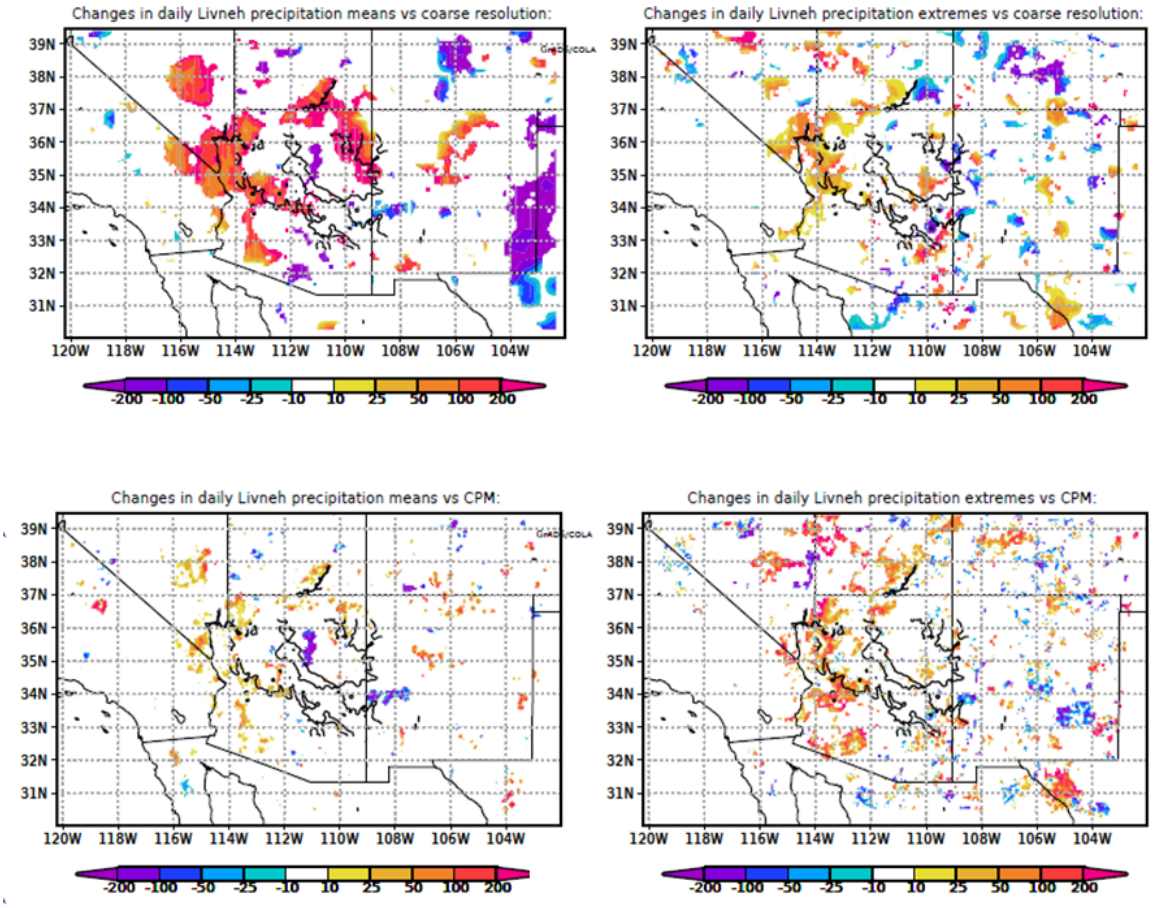

<u>Figure 45:</u> Precipitation trend comparison metric as applied to Liveneh data for changes in means and extremes for coarse resolution (35 km) simulations of severe weather event days and equivalent convective permitting simulations, as labeled. A description of how to interpret the trend comparison metric provided within the text.

d) Simulated changes in downdraft intensity from DCAPE

The changes in mean downdraft intensity (w_{max}) (*Fig. 46*, left) calculated from DCAPE for all CPM-simulated severe weather event days show a decrease in intensity of downdrafts, due to the more moist low-level environment overall. But in the most extreme storms, the convective downdrafts are tending to be more intense in the "present day'' period (*Fig. 46*, right). So the idea of a broadening and flattening of the distribution not only applies for extreme rainfall, but also to DCAPE as well.

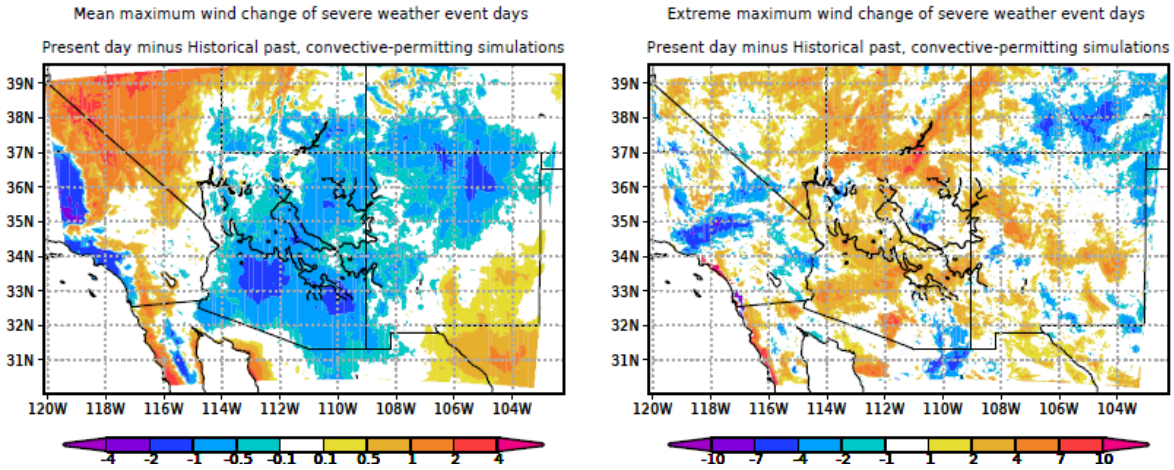

Figure 46: Changes (present day minus historical past) in convective-permitting simulation mean (left) and extreme (right) of downdraft intensity (m s^{-1}). Only grid points that satisfied a statistically significant test are plotted. Location of the Mogollon Rim indicated by terrain relief contours (in black) at 1000 m intervals within the state of Arizona.

d) Changes in precipitation on trough vs. no-trough days in CPM simulations

Precipitation from the NWP-type convective-permitting simulations of severe weather events on no-trough days during the 19 July – 20 August and the 3 August – 4 September intervals are shown in *Fig. 47*. This figure shows widespread precipitation increases over the 60-year analysis period, particularly in Western Arizona. Precipitation increases on no-trough days are consistent with the results from the CPC dataset and are field significant. Precipitation increases in Western Arizona per the NWP-type simulations are greater than those of the CPC dataset. This may reflect the paucity of precipitation gauges in western Arizona and the subsetting of thermodynamically favorable days, as CPC trends are more similar to NWP simulations when only favorable days are selected. The trends for trough days during the same analysis intervals are shown in *Fig. 48*. These results show precipitation decreases in the low deserts of

southeastern and central Arizona on trough days in nearly the same locations as in the CPC dataset. These trends are field significant during the 3 August – 4 September interval. The consistency of the trends derived from the high-resolution simulations and the CPC dataset suggests that these precipitation trends associated with NAM convection can effectively be modeled, using the dynamically downscaled reanalysis data to drive convective-permitting simulations.

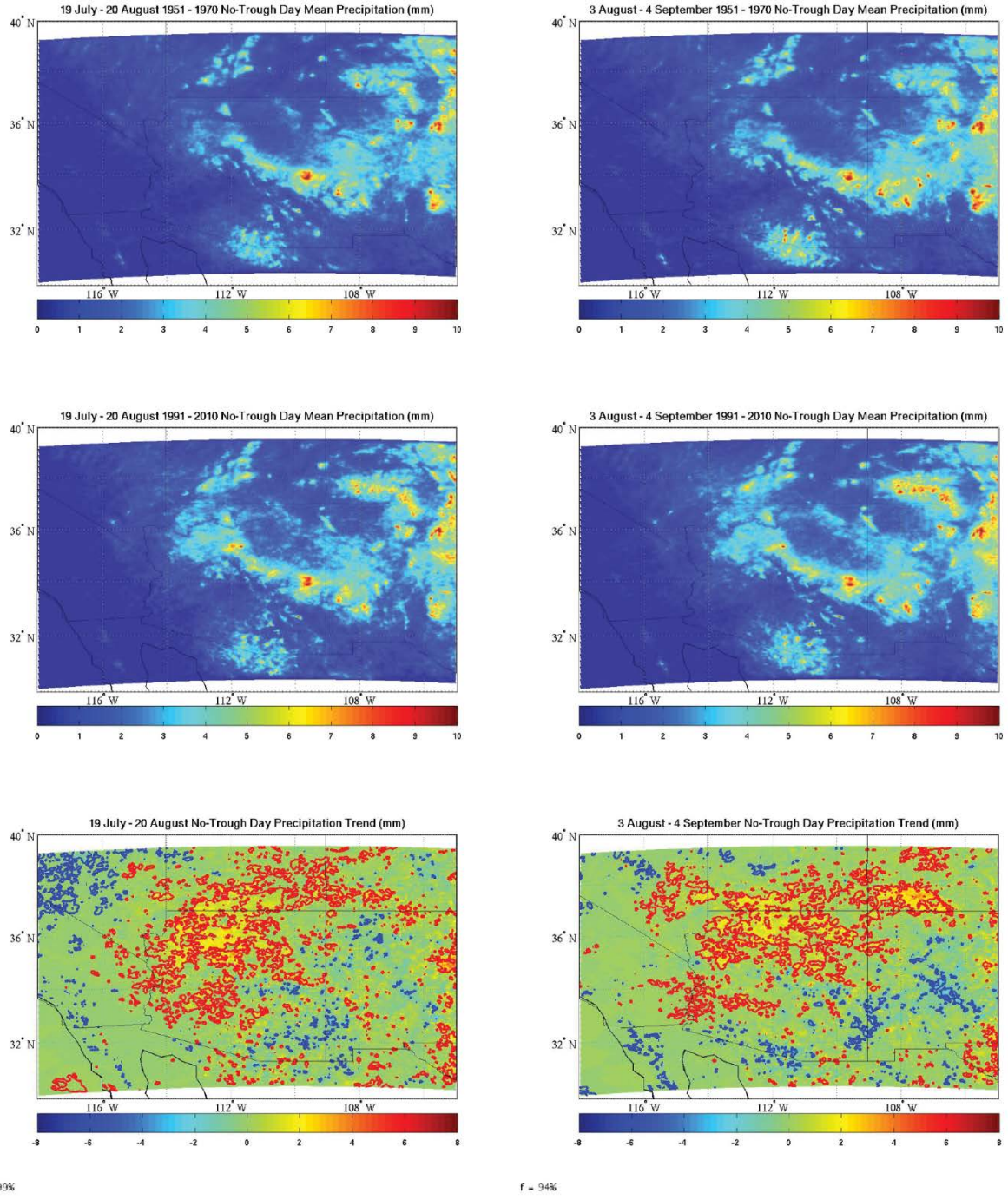

Figure 47: WRF high resolution 24-hour daily average precipitation (mm) on all no-trough days with favorable thermodynamics during the 1951-1970 monsoon seasons (top) and the 1991-2010 monsoon seasons (middle) for the dates 19 July – 20 August (left) and 3 August – 4 September (right). The difference between the two time periods is also shown (bottom). Statistically significant positive (negative) areas are contoured in red (blue). Field significance is shown in the bottom left corners of the bottom plots.

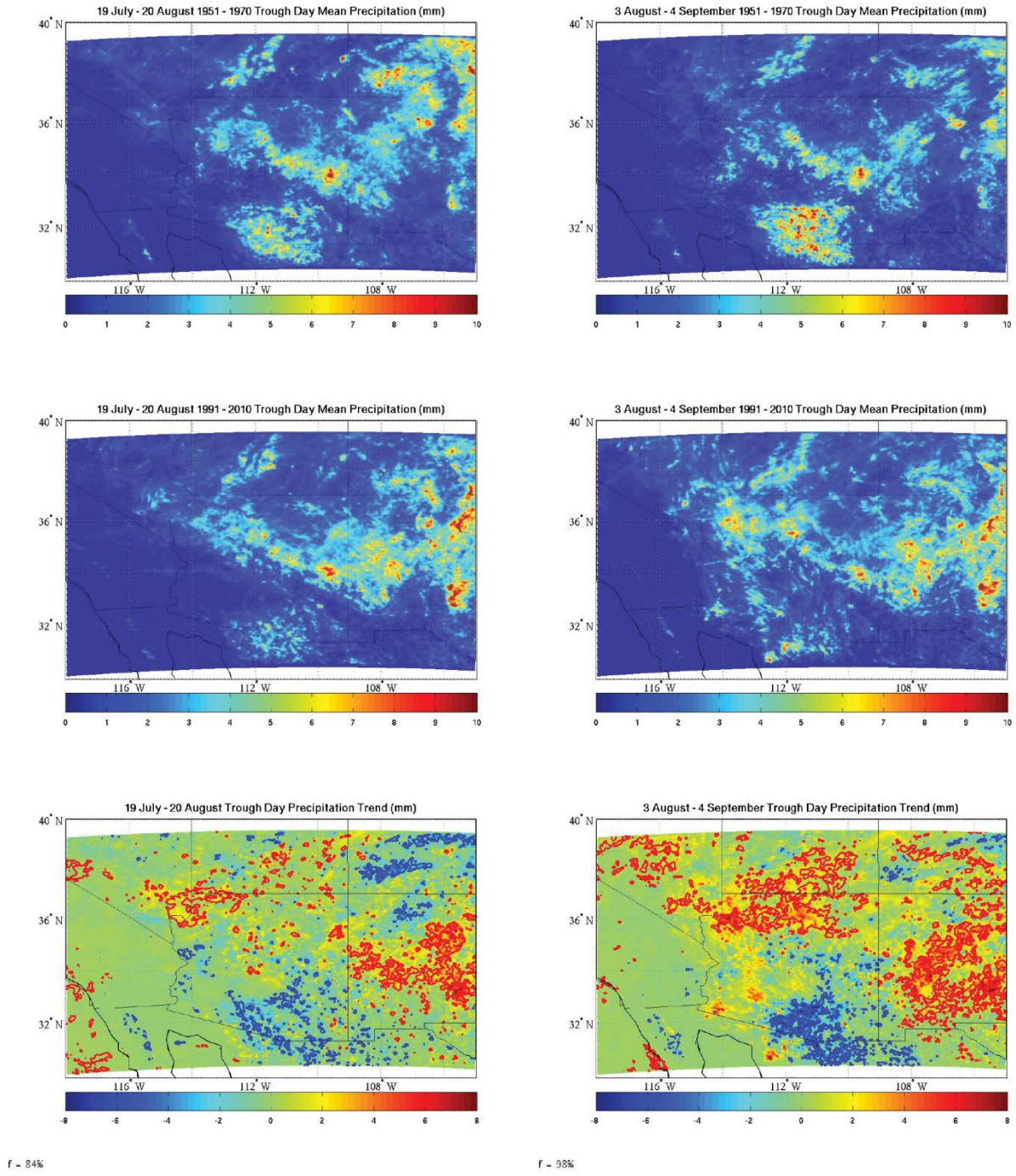

<u>Figure 48:</u> WRF high resolution 24-hour daily average precipitation (mm) on all trough days with favorable thermodynamics during the 1951-1970 monsoon seasons (top) and the 1991-2010 monsoon seasons (middle) for the dates 19 July – 20 August (left) and 3 August – 4 September (right). The difference between the two time periods is also shown (bottom). Statistically significant positive (negative) areas are contoured in red (blue). Field significance is shown in the bottom left corners of the bottom plots.

F. CONVECTIVE-PERMITTING MODEL SIMULATIONS OF SEVERE WEATHER EVENT DAYS, PART TWO: FUTURE PROJECTIONS IN DOWNSCALED CMIP MODELS

The same analysis procedures applied to the downscaled reanalysis as described in the prior Section E were applied to the four downscaled CMIP models. In this case, projected changes in the near future period of 2021-2040 are compared versus the historical period of 1991-2010. For each twenty-year subset in a given modeling paradigm, there are on the order of 200-250 individual severe weather event day NWP-type CPM simulations. Therefore, trends shown here that show the level of ensemble agreement among the models are computed from nearly 2000 event day simulations across the four CMIP models considered in the project.

1. Precipitation from CMIP modeling paradigms vs. Stage IV, downscaled reanalysis

The first step in evaluating the performance of downscaled CMIP models for the convective-permitting simulations was to compare their simulated precipitation to Stage IV observations and the prior dynamically downscaled reanalysis results, as shown in *Fig. 49*. All the CMIP products are generally able to simulate monsoon precipitation for severe weather event days, in a manner that corresponds well to the Stage IV observations in terms of precipitation amount and spatial pattern. This is very important given the wide variability in monsoon precipitation as simulated by CMIP3 and CMIP5 models, as discussed earlier. Maximum precipitation amounts in all the modeling paradigms are correctly centered on the mountain ranges. The ECHAM5 and ECHAM6 simulations tend to be wetter on average than the HadCM3 and HadGEM simulations. The HadCM3 and HadGEM simulations tend to resemble more the downscaled reanalysis. Though there is variation in model simulated precipitation, these simulations were judged suitable by their comparisons with the stage IV product to pass the go/no go decision point of the Interim Report.

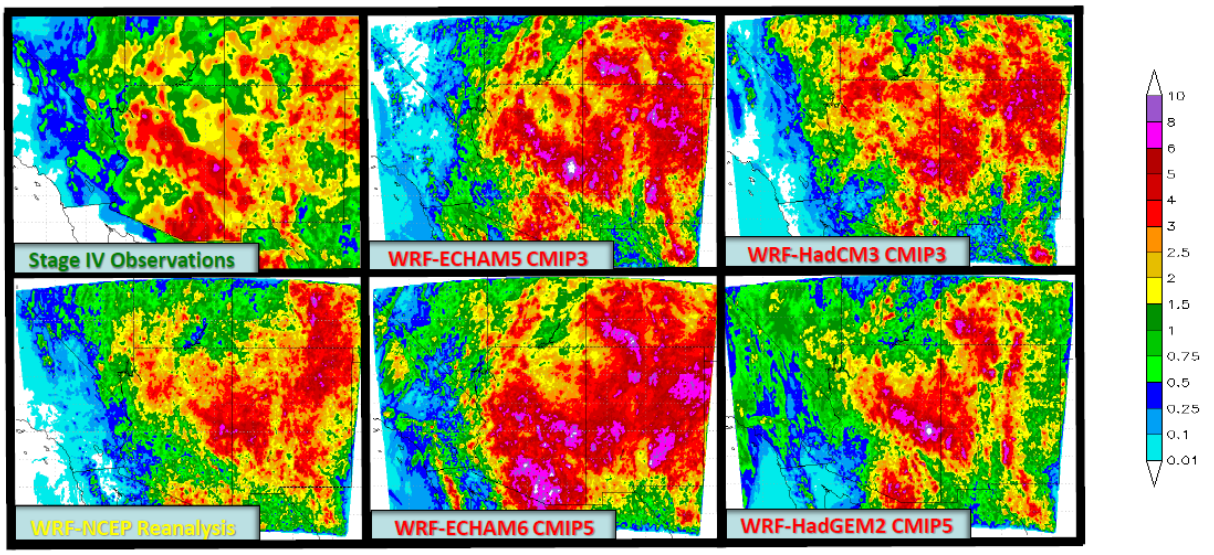

Figure 49: Daily average modeled precipitation (mm day^{-1}) in comparison to Stage IV product observations (2002-2010) for all thermodynamically favorable severe weather event days, all downscaled reanalysis and downscaled CMIP modeling paradigms.

2. Impact of bias correction within context of WRF-CCSM Argonne experiments

The same severe weather event selection methodology was applied to the dynamically downscaled CCSM-WRF 12 km simulation performed by the companion SERDP project at Argonne National Laboratory, for original and bias corrected boundary conditions. The resultant precipitation of the identified severe weather events in both simulations is shown in *Fig. 50*. In comparison to the Stage IV product observations shown in *Fig. 49*, both sets of simulations tend to generally underestimate severe weather event day precipitation in the Southwest. However, the precipitation underestimation is even worse in the bias-corrected simulation. The difference in precipitation between the bias-corrected and original WRF-CCSM simulations is shown in *Fig. 51*. Precipitation is lower in the bias-corrected simulation on the order of 0.3 to 0.6 mm day^{-1} over Arizona. In their published work, Wang and Kotamarthi (2015) note that WRF does improve on the precipitation simulated directly by the CCSM global model. However, they also explicitly note that "driving WRF bias-corrected CCSM does not always reduce the bias." Their conclusion is quite consistent with what is found by the independent analysis of their data in the Southwest within this project, as presented here. Therefore, at least given what the CCSM-WRF experiments show, the evidence is not compelling that use of bias-corrected lateral boundary conditions for any of the CMIP models used this project would result in any consistent and substantial improvements in the climatological representation of monsoon precipitation in WRF simulations of severe weather event days.

The example of severe weather event day precipitation using the original WRF-CCSM data as a lateral boundary condition is additionally shown in *Fig. 52*. The WRF-CCSM CPM data produce a pattern of precipitation that falls within the range of solutions of the other modeling paradigms shown in *Fig. 49*, an encouraging result. However, as mentioned earlier, the project was not able to produce equivalent results for any of the other WRF-CCSM simulations produced by the Argonne SERDP project, owing to technical challenges in working with these data that unfortunately could not be resolved before the end of this project.

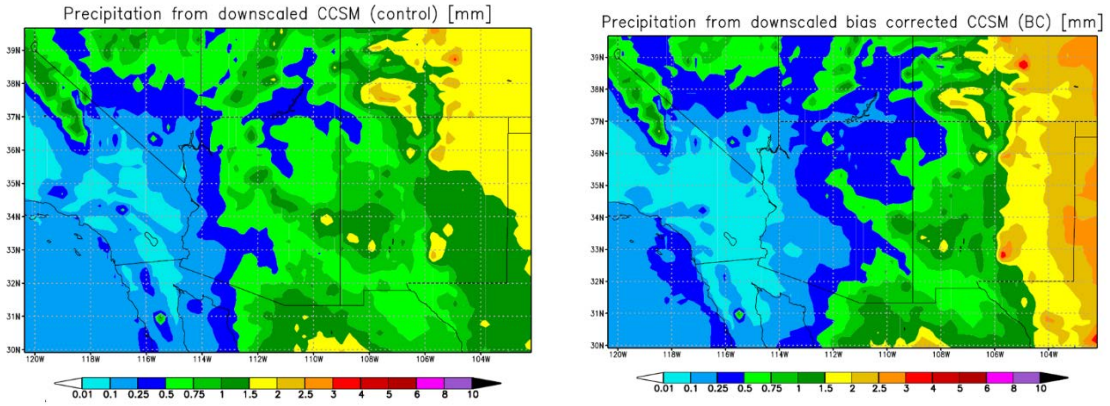

<u>Figure 50</u>: Precipitation from WRF-CCSM 12 km simulations generated at Argonne National Laboratory, for identified severe weather event days during the period 1994-2005. The two simulations utilize unbiased CCSM lateral boundary forcing (left) and bias-corrected CCSM lateral boundary forcing (right). Precipitation in mm day^{-1}.

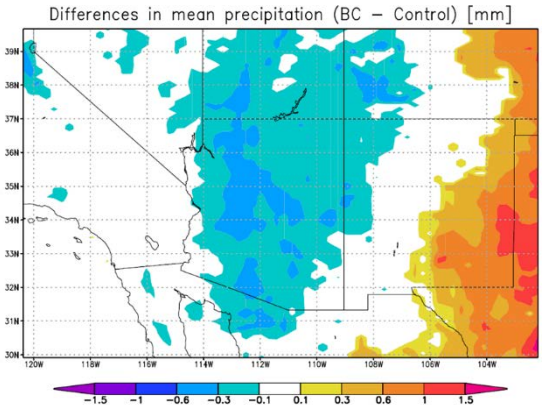

<u>Figure 51</u>: Precipitation difference of WRF-CCSM 12 km simulations (bias-corrected minus original lateral boundary conditions) generated at Argonne National Laboratory, for identified severe weather event days during the period 1994-2005. Precipitation difference in mm day^{-1}.

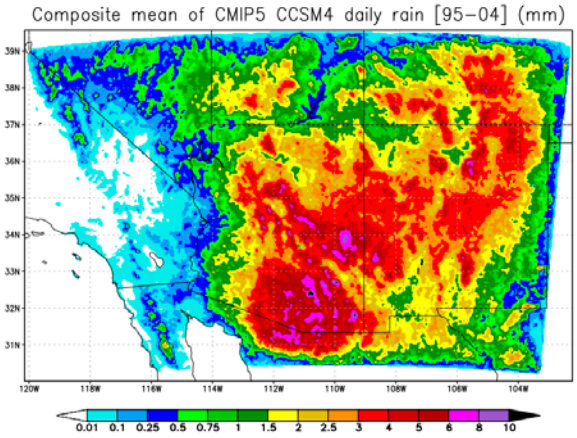

Figure 52: Composite mean of precipitation for simulated severe weather event days at CPM grid spacing (mm day^{-1}), using Argonne WRF-CCSM simulation with original CCSM boundary conditions.

3. Long-term changes in atmospheric thermodynamic conditions

The conclusion from analysis of in-situ radiosonde data and the downscaled reanalysis was that the Southwest has become more thermodynamically favorable for monsoon convection, in terms of increases in atmospheric instability and moisture. The future versus historical changes in MUCAPE and PW as simulated by the four CMIP models is shown in *Fig. 53* for all the individual radiosonde sites used to in the severe weather event day selection procedure. Statistical significance these changes is assessed at the 90% level using a two-tailed student's t-test. Most of these models are in agreement as to statistically significant increases in atmospheric moisture over time. Only two stations (ELP, LAS) exhibit decreases in PW in their modeled future climate in MPI-ECHAM5, but these changes are not statistically significant. The projected changes in CAPE exhibit much less agreement among the four models. Two of the models (HadGEM, MPI-ECHAM5) generally project significant decreases in atmospheric instability while the other two (HadCM3, MPI-ECHAM6) generally project significant increases. So the changes in instability are not very consistent between the models from the two CMIP experiments.

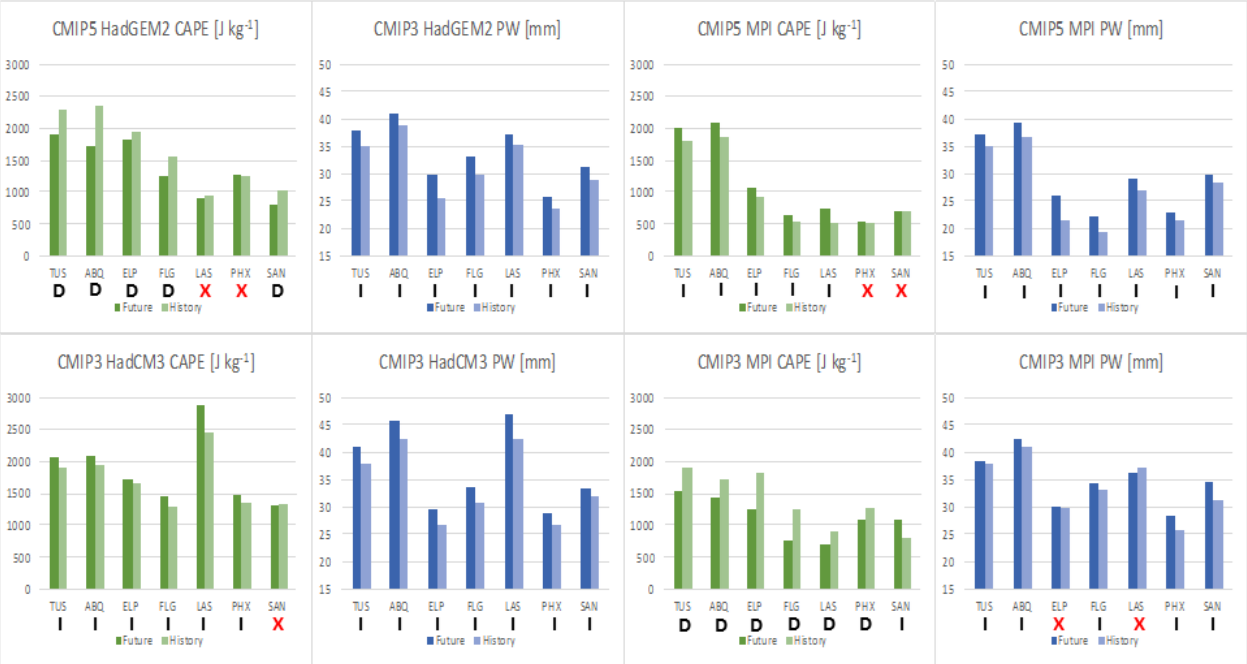

Figure 53: Changes in MUCAPE (J kg^{-1}) and PW (mm) within the dynamically downscaled CMIP models for historical and future periods, for the radiosonde sites used in the severe weather event selection procedure. Direction of change indicated below each station, with "I" a statistically significant increase, "D" a statistically significant decrease, and "X" no significant change.

4. Changes in model-simulated means and extremes of precipitation, maximum wind speed

Even with the variability among the models in their representation of trends of atmospheric instability and moisture, there is surprising consistency in the model simulated results for changes in mean and extreme precipitation. The simulated changes in mean precipitation of the severe weather event days are shown in *Fig. 54* and extreme precipitation in *Fig. 55*. All the models simulate decreases in mean precipitation across the Southwest, but particularly within Arizona. By contrast, extreme precipitation is regionally increasing. Interestingly, the identification of southwest Arizona as a regional "hot spot'' for increases in precipitation intensity starts to become more apparent in the CMIP5 models. Finally, the ensemble mean results for changes in mean and extreme precipitation are shown in *Fig. 56*. Differences are shaded where at least three out of four models are in agreement with respect to the sign of change. Viewed as the ensemble mean change, it becomes quite clear that the CMIP models are capturing well the broadening and flattening of the daily precipitation distribution that is already occurring in the recent historical record, with monsoon precipitation becoming less frequent but precipitation events are becoming more extreme. The CMIP models considered in this work are projecting that the currently observed trends in monsoon precipitation will continue in the future

with a strong level of intermodal agreement—within a paradigm in which the monsoon thunderstorms themselves are explicitly represented in the simulation.

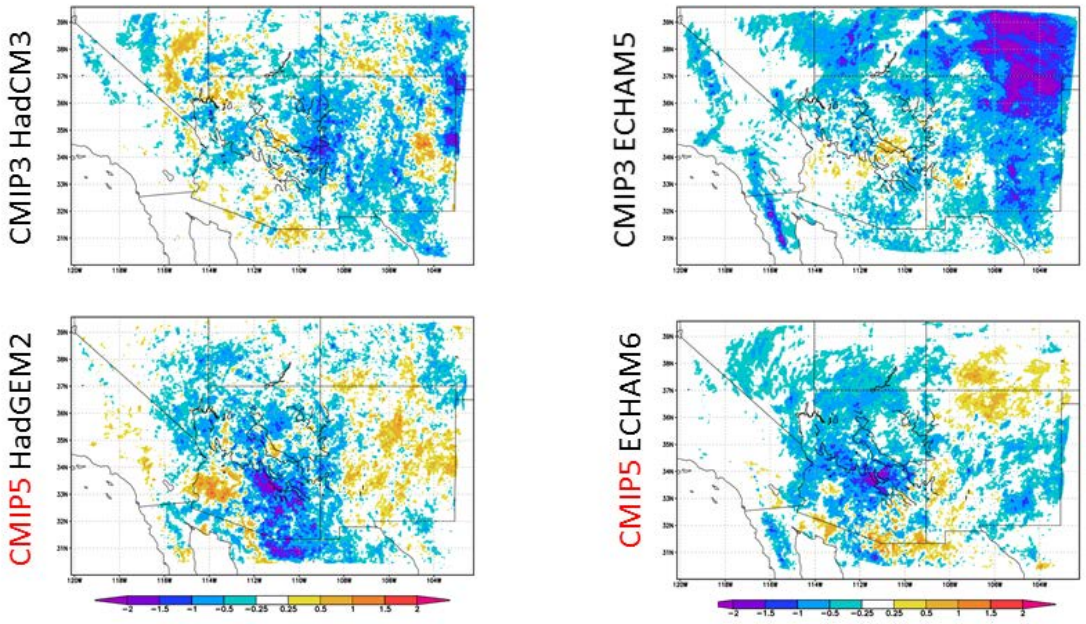

Figure 54: Changes in mean monsoon precipitation (mm day^{-1}) of severe weather event day simulations for all CMIP model downscaling paradigms. Where there is shading indicates areas where changes are statistically significant at the 90% level. Location of the Mogollon Rim indicated by terrain relief contours (in black) at 1000 m intervals within the state of Arizona.

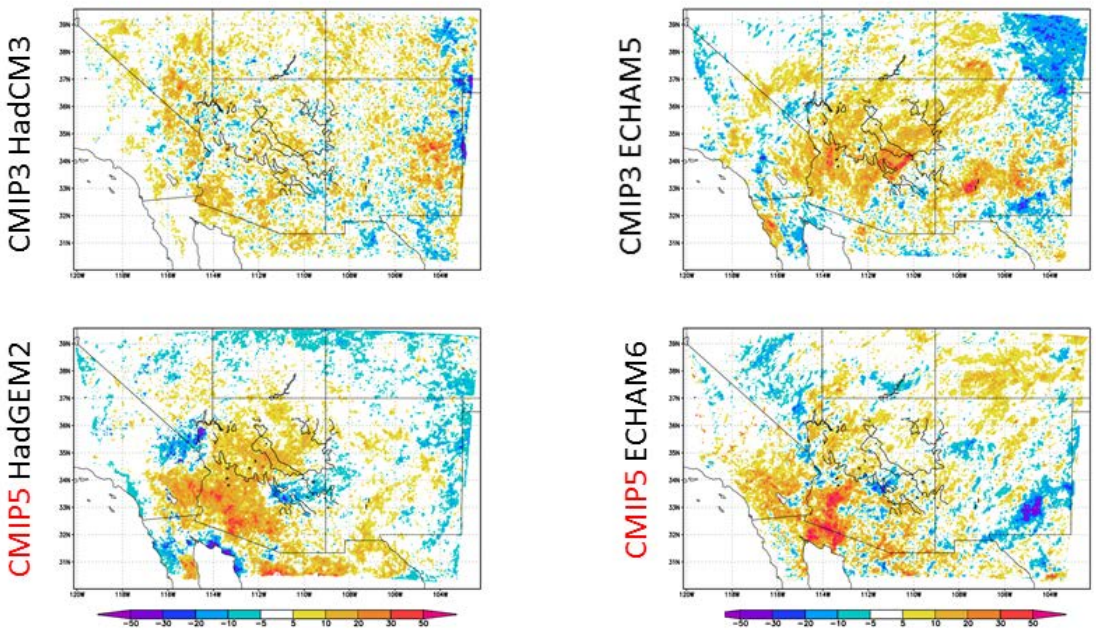

Figure 55: Same as Fig. 54 for changes in precipitation extremes.

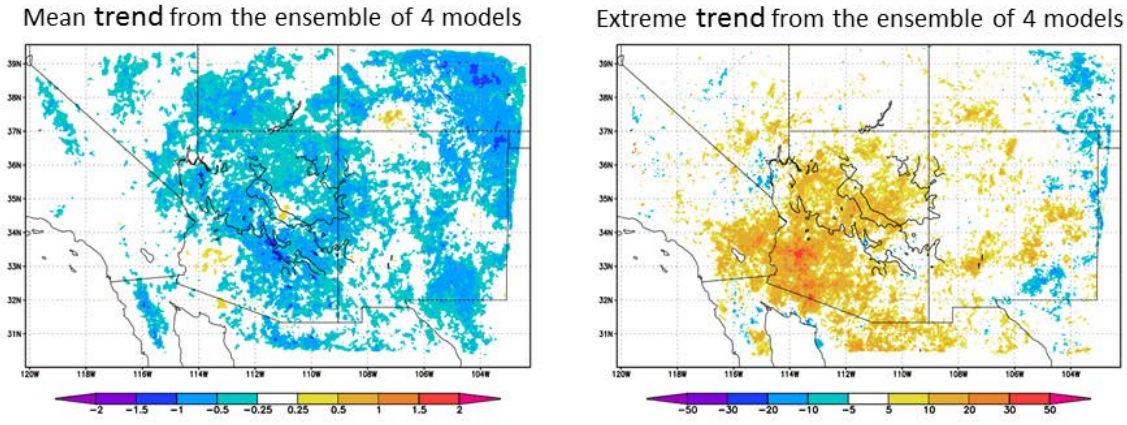

Figure 56: Downscaled CMIP ensemble changes in mean (left) and extreme (right) monsoon precipitation (mm day^{-1}) of severe weather event day simulations for all CMIP model downscaling paradigms. Where there is shading indicates areas where changes are statistically significant at the 90% level and where three out of four models agree as to the sign of trend. Location of the Mogollon Rim indicated by terrain relief contours (in black) at 1000 m intervals within the state of Arizona.

Lastly, the changes in maximum wind gust extremes associated with outflow boundaries from model DCAPE is shown in *Fig. 57*. This figure just shows the results of the ensemble mean of the four models with level of model agreement. Similar to the downscaled reanalysis, areas that are relatively more influenced by organized MCS-type convection (e.g. Southwest Arizona) trend to have largest increases in extreme wind gusts.

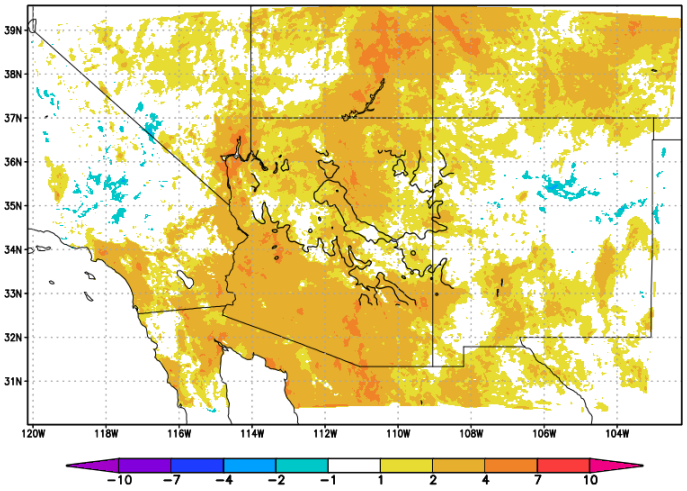

Figure 57: Downscaled CMIP ensemble changes in extreme wind gusts (m s^{-1}) of severe weather event day simulations for all CMIP model downscaling paradigms. Where there is shading indicates areas where changes are statistically significant at the 90% level and where three out of four models agree as to the sign of trend. Location of the Mogollon Rim indicated by terrain relief contours (in black) at 1000 m intervals within the state of Arizona.

G. TRANSLATION OF MODEL INFORMATION TO DOD FACILITY SCALE

The main emphasis in the translation of the information from the convective-permitting model simulations to the DoD facility scale has been the utilization of intensity, duration diagrams. Within the project, proof-of-concept intensity, duration diagrams that consider the changes in precipitation and wind speed (calculated from DCAPE) have been generated for a sample set of installations. Results shown in this report reflect changes in: 1) the WRF downscaled NCEP-NCAR reanalysis from a historical period (1951-1970) to a modern period (1991-2010) and 2) the WRF downscaled CMIP models from historical period (1991-2010) and a future period (2021-2040).

1. Computation of intensity, duration diagrams at sample DoD installations

Five specific DoD installations within the Southwest U.S. area of responsibility (AOR) of 25th OWS were selected for intensity, duration analyses. These represent the DoD facilities that are some of the most spatially expansive in the region and most impacted by monsoon thunderstorms. The facilities (and the number of model grid points in the convective-permitting domain they encompass) are highlighted in *Fig. 58* and these are:

- Fort Bliss, Texas (721 grid points)
- White Sands, New Mexico (1379 grid points)
- Yuma Proving Ground, Arizona (527 grid points)
- Nellis Air Force Range, Nevada (1822 grid points)
- Barry Goldwater Range, Arizona (664 grid points)

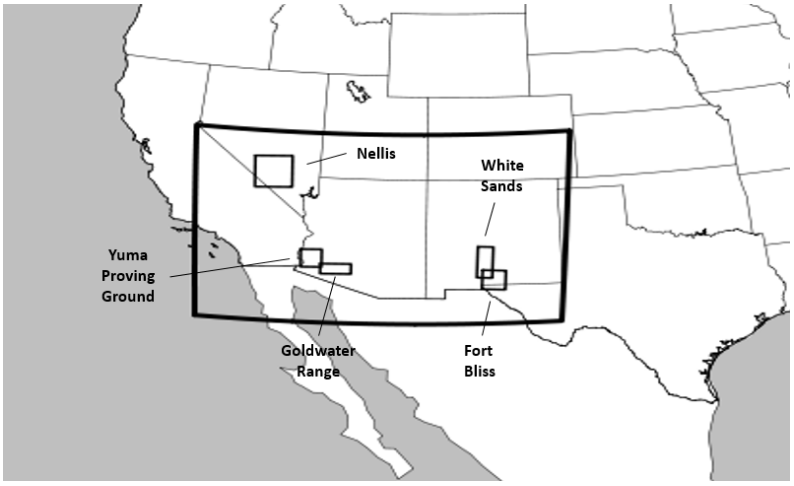

Figure 58: Highlighted DoD installations within the convective-permitting model simulation domain selected for proof-of-concept intensity, duration analyses.

The WRF model simulations output hourly data at each model grid point. For a given facility, the maximum intensity is computed as the maximum grid point value of the variable of interest (precipitation, wind speed) over the time duration of the event. To illustrate, a sample intensity, duration diagram of precipitation for the Barry Goldwater Range is shown in *Fig. 59.* The y-axis shows the rain rate in mm hr^{-1} and the x-axis shows event duration in hours, with the smallest value at one hour corresponding to timescale of model data output. The color bar indicates the frequency of occurrence of events. At this particular location, the highest frequency of event occurrence occurs for rain rates between 0.5 – 10 mm hr^{-1} for events of less than five hours duration.

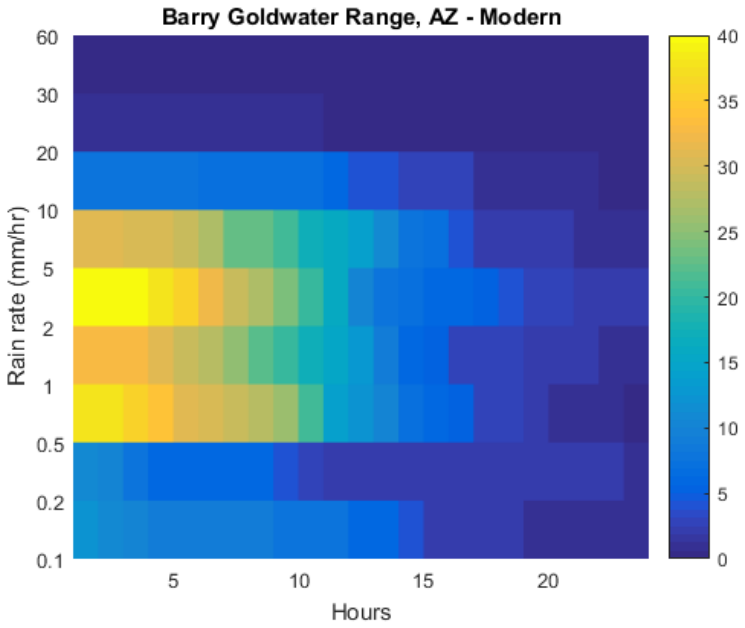

Figure 59: Sample joint PDF intensity, duration precipitation diagram from convective-permitting simulations for Barry Goldwater Range, Arizona. Color bar indicates event frequency.

2. Computation of intensity, duration diagrams at sample DoD installations: downscaled reanalysis data

After computing intensity, duration diagrams for the modern period and historical period the differences between the two joint PDFs is computed, using the downscaled reanalysis convective-permitting simulations. To assess the statistical significance of changes in the joint PDFs between periods a Monte Carlo technique is employed. To construct one randomized

sample, simulation days from the historical period and simulation days from the modern period are combined, and a random subset of 250 sample simulated days are extracted from this combined set using a permutation approach. Then a difference in the joint PDF is computed using two randomly generated samples. This process is repeated 1000 times to construct a null distribution of joint PDF differences, from which the statistical significance of the original sample can be assessed.

Statistically significant differences in the joint PDF of simulated precipitation on the Barry Goldwater Range are shown in *Fig. 60*. The Barry Goldwater Range is selected to demonstrate this procedure because where it is located within Southwest is the exact area which exhibits the largest and most statistically significant increases in precipitation extremes over the last twenty years. The largest statistically significant increases in precipitation intensity occur for rain rates exceeding 20 mm hr^{-1} and events less than 15 hours in duration, that likely correspond to organized mesoscale convective systems. These most intense modeled precipitation events have increased on the order of 5-10% over the past twenty years. The accompanying results for other facilities are included in *Fig. 61*. These also generally show increases in the most intense, shorter duration precipitation events, though not as dramatic as the Barry Goldwater Range.

Ultimately, the particular weather watch or warning criteria used for operational forecasting at these facilities can be superimposed onto these types of diagrams. For the example of precipitation presented here, the watch/warning criteria used by the 25th OWS is over two inches of precipitation (approximately 50 mm) in a 12-hour period. Similar analyses can be constructed for maximum wind speed, computed from DCAPE.

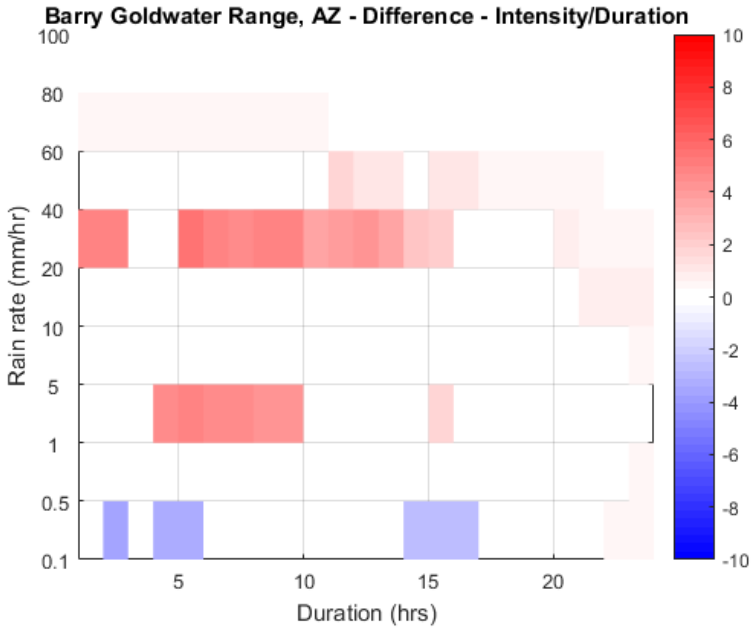

Figure 60: Statistically significant percentage changes in rainfall intensity and duration from convective-permitting simulations dynamically downscaling atmospheric reanalysis for the Barry Goldwater Range, Arizona. Statistical significance at the 90% level.

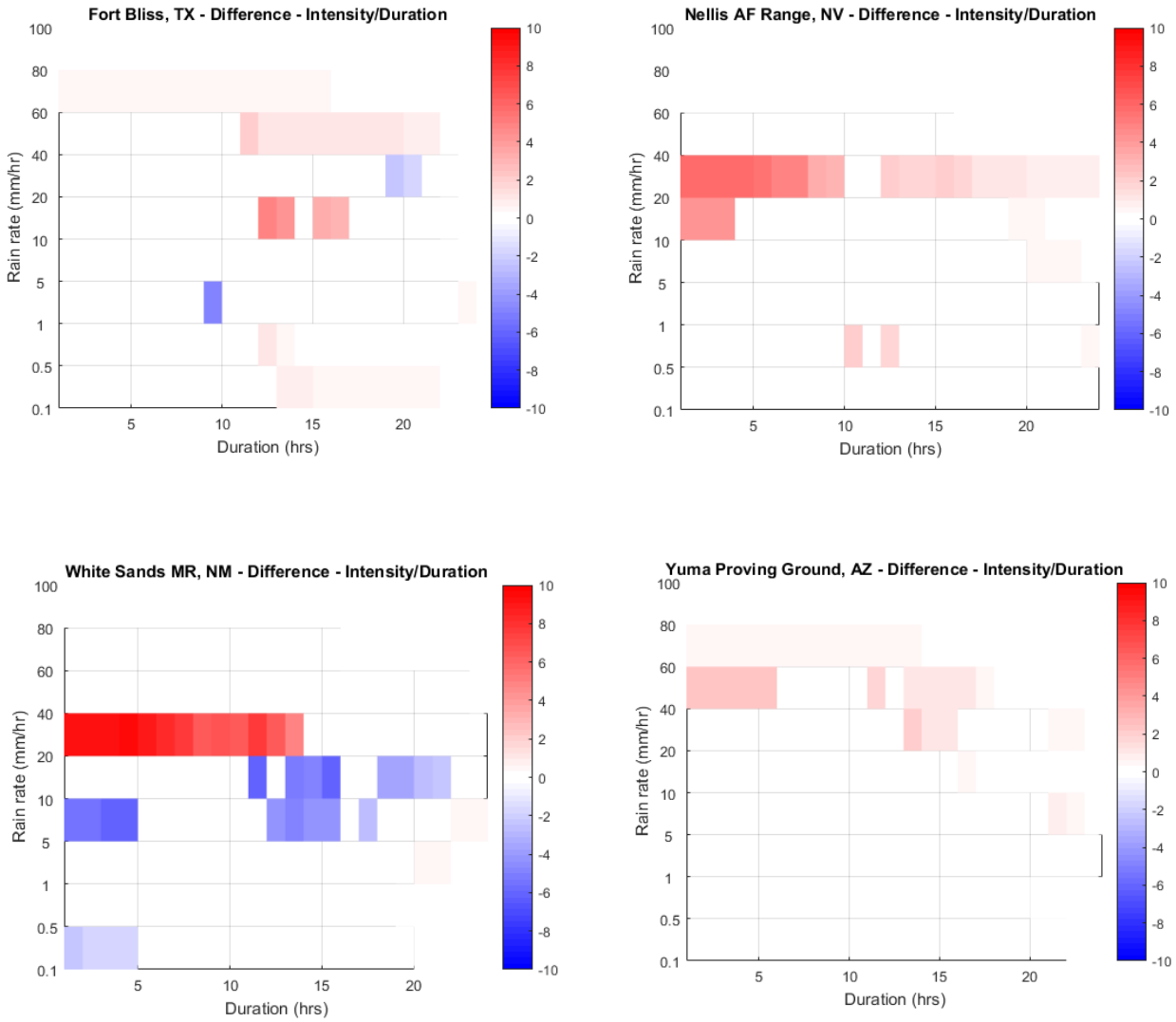

Figure 61: Same as Fig. 60 for other DoD facilities in the Southwest as labeled.

3. Computation of intensity, duration diagrams at sample DoD installations: downscaled CMIP model data

The same intensity duration analysis procedure is then identically applied to the dynamically downscaled CMIP model convective-permitting simulations. Results for all the sample DoD facilities are shown in *Fig. 62*, as the ensemble mean change of all the downscaled CMIP models. A shaded box on the plot means that changes between the historical and future periods are statistically significant and there is agreement as to the sign of change in at least three out of

four of the WRF-CMIP models. Broadly speaking, significant changes occur when there is a change of 3% or more in the joint probability density function. There are two basic categorical groupings for the sample DoD facilities considered here, in terms of the projected changes in precipitation intensity and duration:

- Organized convection dominant: At these facilities, monsoon precipitation is on average lower and more intermittent, relative to the Southwest as a whole. The physical mechanism for precipitation is almost exclusively large, propagating mesoscale convective systems, occurring westward of major mountain ranges (Mogollon Rim) during monsoon burst periods. The geographic areas would include the southwest low desert areas of Arizona extending toward the Colorado River valley, where the Barry Goldwater Range and Yuma Proving Ground are located. At these two facilities, there is generally a significant increase in the high intensity, low duration precipitation events (greater than 40 mm, lasting less than 10 hours) and a significant decrease in in the lower intensity events (less than 40 mm). These changes in the character of precipitation intensity and duration are consistent with the idea of a broadening and flattening of the daily precipitation distribution and more intense organized convective events, as discussed previously.

- Diurnal convection dominant: These facilities are located in closer proximity to mountain ranges, where monsoon precipitation would tend to occur more frequently, is more due to air-mass type thunderstorms, and principally associated with a terrain-induced diurnal cycle of convection. These facilities would include Fort Bliss, White Sands, and Nellis AFB. At these particular facilities, precipitation is generally projected to become significantly less intense, irrespective of duration. These types of changes seem to reflect more the significant decrease in mean precipitation throughout the Southwest that occurs in the ensemble average of all the downscaled CMIP models for their simulated severe weather events.

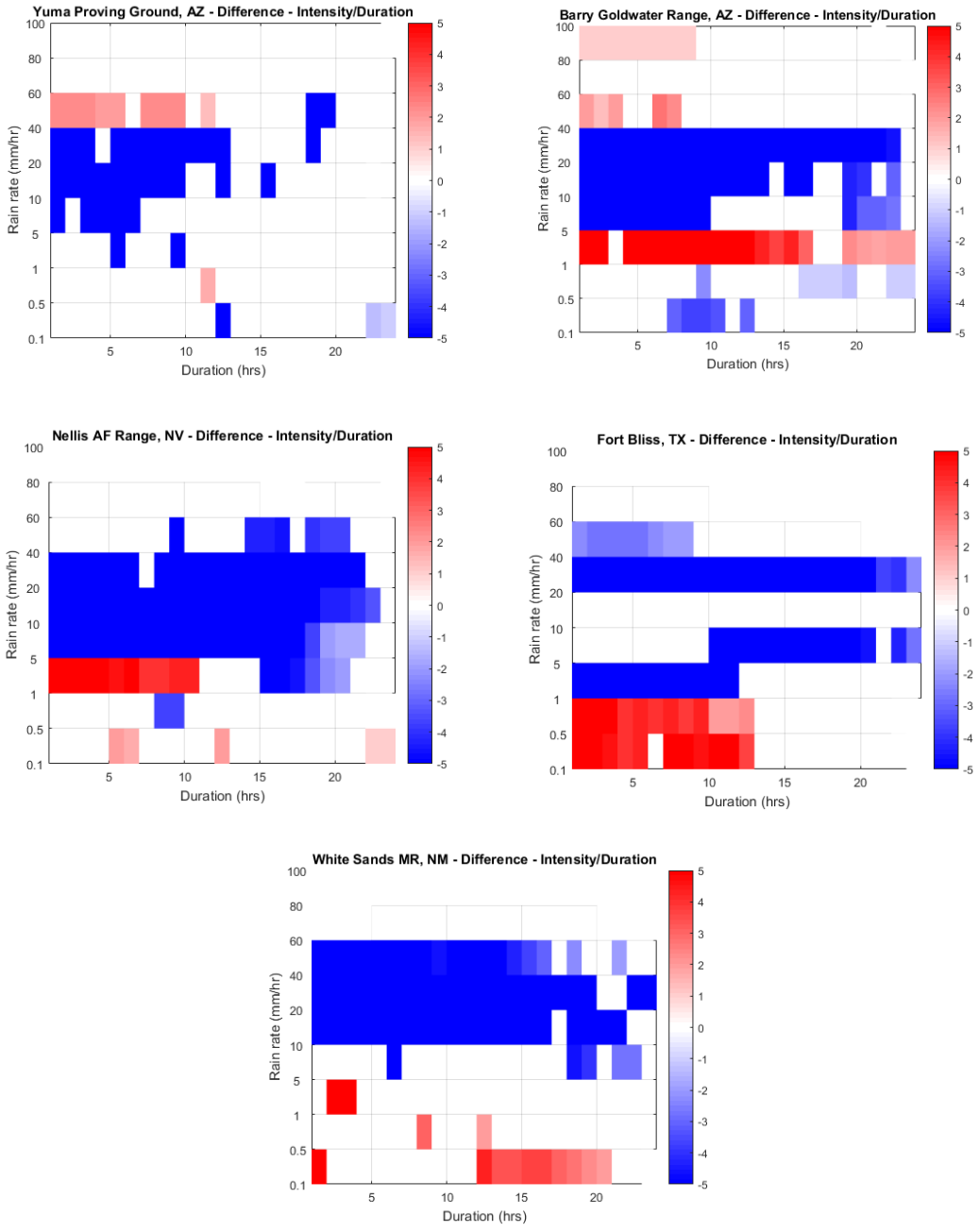

<u>Figure 62:</u> Statistically significant percentage model ensemble changes in rainfall intensity and duration, from convective-permitting simulations using dynamically downscaling CMIP model data for the sample Southwest DoD facilities. Statistical significance at the 90% level. Shaded regions indicate where the sign of change is in agreement between at least three out of four modeling paradigms.

H. PRINCIPAL DISCUSSION POINTS ON PROJECT RESULTS

This section presents some principal discussion points on project results, that synthesize information presented within all the various components of the project.

1. Severe weather event selection methodology

An innovative scientific contribution of this SERDP project has been the development of the severe weather event selection methodology that can be used to objectively identify the severe weather event days. Using this type of approach, any source of climate change model projection data can be utilized as boundary forcing to a convective-permitting regional atmospheric model in a numerical weather prediction-type mode. The underlying philosophical approach to the model exercise might be succinctly summarized as "only use the power of very high resolution modeling when it is most obviously needed." In the example of the Southwest, the ''obvious need'' for convective-permitting simulation is during those days that are thermodynamically and dynamically favored for intense, organized convective systems. Doing weather event-based simulations is much more economically cost-efficient to generate large ensembles of convective-permitting model data, necessary to more robustly quantify statistical uncertainty. The alternative would be to execute continuous convective-permitting simulations for entire seasons or years at a time. Within the National Center for Atmospheric Research, Research Applications Laboratory, these types of simulations are currently being generated with WRF for a domain that considers the entire contiguous U.S. However, these WRF simulations are limited to an approximate period of ten years, generate on the order of a petabyte or more of model data, and can only practically be performed on a supercomputer. The WRF severe weather event-based simulations in this project, even for all the different modeling paradigms, occupy only on the order of 100 terrabytes and were generated using (a more computationally modest) multi-processor linux cluster.

There are several caveats to using an event-based simulation approach for characterizing changes in severe weather. The objective criteria for selecting severe weather events is necessarily place-based. So though thermodynamic criteria (instability, moisture) work well as identifiers monsoon thunderstorms in the Southwest, they would not work as well in other places where the dynamic factors might be more important for severe convective weather, for example in the central United States. Thus, is it necessary in development of the severe weather event selection methodology to work with local operational forecasters and/or professional experts to ascertain what are the most important meteorological factors for severe weather in a given place. The model results will apply only to a specific and confined geographic area, in this project the areas of the Southwest clearly subject to monsoon precipitation. It is impossible to design an objective

severe weather event meteorological criteria that would capture every possible severe weather event hazard. The methodological approach used in this project emphasizes those days mostly when strong and organized monsoon thunderstorms would occur, but not necessarily days which would have a high potential for dry microbursts or heavy precipitation from tropical cyclone remnants, as these days would tend to have more marginal MUCAPE or PW.

2. Present findings for the Southwest within a larger paradigm of anthropogenically-driven climate change

The most important scientific conclusions that have been obtained in this project concerning changes in extreme monsoon precipitation are that 1) monsoon precipitation is generally becoming less frequent but more intense, especially in areas where organized convection accounts for a greater proportion of monsoon precipitation and 2) the predominant dynamic forcing mechanism of the inverted trough for organized monsoon convection is becoming less frequent with the intensification of the monsoon ridge. Even absent the use of any convective-permitting model simulations to substantiate these conclusions, they actually conform quite well to some basic paradigms of how anthropogenic climate change is affecting the global climate system, as mentioned in the introductory section of this report. Global increases in atmospheric moisture are leading to more intense but less frequent precipitation events. Subtropical ridges are getting stronger and expanding in geographic extent. In general, climate is becoming more extreme, with areas that are favored to be wet getting wetter and areas favored to be dry getting drier. All the convective-permitting modeling essentially provides is the more physically realistic framework for how these well-established long-term changes in global translate to changes in Southwest monsoon precipitation on a regional and local scale. But the convective-permitting modeling step therein adds substantial value. It is especially notable that the simulated pattern of changes in precipitation extremes in the Southwest exist in both the dynamically downscaled atmospheric reanalysis and the ensemble mean of dynamically downscaled CMIP model projections, in a manner that better matches observations as compared to a coarser resolution model.

3. Assessing the impact of bias correction of global climate model data

A particular and persistent concern of SERDP in their internal evaluation of this project was the fact that all the regional model simulations performed used the original global climate model data as lateral boundary forcing. There was an explicit desire to ascertain the effect of a “better” specification of lateral boundary conditions, obtained by bias correcting the global climate model data to an atmospheric reanalysis. However, when data from the companion SERDP project

from Argonne National Laboratory were considered, WRF model simulations that utilized a bias correction to CCSM actually generated a poorer result for precipitation during the identified severe weather event days in the Southwest. Assessing the physical reasons why that may be is beyond the scope of this present project. All of the CMIP-WRF model paradigms exhibit a reasonable result in terms of their climatological representation of monsoon precipitation during the severe weather events. There is also good correspondence of simulated precipitation changes to observed precipitation changes for both means and extremes. It may be that a bias correction step is more appropriately applied as a post-processing exercise to the convective-permitting model simulation data, prior to use of these data for any subsequent impacts assessment.

4. A unique database of information

There are many potential impacts assessment applications for use of the convective-permitting model simulation data generated by this project, for both civilian and DoD purposes, which this project simply did not have the time or resources to fully explore. The intensity-duration analyses performed for precipitation at DoD facilities is designed to provide a template example of how these data may be put to practical use, to match DoD operational decision making criteria for severe weather. In the interactions with the 25th Operational Weather Squadron and 14th Weather Squadron, it become clearer and clearer that same practical and feasible route needed to be found for provision of the complete set of model data to multiple potential users. The most economically efficient solution is to place these data on a cloud storage system called Cyverse (www.cyverse.org).

VI. CONCLUSIONS AND IMPLICATIONS FOR FUTURE RESEARCH/IMPLMENTATION

A. SYNTHESIS OF RESULTS PER PROJECT OBJECTIVES

1. Thermodynamic classification of severe weather event days

- The methodological approach to identifying thermodynamically favorable days for severe monsoon thunderstorms is robust because approximately 60% of reported severe weather events in southern Arizona are accounted for by use of observational sounding data. The percentage accounted for by use of the long-term dynamically downscaled NCEP-NCAR reanalysis is similar.

- When this same methodology is applied to dynamically downscaled CMIP3 and CMIP5 data, all these RCM data contain a subset of days that meet or exceed operational thermodynamic criteria for severe monsoon thunderstorms.

- It is feasible to identify thermodynamically favorable severe weather event days for the Southwest U.S. region as a whole.

2. Dynamic classification of severe weather event days:

- The dominant modes of 500-mb geopotential height for thermodynamically favorable severe weather event days in the recent observational record reflect well the prior, subjectively determined severe weather modes by Maddox et al. (1995). For three out of the four downscaled CMIP models considered, the climatological monsoon ridge positioning and dominant modes of the monsoon ridge for thermodynamically favorable severe weather event days appear to be reasonable. The one downscaled CMIP model (MPI-ECHAM6) that is most challenged to represent the monsoon ridge climatologicallly also does not represent the severe weather modes as well, but the modes nonetheless reflect a northward displacement of the ridge.

- It is possible to objectively identify gulf surges using NWS operational forecast criteria. The downscaled reanalysis and downscaled CMIP models can represent the physical structure of an observed gulf surge well, in terms of the low-level wind speed, dew point, and wind direction from the southeast at Yuma, Arizona, as well as the entire northern end of the Gulf of California. The vast majority of thermodynamically favorable severe weather event days (80-90%) in all the sources of downscaled CMIP data are also gulf surge event days.

- IVs can be objectively tracked in all sources of dynamically downscaled data. The IV track density climatology of the downscaled reanalysis, objectively determined with a

vortex tracking algorithm, generates comparable results to a prior documented approach to IV tracking by using a more subjective analysis of weather maps and satellite data. For three downscaled CMIP models considered, all have at least some representation of IV features during the period of the monsoon, the principal synoptic mechanism to facilitate organized convection in the Southwest.

3. Long term climatological changes in North American monsoon

- Considering the changes in atmospheric thermodynamic conditions during the monsoon in the downscaled reanalysis and in-situ radiosonde data for sites within the Southwest, both atmospheric moisture and instability are being more favorable for intense monsoon thunderstorms. Increases in at least precipitable water are also observed with the dynamically downscaled CMIP models, though there is not a clear signal of increases in instability.

- The frequency of inverted troughs (IVs) in the Southwest is decreasing during the latter part of the monsoon (August), so convection originating on the mountains is less likely to organize and propagate westward into the urban areas and low southwestern desert areas of Arizona. It is as yet unknown whether downscaled CMIP models exhibit similar long-term changes in IVs, but the influences of thermodynamic versus dynamic forcing on monsoon precipitation can nonetheless be objectively separated by considering trough versus no trough days. Assessing long-term changes in IVs within dynamically downscaled CMIP models, and the associated precipitation response, is problematic because of the differences in their climatological representation of IVs.

4. Changes in monsoon precipitation in the context of convective-permitting simulations

- High-resolution, convective resolving simulations that downscale thermodynamically favorable severe weather event days, identified in all sources of baseline dynamically downscaled data, are able to reasonably represent widespread monsoon precipitation across the Southwest, the diurnal evolution of monsoon thunderstorms, and gulf surges. This conclusion generally applies to all paradigms of WRF dynamically downscaled data, that use the NCEP-NCAR reanalysis and CMIP models as boundary forcing.

- Considering the severe weather event days simulated by downscaling the NCEP-NCAR reanalysis, there have been distinct differences in the changes in simulated mean and extreme monsoon precipitation in the Southwest during the past 20-30 years. Mean monsoon precipitation during the severe weather event days is generally decreasing. By contrast, the most extreme precipitation events are becoming more intense in those areas where organized convective precipitation accounts for a greater proportion of total monsoon precipitation. Specifically, the low desert areas of southwestern Arizona seem to be a local “hot spot” where the most intense precipitation events due to organized convection are becoming even more intense.

- The changes in model simulated precipitation were verified by observed daily precipitation data derived from the original gauge-derived coop observations. Therefore the model simulated changes in precipitation in the downscaled reanalysis are physically realistic and tied to observed increases in moisture and instability.

- The changes in daily monsoon precipitation in the Southwest just described may be interpreted as a broadening and flattening of the daily precipitation distribution, with less frequency of precipitation events overall, but an increase in the frequency of the most extreme precipitation events. This conclusion fits well with the well-accepted paradigm of increasing weather and climate extremes in an anthropogenically-altered climate.

- The exact same types of changes also occur in the dynamically downscaled CMIP data considered in the scope of the project, with a high level of inter-model agreement as to the sign and spatial location of where significant changes occur. Because these types of projected changes have already determined to be happening in the Southwest over the past twenty to thirty years, these climate projections should be quite robust for impacts assessment purposes.

- The modeled maximum wind gusts in the downscaled reanalysis (computed from DCAPE) associated with thunderstorm outflow boundaries are increasing in intensity for the most extreme events of organized convection, in nearly the exact same geographic locations where extreme precipitation is intensifying (i.e. southwestern Arizona).

- Convective-permitting modeling adds substantial value in projecting changes in monsoon thunderstorms, as these results are very different from coarser resolution simulations. CPMs seem to be able to get the exact spatial locations correct with respect to where precipitation is becoming more intense in the Southwest.

5. Assessment of changes in monsoon thunderstorms at the DoD facility scale

- The approach of using intensity, duration diagrams is a means to graphically express changes in event intensity in relation to duration at the facility scale, in a manner that is easily relatable to USAF operational decision making criteria for issuance of weather watches and warnings.

- Important DoD assets are located in areas where monsoon thunderstorms are clearly becoming more intense, with respect to rainfall rates and maximum wind gusts. Namely, the area of southwestern Arizona where the Barry Goldwater Range is located seems to be one of the most affected facilities in the region.

6. Limitations and caveats to project methodological approach and results

- Selection criteria for severe weather event days: The selection criteria for the severe weather event days to model at convective-permitting grid spacing is based solely on thermodynamic conditions (atmospheric instability and moisture). While these selection criteria result in a good correspondence to observed severe weather events in the Southwest during the period of the monsoon, it still misses approximately 40% of the observed severe weather reports if applied to historical radiosonde data.

- High based convection and tropical cyclone remnants: The methodological approach for the selection of severe weather event days exclude any days that have relatively more marginal instability and/or moisture, favoring days where organized convection and heavy precipitation are more likely to occur. Therefore, two important types of severe weather conditions that occur in the Southwest are not well accounted for. First, days wore high-based convection, with precipitation that evaporates before it reaches the ground (virga) causing the severe weather hazard of a dry microburst. During these types of days with deep warm and dry boundary layers the atmospheric moisture would be relatively more marginal. However, dry microbursts and high-based thunderstorms are an important severe weather hazard to account in terms of a potential aviation hazard, lightning-triggered wildfire, and wind gusts that can help spread wildfire. Second, days with the occurrence of tropical cyclone remnants typically are very moist, but have very little convective available potential energy. Tropical cyclone remnants are an important trigger for extreme precipitation in the Southwest, but tend to occur more in late summer and early fall (August-October). In any case, tropical cyclones are not represented as salient features within CMIP models that were used to force the WRF simulations in this project.

- Geographic range of monsoon precipitation: There is a confined geographic range where the results concerning changes in monsoon precipitation as reported here apply, namely those areas within the Southwest that have a clear, coherent signal in monsoon precipitation. The approximate range of where the monsoon substantially influences warm season precipitation is well indicated by *Fig. 15* and *Fig. 16*. Roughly speaking, monsoon convective precipitation is relevant only in those places where the coherency of the dominant mode of MUCAPE for the Southwest radiosonde stations is statistically significant at the 90% level or above (a correlation value of approximately 0.3). These would include: all of Arizona, southwestern Nevada (south of 40°N latitude and east of 116°W longitude), western New Mexico (west of the continental divide), southwest Colorado (west of the continental divide and south of 40°N latitude), southern Utah

(south of 40°N latitude), and far southeast California (east of 116°W longitude). This project is not able to confidently consider changes in warm season severe weather for any DoD facilities that fall outside of these geographic bounds. Edwards AFB in California is perhaps the best example of a very important DoD facility that falls outside of the geographic range of where the monsoon substantially influences warm season precipitation in the Southwest. So the severe weather event simulations produced in this project cannot well account any potential changes there, as they do for other facilities like Nellis AFB or the Barry Goldwater Range.

Nearly all of these methodological limitations (save the representation of tropical cyclone remnants) could certainly be addressed if the convective-permitting simulations were performed continuously for at least the entire warm season for every year, rather than for just the severe weather event days. But doing this would require substantially more computational resources, likely limiting the number of years that could be considered in the statistical characterization of changes in means and extremes, reducing the level of confidence in results.

B. RECOMMENDATIONS FOR FUTURE WORK AND ACTIVITIES PENDING POST-PROJECT

- The main interest of SERDP in this project was to develop a template methodological approach to climate change projection using convective-permitting modeling. Though the particular criteria would have to be modified, the project results presented here indicate an event-based simulation approach produces physically and statistically confident climate projection results. This can be achieved with a relatively modest amount of computational resources. It is therefore recommended to expand these types of studies to other geographic regions.

- Maintaining operational capability within DoD theatres of operation outside of the territory of the United States was strongly expressed as a high priority need by USAF collaborators on this project. A means to explore projected changes in extreme convective weather such as this can basically be applied to subtropical and tropical regions throughout the world.

- As of the official conclusion of this SERDP project, the project team is still working with 25th OWS and 14th WS on the matter of final transfer of model simulation data, subsequent to the final project webinar that took place in December 2016. A DoD user's guide to these model data (as stated in the original proposal) is pending post-project, but it must be verified that 14th WS can successfully access these data remotely, given DoD cybersecurity restrictions, before that is possible. 14th WS has requested access to the entire suite of WRF model simulation data, on the order of 100 terrabytes worth of information. As project resources did not allow for purchase of external disk storage to

exchange these data, they are being uploaded to the Cyverse cloud data storage server (see Appendix for description), a process which will take approximately two months. This final project report will be made accessible to 25th OWS and 14th WS in the meantime, to immediately motivate these pending activities.

C. AFFIRMATION OF FINAL REPORT

The information presented in this interim technical report represents an accurate reporting of the most pertinent research results obtained in SERDP Project RC-2205 in relation to the originally proposed work, to the conclusion of funding period of this project.

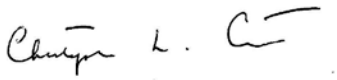

Christopher L. Castro, Ph.D.
Principal Investigator

LITERATURE CITED

Adams, D. K., S. Gutman, K. Holub and D. Pereira, 2013. GNSS Observations of Deep Convective timescales in the Amazon, 2013: *Geophys. Res. Lett*., **40**,1-6,doi:10.1002/grl.50573

Adams, D. K., and E. P. Souza, 2009. CAPE and Convective Events in the Southwest during the North American Monsoon. *Mon. Wea. Rev.*, **137**, 83–98.

Adams, D.K., and A.C. Comrie, 1997. The North American Monsoon. *Bull. Amer. Meteor. Soc*., **78**, 2197-2213.

Anderson, B. T., Wang, J., Salvucci, G., Gopal, S., and Islam, S., 2010. Observed trends in summertime precipitation over the southwestern United States. *J. Climate*. **23**, 1937–1944.

Archer, C. L., and K. Caldeira, 2008. Historical trends in the jet streams, *Geophys. Res. Lett.*, **35**, L08803, doi:10.1029/2008GL033614.

Bieda, S. W., C. L. Castro, S. L. Mullen, 2009. The relationship of transient upper-level troughs to variability of the North American monsoon system. *J. Climate*, **22**, 4213-4227.

Bretherton, C.S., M.E. Peters, and L.E. Back, 2004. Relationships between water vapor path and precipitation over the tropical oceans. *J. Climate*, **17**, 1517-1528.

Bretherton, C.S., C. Smith, J.M. Wallace, 1992. An intercomparison of methods for finding coupled patterns in climate data. *J. Climate*, **5**, 541-560.

Bukovsky M. S., and co-authors, 2015. Toward Assessing NARCCAP Regional Climate Model Credibility for the North American Monsoon: Future Climate Simulations. *J. Climate*, **28**, 6707-6728.

Bukovsky, M., D. J. Gochis, and L. O. Mearns, 2013. Towards Assessing NARCCAP Regional Climate Model Credibility for the North American Monsoon: Current Climate Simulations. *J. Climate*, **26**, 8802–8826.

Cassell, W. W., C. L. Castro, T. M. Luong, and Q. Xiao, 2015. Simulating organized convection during the 2004 North American Monsoon Experiment and its sensitivity to the specification of initial conditions. *Mon. Wea. Rev*. Submitted.

Castro, C.L., H-I. Chang, F. Dominguez, C. Carrillo, J. Kyung-Schemm, H. H-M. Juang, 2012. Can a regional climate model improve warm season forecasts in North America? *J. Climate*, **25**, 8212-8237.

Castro, C. L., R. A. Pielke, Sr., and J. O. Adegoke, 2007. Investigation of the Summer Climate of the Contiguous U.S. and Mexico Using the Regional Atmospheric Modeling System (RAMS). Part I: Model Climatology (1950-2002). *J. Climate*, **20**, 3866-3887

Chang, H.-I., C. L. Castro, C. M. Carrillo, and F. Dominguez, 2015. The more extreme nature of U.S. warm season climate in the recent observational record and two "well-performing" dynamically downscaled CMIP3 models, *J. Geophys. Res*., **120**, 8244–8263

Chou, M.-D., and M. J. Suarez, 1994. An efficient thermal infrared radiation parameterization for use in general circulation models. *NASA Tech. Memo. 104606*, 85pp.

Cook, B.I., and R. Seager, 2013. The response of the North American Monsoon to increased greenhouse gas forcing. *J. Geophys. Res.*, **118**, 1690-1699, doi:10.1002/jgrd.50111.

Dominguez, F., E. Rivera, D. P. Lettenmaier, and C. L. Castro, 2012. Changes in winter precipitation extremes for the western United States under a warmer climate as simulated by regional climate models, *Geophys. Res. Lett*., **39**, L05803.

Dominguez, F., J. Cañon, and J. Valdes, 2009. IPCC-AR4 climate simulations for the southwestern U.S.: the importance of future ENSO projections. *Clim. Change*, DOI: 10.1007/s10584-009-9672-5.

Doswell, C. A., and E. N. Rasmussen, 1994. The effect of neglecting the virtual temperature correction on cape calculations. *Wea. Forecasting*, **9**, 625–629.

Douglas, M.W., 1995. The Summertime Low-Level Jet over the Gulf of California. *Mon. Wea. Rev*., **123**, 2334-2347.

Douglas, A.V, and P.J. Englehart, 2007. A Climatological Perspective of Transient Synoptic Features during NAME 2004. *J. Climate*, **20**, 1947-1954.

Dudhia, J., 1989: Numerical Study of Convection Observed during the Winter Monsoon Experiment Using a Mesoscale Two-Dimensional Model. *J. Atmos. Sci*. **46**, 3077-3107.

Emanuel, K. A., 1994. Atmospheric Convection. Oxford University Press, 592 pp.

Finch, Z. O., and R. H. Johnson, 2010: Observational Analysis of an Upper-Level Inverted Trough during the 2004 North American Monsoon Experiment. *Mon. Wea. Rev*., **138**, 3540–3555.

Garfin, G., A. Jardine, R. Merideth, M. Black, and S. Leroy, Eds. 2013. Assessment of Climate Change in the Southwest United States: A Report Prepared for the National Climate Change Assessment. A report by Southwest Climate Alliance. Washington, DC: Island Press.

Geil, K. L., Y. L. Serra, and X. Zeng, 2013. Assessment of CMIP5 Model Simulation of the North American Monsoon System. *J. Climate*, **26**, 8787-8801. doi: http://dx.doi.org/10.1175/JCLI-D-13-00044.1.

Griffiths, P. G., C. S. Magirl, R. H. Webb, E. Pytlak, P. A. Troch, and S. W. Lyon, 2009: Spatial distribution and frequency of precipitation during an extreme event: July 2006 mesoscale convective complexes and floods in southeastern Arizona. *Water Resour. Res.*, **45**, W07419, doi:10.1029/2008WR007380.

Groisman, P.Y., R.W. Knight, D.R. Easterling, T.R. Karl, G.C. Hegerl, and V.N. Razuvaev, 2005. Trends in intense precipitation in the climate record. *J. Climate*, **18**, 1326-1350.

Grossman-Clarke, S., Zehnder, J. A., Loridan, T., and C. S. B. Grimmond, 2010: Contribution of Land Use Changes to Near Surface Air Temperatures during recent Summer Extreme Heat Events in the Phoenix Metropolitan Area. *J. Appl. Meteorol. Climatol*., **49**, pp. 1649-1664.

Hales, J.E., Jr., 1977: On the relationship of convective cooling to nocturnal thunderstorms at Phoenix. *Mon. Wea. Rev*., **105**, 1609-1613.

Higgins, R.W., and W. Shi, 2005. Relationships between Gulf of California Moisture Surges and Tropical Cyclones in the Eastern Pacific Basin. *J. Climate*, **18**, 4601-4620.

Hodges, K. I., 1999. Adaptive Constraints for Feature Tracking. *Mon. Wea. Rev.*, **127**, 1362–1373.

Hodges, K. I., 1996. Spherical Nonparametric Estimators Applied to the UGAMP Model Integration for AMIP. *Mon. Wea. Rev.*, **124**, 2914–2932.

Hong, S-.Y., J. Dudhia, S.-H. Chen, 2004. A revised approach to ice-microphysical processes for the bulk parameterization of cloud and precipitation. *Mon. Wea. Rev.*, **132**, 103-120.

Hong, S.-Y., H.-M. H. Juang, and Q. Zhao, 1998. Implementation of prognostic cloud scheme for a regional spectral model. *Mon. Wea. Rev.*, **126,** 2621–2639

IPCC, 2013. Climate Change 2013. The Physical Science Basis. Contribution of Working Group I to the Fifth Assessment Report of the Intergovernmental Panel on Climate Change [Stocker, T.F., D. Qin, G.-K. Plattner, M. Tignor, S.K. Allen, J. Boschung, A. Nauels, Y. Xia, V. Bex and P.M. Midgley (eds.)]. Cambridge University Press, Cambridge, United Kingdom and New York, NY, USA, 1535 pp.

Ivanova, D.C., and D.L. Mitchell, 2003. Sensitivity of the atmospheric boundary layer and circulation to sea surface temperatures in the Gulf of California: Results of a MM5 modeling study. *12th conference on Interactions of the Sea and Atmosphere. AMS Annual Meeting*, Long Beach, California, February 9-13.

Janiga, M.A., and C.D. Thorncroft, 2014. Convection over tropical Africa during the West African Monsoon: Regional and diurnal variability. *J. Climate*, **27**, 4159-4188.

Janjic, Z. I., 2002. Nonsingular Implementation of the Mellor-Yamada Level 2.5 Scheme in theNCEP Meso model. NCEP Office Note No. 437, 61 pp.

Janjic, Z. I., 1996. The Surface Layer in the NCEP Eta Model. 11th Conf. on NWP, Norfolk, VA, *Amer. Meteor. Soc.*, 354–355.

Janjic, Z. I., 1990. The step–mountain coordinate: physical package. *Mon. Wea. Rev.*, **118**, 1429-1443.

Kain, J. S., and J.M. Fritsch, 1993. Convective parameterization for mesoscale models: The Kain- Fritsch scheme. The representation of cumulus convection in numerical models. *Meteor. Monogr.*, No. 24, *Amer. Meteor. Soc.*, 165-170.

Kain, J. S., 2004. The Kain-Fritsch convective parameterization: An Update. *J. Appl. Meteror*., **43,** 170-181.

Karl, T.R., and R.W. Knight, 1998. Secular trends in the precipitation amount, frequency, and intensity in the United States. *Bull. Amer. Meteor. Soc*., **79**, 231-241.

Karl, T. R., and K. E. Trenberth, 2003. Modern climate change. *Science*, **302**, 1719–1723.

Katz, R. W., 2010. Statistics of extremes in climate change, *Clim. Change*, **100**, 71–76.

Kendon, E. and co-authors, 2016. Do convection-permitting regional climate models improve projections of future precipitation change? *Bull. Amer. Meteor. Soc*., in press.

Kendon, E., and co-authors, 2014. Heavier summer downpours with climate change revealed by weather forecast resolution model. *Nature Climate Change*, **4**, 570–576.

Kharin, V., and F. Zwiers, 2005. Estimating extremes in transient climate change simulations, *J. Climate*, **18**, 1156–1173.

Kunkel, K. E., and co-authors, 2013. Monitoring and Understanding Trends in Extreme Storms: State of Knowledge. *Bull. Amer. Meteor. Soc*., **94**, 499–514.

Kursinski, E.R., and co-authors, 2008a. Water vapor and surface observations in northwestern Mexico during the 2004 NAME enhanced observing period, *Geophys. Res. Lett*., **35**, L03815, doi:10.1029/2007GL031404.

Kursinski, E.R., D.K. Adams, and M. Leuthold, 2008b. GPS Observations of Precipitable Water and Implications for the Predictability of Precipitation during the North American Monsoon, *CLIVAR Exchanges*, **45**, 13-21.

Kutzbach, J. 1967: Empirical eigenvectors of sea-level pressure, surface temperature, and precipitation complexes over North America. *J. Appl. Meteor*., **6**, 791-802.

Lahmers, T., C. Castro, D.K. Adams, Y. Serra, and J.J. Brost, 2016. Long-term changes in the climatology of transient inverted troughs over the North American Monsoon region and their effects on severe weather. *J. Climate*, in press.

Lang. T. J., D. A. Ahijevych, S.W. Nesbitt, R.E. Carbone, S.A. Rutledge, and R. Cifelli, 2007. Radar-Observed Characteristics of Precipitating Systems during NAME 2004. *J. Climate*, **20**, 1713-1733.

Lin, Y.-L., R. D. Rarley, and H. D. Orville, 1983. Bulk parameterization of the snow field in a cloud model. *J. Appl. Meteor*, **22**, 1065-1092

Livezey, R.E, and W.Y. Chen, 1983. Statistical Field Significance and its Determination by Monte Carlo Techniques. *Mon. Wea. Rev.*, 111, 46-59.

Liveneh, B., E.A. Rosenberg, C. Lin, B. Nijssen, V. Mishra, K.M. Andreatis, E.P. Maurer, and D.P. Lettenmaier, 2013. A Long-Term Hydrologically Based Dataset of Land Surface Fluxes and States for the Coterminous United States: Update and Extensions. *J. Climate*, **26**, 9384-9392.

Lu, J., C. Deser, and T. Reichler, 2009. Cause of the widening of the tropical belt since 1958, *Geophys. Res. Lett*., **36**, L03803, doi:10.1029/2008GL036076.

Lu, E., X. Zeng, Z. Jiang, Y. Wang, and Q. Zhang, 2009. Precipitation and precipitable water: Their temporal-spatial behaviors and use in determining monsoon onset/retreat and monsoon regions. *J. Geophys. Res.*, **114**, D23105.

Maddox, R. A., D. M. McCollum, and K.W. Howard, 1995. Large-scale patterns associated with severe summertime thunderstorms over central Arizona. *Wea. Forecasting*, **10**, 763–778.

Magirl, C. S., and Coauthors, 2007. Impact of recent extreme Arizona storms, *Eos.Trans. AGU*, **88**, 191– 193, doi:10.1029/2007EO170003.

Maurer, E.P., A.W. Wood, J.C. Adam, D.P. Lettenmaier, and B. Nijssen, 2002. A Long-Term Hydrologically Based Dataset of Land Surface Fluxes and States for the Conterminous United States, *J. Climate*, **15**, 3237-3251.

Mearns, L.O., and co-authors, 2012. The North American Regional Climate Change Assessment Program: Overview of Phase I Results. *Bull. Amer. Meteor. Soc.*, **93**, 1337–1362.

Meehl, G.A., F. Zwiers, J. Evans, T. Knutson, L. Mearns, and P. Whetton, 2000. Trends in Extreme Weather and Climate Events: Issues Related to Modeling Extremes in Projections of Future Climate Change. *Bull. Amer. Meteor. Soc*., **81**, 427-436.

Mesinger, F., and co-authors, 2006. North American Regional Reanalysis. *Bull. Amer. Meteor. Soc.*, **87**, 343-360.

Miguez-Macho, G., G. L. Stenchikov, and A. Robock, 2005. Regional climate simulations over North America: Interaction of local processes with improved large-scale flow. *J. Climate*, **18**, 1227-1246.

Min, S-K., X. Zhang, F.W. Zwiers, and G.C. Hegerl, 2011. Human contribution to more-intense precipitation extremes. *Nature*, **470**, 378-381.

Min, S.-K., X. Zhang, F. W. Zwiers, P. Friederichs, and A. Hense, 2009. Signal detectability in extreme precipitation changes assessed from twentieth century climate simulations. *Climate Dyn.*, *32*, 95–111

Mlawer, E. J., S. J. Taubman, P. D. Brown, M. J. Iacono, and S. A. Clough, 1997. Radiative transfer for inhomogeneous atmospheres: RRTM, a validated correlated-k model for the longwave, *J. Geophys. Res.*, **102(D14)**, 16,663–16,682.

Mo, K.C., and E.H. Berbery, 2004. Low-level jets and summer precipitation regimes over North America. *J. Geophys. Res*., **109, D06117**, doi:10.1029/2003JD004106.

Moncrieff, M., and M. Miller, 1976. The dynamics and simulation of tropical cumulonimbus an squall lines. *Quart. J. Roy. Meteor. Soc.*, **102**, 373–394.

Nesbitt, S.W., D.J. Gochis, and T.J. Lang, 2008. The Diurnal Cycle of Clouds and Precipitation along the Sierra Madre Occidental Observed During NAME-2004: Implications for Warm Season Precipitation Estimation in Complex Terrain, *J. Hydrometeor.*, **9**, 728-743.

Niu, G.-Y. and co-authors, 2011. The community Noah land surface model with multiparameterization options (Noah-MP): 1. Model description and evaluation with local-scale measurements. *J. Geophys. Res*., **116**, D12109.

North, G., T. Bell, R. Cahalan, and F. Moeng, 1982: Sampling errors in the estimation of empirical orthogonal functions. *Mon. Wea. Rev*., **110**, 699-706.

Petrie, M., Collins, S., Gutzler, D., Moore, D., 2014. Regional trends and local variability in monsoon precipitation in the northern Chihuahuan Desert, USA. *J. Arid Environments*, **103**, 63–70.

Prein, A. F., and co-authors, 2015. A review on regional convection-permitting climate modeling: demonstrations, prospects and challenges. *Rev. Geophys*., **53**, 323–361.

Probhaska, J., 1976. A technique for analyzing the linear relationships between two meteorological fields. *Mon. Wea. Rev*., **104**, 1345-1353.

Pytlak, E., M. Goering, and A. Bennett, 2005. Upper-tropospheric troughs and their interaction with the North American monsoon. Preprints, *19th Conf. on Hydrology*, San Diego, CA, Amer. Meteor. Soc., JP2.3.

Raman, A., A.F. Arellano, and J.J. Brost, 2014. Revisiting haboobs in the southwestern United States: An observational case study of the 5 July 2011 Phoenix dust storm, *Atmos. Environ.*, **89**, 179-188, 10.1016/j.atmosenv.2014.02.026.

Rivera, E., F. Dominguez, and C. L. Castro, 2014. Atmospheric Rivers and Extreme Cool Season Precipitation Events in the Verde River Basin of Arizona. *J. Hydromet.*, **15**, 813-829.

Santer, B. D. and co-authors, 2007. Identification of human-induced changes in atmospheric moisture content. *Proc Natl Acad Sci USA*, **104**, 15248–15253.

Serra, Y., D.K. and co-authors, 2016. The North American Monsoon GPS Transect Experiment 2013. *Bull. Amer. Meteor. Soc.*, doi: http://dx.doi.org/10.1175/BAMS-D-14-00250.1

Sheffield, J., and Coauthors, 2013. North American climate in CMIP5 experiments. Part I: Evaluation of historical simulations of continental and regional climatology. *J. Climate*, **26**, 9209–9245, doi:10.1175/JCLI-D-12-00592.1.

Seidel, D.J., Q. Fu, W.J. Randel, and R.J. Reichler, 2008. Widening of the tropical belt in a changing climate. *Nature Geosci.*, **1**, 21-24, doi:10.1038/ngro.2008.38.

Skamarock, W.C., and co-authors, 2008. A description of the Advanced Research WRF Version 3. NCAR Tech Notes-475+STR.

Taylor, K.E., R.J. Stuoffer, G.A. Meehl, 2012. An Overview of CMIP5 and the Experimental Design. *Bull. Amer. Meteor. Soc.*, **93**, 485-498.

Tripathi, O. P. and F. Dominguez, 2013. Effects of spatial resolution in the simulation of daily and subdaily precipitation in the southwestern US. *J. Geophys. Res*., **118**, 7591-7605.

Wallace, J.M., C. Smith, and C.S. Bretherton, 1992. Singular value decomposition of wintertime sea surface temperature and 500-mb height anomalies. *J. Climate*, **5**, 561-576.

Wang., J., and R. Kotamarthi, 2015. High-resolution dynamically downscaled projections of precipitation in the mid and late 21st century over North America. *Earth's Future*, **3**, 268-288.

Wilks, D. 2006. *Statistical Methods in the Atmospheric Sciences*, Second Ed. Academic Press, 627pp.

Willett, K. M., N. P. Gillett, P. D. Jones, and P. W. Thorne, 2007. Attribution of observed surface humidity changes to human influence. *Nature*, **449**, 710-712.

Wood, K.M., and E.A. Ritchie, 2013. An Updated Climatology of Tropical Cyclone Impacts on the Southwestern United States. *Mon. Wea. Rev.*, **141**, 4322-4336.

Zehnder, J.A., 2004. Dynamic Mechanisms of the gulf surge. *J. Geophys. Res*., **109**, D10107, doi:10.1029/2004/JD004616.

Zehnder, J., L. Zhang, D. Hansford, A. Radzan, N. Selover, and C. Brown, 2006. Using digital cloud photogrammetry to characterize the onset and transition from shallow to deep convection over orography. *Mon. Wea. Rev.*, **134**, 2527–2546.

Zhang, J., and co-authors, 2011. National Mosaic and Multi-Sensor QPE (NMQ) System. Description, Results and Future Plans. *Bull. Amer. Meteor. Soc*., **92**, 1321-1338.

APPENDICES

A. SUPPORTING DATA

Data Portal and Data Access

CyVerse Data Portal (http://www.cyverse.org/) is a cloud infrastructure to use remote servers for computation, analysis, and storage. Funded by National Science Foundation Directorate for Biological Sciences and lead by the University of Arizona and other partners (Texas Advanced Computing Center, Cold Spring Harbor Laboratory, and the University of North Carolina at Wilmington), CyVerse is designed to be an interactive analytical platform that provides data storage, bioinformatics tools, image analyses, cloud services, and also support computational algorithms to run on large, high-speed computers. Current Cyverse data storage is free of charge for domestic and international users, individual user has 1TB (1 terabyte) space for data storage. Larger data storage between group members and collaborators are upon request.

CyVerse has proven to be a powerful and easy-to-use data sharing portal; the UA research team is able to allocate 50TB of storage space and share multi-terabyte datasets with domestic and international collaborators. Data Commons Repository (DCR) from CyVerse allows users to access a suite of large-scale computational analysis resources, so that users can seamlessly analyze, manage, and publish new results. The PIs also have the option to assign permanent identifier (a Digital Object Identifier, DOI, or Archival Resource Key, ARK) to the data archive uploaded on CyVerse. Project PIs and related personnel have various privilege to upload/edit/download the data directories. The archive can also be accessed externally via a login system and request to the data management staff. To date, the UA research group has used the Cyverser portal to exchange past research outcomes with more than a dozen users within U.S. and international collaborators in Europe, Central and South America.

B. LIST OF SCIENTIFIC/TECHNICAL PUBLICATIONS

Publications:

Chang, H., C.L. Castro, C.M. Carrillo, and F. Dominguez, 2015. The more extreme nature of U.S. warm season climate in the recent observational record and two "well performing dynamically downscaled CMIP3 models. *J. Geophys. Res. Atmos*., **120,** 8244-8263. doi:10.1002/2015JD023333.

Lahmers, T.M., C.L. Castro, D.K Adams, Y.L. Serra and J.J. Brost, 2016. Long-term changes in the climatology of transient inverted troughs over the North American Monsoon region and their effects on severe weather. *J. Climate*, **29**, 6027-6064.

Mazon, J.J., C.L. Castro, D.K. Adams, C. Carrillo, and J. J. Brost, 2016. Objective Climatological Analysis of Extreme Events During the North American Monsoon. *J. Appl. Meteor. and Climatol*., DOI: http://dx.doi.org/10.1175/JAMC-D-16-0075.1

Luong, T. M. C. L. Castro, H. Chang, Timothy Lahmers, David K. Adams, and Carlos A. Ochoa-Moya, 2017. The More Extreme Nature of North American Monsoon Precipitation in the Southwestern U.S. as Revealed by a Historical Climatology of Simulated Severe Weather Events, *J. Appl. Meteor. and Climatol*. in revision.

Presentations:

Chang, H., C. L. Castro, S. Megdal, and E. M. Tapia, 2017: Toward Improved Seasonal Forecasting of Water Resources and North American monsoon Precipitation in the Southwestern United States.97th American Meteorological Society Annual meeting, January 22-26, Seattle, WA.

Castro, C. L., H. I. Chang, T. Luong, C. M. Carrillo, T. Lahmers, M. Jares, and J. J. Mazon, 2017: Evaluating Changes in Extreme Weather During the North American Monsoon in the Southwest U.S. Using High Resolution, Convective-Permitting Regional Atmospheric Modeling. 97th American Meteorological Society Annual meeting, January 22-26, Seattle, WA.

Castro, C. L., H. Chang, T. M. Luong, T. M. Lahmers, M. Jares, J. Mazon, C. M. Carrillo, and D. K. Adams, 2016: Evaluating Changes in Extreme Weather During the North American Monsoon in the Southwest U.S. Using High Resolution, Convective-Permitting Regional Atmospheric Modeling. Water Availability Grand Challenge for North America, May 3-5, Columbia, MD.

Castro, C. L., H. Chang, T. M. Luong, T. M. Lahmers, M. Jares, J. Mazon, C. M. Carrillo, and D. K. Adams, 2015: Evaluating Changes in Extreme Weather During the North American Monsoon in the Southwest U.S. Using High Resolution, Convective-Permitting Regional Atmospheric Modeling (Invited). American Geophysical Union Fall Meeting, December 14-18, San Francisco, CA.

Castrol, C. L., T. M. Lahmers, Y. Serra, J. J. Brost, T. M. Luong and D. K. Adams, 2015: Assessment of the Long-Term Trends of Transient Inverted Troughs within the North American Monsoon Region: Mechanisms and Implications for Warm Season Precipitation. American Geophysical Union Fall Meeting, December 14-18, San Francisco, CA.

Lahmers T. M., C. L. Castro, Y. Serra, and J. J. Brost, 2015: Assessment of the long-term trends of transient inverted trough climatology over the North American Monsoon Region from four dynamically downscaled GCMs, 29th Conference on Hydrology, Phoenix, AZ, American Meteorological Society 7.3.

Castro, C. L., H. Chang, T. M. Luong, T. M. Lahmers, M. Jares, and C. M. Carrillo, 2014: Projecting Future Changes in Extreme Weather During the North American Monsoon in the Southwest with High Resolution, Convective-Permitting Regional Atmospheric Modeling. American Geophysical Union Fall Meeting, December 14-19, San Francisco, CA.

Jares, M., C. L. Castro, H. I. Chang, C. Carrillo, J. J. Mazon, J. Stutler, and J. J. Brost, 2014: High Resolution WRF Simulation and Climatological Analysis of Severe Weather Events during the North American Monsoon. 94th American Meteorological Society Annual meeting, February 2-4, Atlanta, GA.

Lahmers, T. M., C. L. Castro, Y. Serra, and J. J. Brost, 2014: Long-term changes in the climatology of transient inverted troughs over the North American Monsoon region and their effects on severe weather. 94th American Meteorological Society Annual meeting, February 2-4, Atlanta, GA.

Chang, H., C.L. Castro, P.A. Troch, M. B. Switanek, T. Luong, and F. Dominguez, 2013: Dynamically Downscaled IPCC RCM Climate Projections for the Southwest U.S. and Their Applicability in Hydrologic Resource Projection. 93rd American Meteorological Society Annual meeting, January 5-10, Austin, TX.

Mazon, J. J., C. L. Castro, H. I. Chang, M. Leuthold, and J. J. Brost, 2013: Objective Climatological Analysis of Warm Season Extreme Events during the North American Monsoon. 93rd American Meteorological Society Annual meeting, January 5-10, Austin, TX.

Stutler, J., C. L. Castro, J. J. Brost, and H. I. Chang, 2013: Determining Gulf Surge Contributions to NAM Precipitation Using Observational and Reanalysis Data. 93rd American Meteorological Society Annual meeting, January 5-10, Austin, TX.

Chang, H., C. L. Castro, and M. Leuthold, 2013: Assessing Climate Change Impacts for Military Installations in the Southwest United States During the Warm Season. 93rd American Meteorological Society Annual meeting, January 5-10, Austin, TX.